ROADMAP

Nanostructured photovoltaics

NANO FUTURES

ROADMAP

Nanostructured photovoltaics

Katerina Nikolaidou, Som Sarang and Sayantani Ghosh

Department of Physics, University of California, Merced, CA 95343, United States of America

E-mail: sghosh@ucmerced.edu

Keywords: nanomaterials, photovoltaics, solar concentrators, nanowires, quantum dots

RECEIVED
10 December 2018

ACCEPTED FOR PUBLICATION
29 January 2019

PUBLISHED
25 February 2019

Abstract

In this review, we begin by discussing the need for harnessing renewable energy resources in the context of global energy demands. A summary of first- and second-generation solar cells, their efficiency and grid parity is provided, followed by the need to reduce material and installation costs, and achieve higher efficiencies beyond the Shockley–Queisser limit imposed on single junction cells. We also discuss the specific advantages offered by nanomaterials in enhanced energy harvesting, what design platforms comprise nanostructured photovoltaics, and list the prominent categories of nanomaterials used in the design of third generation solar cells. We review the significant nanostructured photovoltaic platforms that have encouraging power conversion efficiencies, have the potential for long term stability (both structural and functional) and have received attention in the field. In addition to their operational principle, we highlight both their advantages and shortcomings, along with insights into possible improvements. We include alternate routes to improving power conversion efficiency, not by tuning material properties to match the solar spectrum but using additives and/or structural modifications to allow more efficient harvesting of sunlight, either by reducing losses or by altering the spectral properties. The properties of nanomaterials that make them well-suited as active materials in photovoltaic devices (broadband absorption, high quantum yield, etc.) also make them ideal candidates for luminescent solar concentrators (LSCs). These devices also harvest solar energy, but instead of directly allowing charge generation, they act as downconverters for other photovoltaic cells. We review dye, thin film, and quantum dot based LSCs that have garnered a lot of attention in recent years as these devices face a resurgence given the advances in materials science and engineering which have led to novel quantum dots and hybrid semiconductors. The review ends with where the future of nanostructured photovoltaics is headed, what device designs and materials development are needed to achieve efficiencies beyond the Shockley–Queisser limits and fulfil the goal of the 3rd and 4th generation photovoltaics.

1. Introduction

Global energy consumption has steadily risen since the 1960s, and the last two decades have seen an increase by roughly 53% [1]. A conservative estimate predicts an additional 35% increase in the next two decades, putting our power needs at an overwhelming ~30 TW by 2050. While there is a strong possibility that fossil fuels will continue to be a mainstay, an optimistic perspective would be to assume that renewable sources will be tapped more substantively in the coming decades, both for resource conservation and climate preservation purposes. Among the various options available on that front, biomass, hydroelectricity, wind and geothermal resources together can account for almost 14 TWy, but solar energy incident at the Earth's surface is a phenomenal 10^5 TWy [2]. Needless to say, efficient harnessing of solar energy could not only more than satisfy global energy needs, but do so in a clean, carbon-neutral manner. These obvious advantages have spurred extensive research efforts worldwide, and the influence in the commercial sphere has been notable. The sale of photovoltaic (PV) modules has grown from 1 GW to 100 GW between 2004 and the present [3], reflective of market demand and manufacturing growth. Simultaneously, module prices have dropped by a factor of 5 [4], bringing solar energy

closer to achieving grid parity. It is estimated that globally, almost 2% of electrical needs are currently provided by PVs [5], and nearly 90% of the PV market consists of crystalline silicon (Si) solar cells [6].

Si PV belongs to the 1st generation of solar cells and is still the most economically viable PV in use. It has some drawbacks, which have contributed to PVs not having more widespread applications. In the simplest terms, these boil down to the net cost of installing and using solar panels to generate electricity rather than conventional sources. This is measured in terms of grid parity, which currently stands at about 0.1$/kWh [7]. Si PVs are close, but the additional inconvenience of switching over to solar energy would be more attractive to the general populace if this price was closer to $0.03/kWh. There are two routes to achieving this: lowering the manufacturing and installation costs of solar panels or producing panels with higher power conversion efficiency (PCE), or both. And this is where the 1st generation Si panels are problematic. Module and installation prices are unlikely to reduce much more than the present value, and PCE has remained unchanged at a peak value of 25% for the last 15 years [8]. And this limitation is rooted in the inherent material properties. Si has an indirect band gap, which results in low absorptivity, which in turn requires the solar cells be thick to have adequate solar absorption. The cell thickness adds to material costs, to panel weight, and to low PCE as this extra path length gives the photogenerated carriers increasing opportunities to recombine, rather than be extracted as photocurrent. Some of these issues were addressed in the 2nd generation solar cells, which are direct band gap semiconductors and can be fabricated as thin films. Gallium arsenide (GaAs), cadmium telluride (CdTe) and copper indium germanium selenide (CIGS) are representative of this generation, and the most successful is GaAs, with a reported record PCE of 29% [9]. These are commercially even less viable though, given their very high price point. But, these can be fashioned into multijunction cells that are not restrained by the Shockley–Queisser limit and have demonstrated PCEs >40% [10]. The theoretical efficiency of a single junction solar cell is limited to ~33% by the Shockley–Quiesser [11] formulation, and in practice, single junction cells have not achieved this full potential due to spectral limitations. The inherent inability of a semiconductor to absorb photons with energy lower than its band gap, added to the thermalization of photons with energy higher than it, are both unavoidable loss mechanisms and the only way to overcome them is to fabricate multijunction cells. These make them ideally suited for applications where expense is not a limiting factor, but poundage is, such as space exploration. Returning to terrestrial use, research in the newest generation (3rd) of emergent PVs is motivated by the desire to develop solar cells that allow lost cost synthesis while exhibiting high enough efficiency that would allow them to compete with conventional power generation infrastructure. And a large proportion of these emerging solar cells focus on nanostructured components, both organic and inorganic, which is what this review will emphasize. Before we delve into the wide range of nanostructured PV and their successes and limitations, we take a brief look into the broad context as to why nanostructured materials are considered to have such potential as photovoltaics.

'Small is different' is an oft-repeated but very apt phrase to succinctly describe the unique aspect of nanoscale materials. The reduced spatial dimensions lead to quantization of energy and momentum, and this phenomenon, known as quantum confinement [12], is at the origin of their unique optical, electronic, and magnetic properties that are so different from their bulk counterparts. Additionally, these properties are easily tunable by varying the size of the nanomaterials, or by surface modification [13]. In the specific context of photovoltaic devices, the large absorption coefficient of nanoscale materials is particularly advantageous. less material is needed to harness sunlight, which not only makes the device lightweight and less expensive from the raw materials perspective but allows easier extraction of photogenerated carriers by virtue of a shorter effective path length. And while these will key issues of reducing price while improving efficiency, there are additional advantages offered by nanostructured photovoltaic. The nanomaterials are typically chemically synthesized via low temperature, solution-based methods and therefore, suited for deposition on flexible substrates. The devices thus designed can be applied far more broadly than current rigid solar panels, especially for mobile deployment. This also allows the use of organic materials and others like these that have low mobility. Nanostructured surfaces have lower reflectivity, negating the need for AR coatings and subsequently, the added weight and expense. The definition of what constitutes a nanostructured photovoltaic is quite broad, comprising not only devices that use nanoscale semiconductors as the active material, but also those that incorporate nanoscale optoelectronic components to enhance absorption, induce reflective losses and increase light trapping. In our review, we have exhaustively covered both various, focusing on those platforms that have demonstrated encouraging power conversion efficiencies accompanied by the potential for long term structural and functional stability. While discussing the advantages of each type, we will touch upon the shortcomings, along with any insights into arresting the latter and improving the performance. We include a third category of devices as well, luminescent solar concentrators (LSCs), where the active material is not utilized to directly generate photocarriers. Instead, they act as down converters by absorbing solar radiation and re-emitting it in a spectral region more suited for solar cells attached at the edges. LSCs were initially marketed as a less expensive alternative to silicon solar panels, but with the change in pricing all around, this is no longer a valid motivation. However, LSCs do indeed have unique properties, as they can harvest diffuse radiation in addition to direct sunlight. This is a major advantage over solar cells that require tracking to optimize performance. Further, they are better suited for building-integrated photovoltaic installations than solar panels and will round off our review of nanostructured devices for solar energy harvesting.

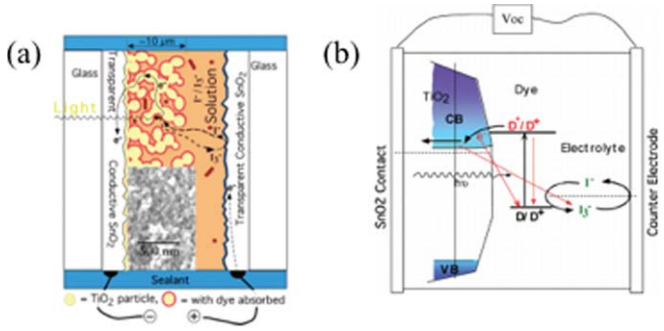

Figure 1. (a) Schematic of a DSSC, and (b) electron transfer processes in a DSSC. Reprinted with permission from [15]. Copyright (2009) American Chemical Society.

We segregate the nanostructured devices in to two broad categories for the purposes of this review. In the first section we will describe and discuss the significant nanostructured PV platforms where the nanomaterials are the active material. These will include dye-sensitized solar cells, quantum dot-sensitized solar cells, quantum dot solar cells, and solar cells that utilize nanowire arrays. In the next section we focus on an alternate route to improving PCE, not by tuning material properties to match the solar spectrum but using nanoscale additives and/or structural modifications to allow more efficient harvesting of sunlight, either by reducing losses or by altering the spectral properties. We will cover plasmonic inclusions that enhance scattering, and absorption, or offer resonant energy transfer and hot carrier injection into the semiconducting photovoltaic, as well as rare earth ions and compounds that act as up or down converters of the solar spectrum to match the absorption band of the active medium to improve performance. We finish off with a description of alternative nanostructured platforms, devices that also harvest solar energy, but instead of directly allowing charge generation, they act as down converters for other PV cells. We will review dye, thin film, and quantum dot based LSCs that have garnered a lot of attention in recent years as these devices face a resurgence given the advances in materials science and engineering which have led to novel QDs and hybrid semiconductors.

2. Nanostructured PV platforms

Nanostructured PVs offer the possibility of increased surface area due to their nanostructured components without increasing the physical size of the device, whereas tailoring of their individual components is significantly easier than conventional Si-based PV as different processes occurring under illumination are decoupled. In this section we highlight the nanostructured PV platforms that have significant and encouraging power conversion efficiencies, and the potential for long term stability. The various technologies that currently satisfy these criteria, and those we will describe and discuss here include dye-sensitized solar cells (QDSSCs) , colloidal quantum dot solar cells, and nanowire-based solar cells. In addition to their operational principle, we will discuss both their advantages and shortcomings, along with insights into possible improvements.

2.1. Dye sensitized solar cells (DSSCs)

DSSCs were first introduced by O'Regan and Grätzel in 1991 [14]. Their work challenged the conventional solid-state photovoltaic cells, by introducing a device that incorporated nanomaterials and separated the processes of light absorption and charge carrier transport. This new device offered the possibility of low-cost photovoltaic devices, which would provide an alternative to power generation from conventional sources.

The first example of DSSC was prepared using a ruthenium complex as sensitizer, deposited on a TiO_2 (titanium dioxide) film, and employed a liquid re-dox electrolyte of tetrapropylammonium iodine mixed with iodine. This device achieved a fill factor of 0.76, and in addition to a PCE of 7.9% [14], it also demonstrated an efficiency of 12% under diffuse sunlight, revealing unexpected benefits of these devices compared to conventional silicon based solar cells. Furthermore, under conditions of low light intensity (<5 W m^{-2}), the fill factor remained above 0.7, which is not observed for conventional devices. This was an initial indication of the absence of recombination processes that normally limit device performance in semiconductor devices. The promise shown by this first DSSC encouraged further research into the processes occurring within the device and potential enhancements of the device design to achieve higher PCE .

A typical DSSC is shown in figure 1. The device consists of a glass or plastic substrate, which is coated with a transparent conductive oxide (TCO)—common examples include indium tin oxide (ITO) or fluorine-doped tin oxide (FTO). The substrate is coated with a mesoporous oxide layer, which typically serves as the electron

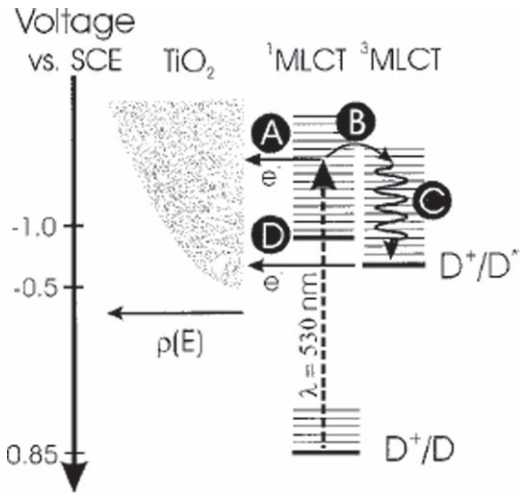

Figure 2. Energy level diagram of the RuN3–TiO_2 system. Processes: (A) electron injection from the singlet excited state, (B) intersystem crossing, (C) thermalization of triplet state, (D) electron injection from triplet state. Reprinted with permission from [19]. Copyright (2002) American Chemical Society.

transport layer (ETL) that guides electrons to the anode, and TiO_2 has been a particularly popular material for this purpose. Dye is deposited onto the ETL and is employed for light absorption followed by electron injection into the conduction band of the ETL. The dye is then regenerated via electron transfer from the redox electrolyte, typically an iodide/triiodide system. Finally, the triiodide formed is reduced to iodide by capture of electron from the cathode, which usually consists of platinum on TCO glass. These processes are shown in figure 1(b). Therefore, at the end of the process the device has returned to its original state [15]. While extensive research has been done on the materials incorporated in these devices, certain dyes have shown great promise. The most impressive PCE from a single sensitizer so far has been achieved by implementing porphyrin sensitizer (SM315) that has been engineered to improve its light harvesting properties, resulting in a PCE of 13.0% [16].

2.1.1. Charge separation, transport, and transfer at dye/ETL interface

Figure 1(b) also shows loss mechanisms that DSSCs are susceptible to. These include direct recombination of the electron and hole pairs in the dye, and recombination of the electrons in the ETL with the oxidized dye or the electrolyte [17, 18]. Hence, optimizing charge injection from the dye to the ETL is crucial for efficient device operation. The dye molecule is responsible for harvesting the incident light energy, resulting in a long-lived excited state, followed by electron injection into the conduction band of the ETL. Two different charge transfer pathways have been identified via femtosecond transient absorption spectroscopy: electron injection from non-relaxed higher-lying excited state, which has been associated with the singlet excited state of the dye, and injection from the fully relaxed excited state, which is associated to the triplet excited state of the dye [18, 19]. These processes compete with back electron transfer from the ETL to the dye, implying that for efficient power conversion, fast electron transfer and slow back electron transfer are needed.

The electron kinetics have been studied extensively in the $Ru(dcbpy)_2(NCS)_2$ (RuN3)–TiO_2 system, as it is one of the most efficient dye/ETL combinations. Since the lowest excited state of RuN3 is 0.3 eV higher than the conduction band minimum of TiO_2, electron injection can occur from the singlet and triplet states of RuN3 [19–22]. By comparing transient absorption signals of the dye deposited on TiO_2 and the dye in solution, a shorter time constant was observed for the former case, indicating that a depopulation channel is available. Furthermore, by probing the triplet state absorption, it was concluded that excited state evolution from the singlet to the triplet state is also occurring, with a time constant of approximately 70 fs [19]. The fast component of electron injection from the singlet states has been estimated to occur on a time scale of $<$100 fs [19, 23–26]. On the other hand, the slow component of electron injection, associated with the transfer from the triplet states of the dye, has been associated with time constants ranging from 1.7 to 100 ps [19, 24–27]. These processes are depicted in figure 2.

Figure 2 also shows the energy dependence of the states in the conduction band of TiO_2, which has been associated with the variation of the electron injection rate, as it was observed to increase with higher density of states. This has been used to rationalize the presence of a slow component of electron transfer, as the triplet states are close to the energy of the conduction band minimum of TiO_2, meaning that there is a reduced density of states available [19, 22, 28]. In addition, while the fast component of electron transfer could occur adiabatically, the slow component could be associated with non-adiabatic processes resulting from the formation of the triplet state [19]. The slow component could also be a consequence of the binding of the dye on the ETL and surface defects [19].

On the other hand, back electron transfer has been observed to happen non-exponentially and is associated with timescales of microseconds to milliseconds, and a negligible picosecond/nanosecond component, therefore reducing competition for the aforementioned electron transfer processes [18, 19]. This difference in timescales justifies the high efficiency of the RuN3–TiO_2 system in DSSCs. The slow back electron transfer has been attributed to weak electronic coupling between the oxidized dye and the electron in the ETL, trapping of the electron in the ETL, as well as the inverted Marcus region that slows outer sphere electron transfer [19, 29].

Electron injection studies have been extended to other dyes as well. Work on the Ruthenium bipyridyl sensitizer dye N719 has demonstrated that unlike the RuN3 dye, in which electron injection from the singlet and triplet states is occurring in parallel, electron injection from the triplet state of the N719 dye is the more efficient injection pathway [30]. It was estimated that singlet injection occurs within 1–10 ps, triplet injection occurs within ~100 ps, whereas intersystem crossing from the singlet to the triplet state occurs within ~100 fs [19] and decay of the triplet state to ground state requires ~10 ns. Therefore, Koops *et al* [30] concluded that electron injection from singlet states occurs only for systems with very favorable interfacial energetics, as is the case in the RuN3–TiO_2 system, but for typical devices, due to the presence of the electrolyte which influences the potential, it is unlikely that singlet injection can compete with intersystem crossing. Consequently, electron injection will most likely originate from the triplet state, which results in a ten-fold retardation of injection. This work [30] also investigated the various factors that could influence the electron injection kinetics in a DSSC. While the application of electrical bias or the mere presence of the electrolyte in the device did not affect the injection kinetics, it was found that the composition of the electrolyte had a larger effect. The concentration of tert-butylpyridine (tBP) and lithium cations (Li^+) significantly modified kinetics. Incorporation of tBP in the electrolyte is observed to shift the density of states of TiO_2 to more negative potentials, whereas Li^+ results in less negative potentials. The former changes the conduction band of TiO_2 by coordination to the TiO_2 surface, or by diminishing the cation concentration on the surface [30–32]. On the other hand, Li^+ adsorb or intercalate into the TiO_2 layer, eventually modifying the charge and energy levels [28, 30, 33]. However, it was demonstrated that despite the retardation of injection kinetics because of these electrolyte additives, resulting in reduction of the device photocurrent, their presence increases the Fermi level of TiO_2 and, consequently, enhances the open circuit voltage of the device, therefore resulting in higher device efficiency. This further establishes the fact that it is not necessary to have the faster injection kinetics for best device performance, but rather a good compromise between driving force that allows competition with dye relaxation and raising the conduction band of TiO_2 to reduce recombination losses [30]. Hence, the only requirement is that electron injection from the dye to the ETL happens faster than decay of the excited state.

Although Ruthenium bipyridyl dyes were originally believed to be the best choice for DSSCs, record devices have been prepared with porphyrin sensitizers [16, 34]. Therefore, it is imperative that we discuss the electron injection kinetics of these sensitizers and how they compare with Ruthenium bipyridyl dyes. Ruthenium bipyridyl dyes are characterized by long-lived excited state, good visible absorption, and good photochemical stability [21], as well as a high degree of charge transfer character and mixed singlet/triplet states as discussed previously. On the other hand, other common dyes, including porphyrins, do not show as much mixing of singlet/triplet states and charge transfer, but they also demonstrate long-lived singlet excited states [26, 35–37]. The photophysical characteristics of the two types of dyes are different when in solution; RuN3 exhibits very low emission yield and large red shift of emission, associated with the relaxation of the singlet state to the triplet states, whereas porphyrin dyes (zinc and free base tetracarboxyphenyl porphyrins: ZnTCPP and H_2TCPP respectively) show a series of narrow visible absorption bands and small red shift with high emission intensity, characterized by relatively long excited state lifetime [26]. After deposition of all dyes on TiO_2, almost indistinguishable, multi-exponential injection kinetics are observed for all, with essentially the same lifetimes and relative amplitudes. This result demonstrates that while for porphyrin dyes electron injection occurs from the singlet state, and for ruthenium bipyridyl dyes charge transfer and relaxation to the triplet state is involved, it does not dominate electron injection kinetics. Furthermore, the recombination kinetics for RuN3 and ZnTCPP are also indistinguishable, whereas H_2TCPP demonstrates recombination kinetics that are eight times slower. This result further supports the model that recombination in dyes is mostly controlled by the electron transfer between trap sites in the mesoporous ETL, rather than the electronic structure of the dye [26]. Once the electron is injected into the ETL mesoporous layer, it is transported to the contact, so it can be extracted from the device. Materials such as ZnO and SnO_2 have been used in DSSCs, but nanocrystalline porous TiO_2 appears to be the best option so far, due to good energy level matching with dyes [38, 39]. The efficient electron transport through the nanocrystalline TiO_2 layer is believed to occur by electron hopping from one particle to another [18, 20]. Mesoporous layers are unlike the bulk material as they are characterized by low conductivity, the particles making up the layer are too small to support an electrical field, whereas the mesoporous layer allows for formation of interpenetrating networks that result in a large contact area with the other components of the device [18].

The transport of electrons through the ETL is a complex procedure that has been investigated by multiple research groups. Since the electrons are transported through a trapping and de-trapping mechanism, the traps play a crucial role for both electron transfer and recombination in TiO_2 [23, 40, 41]. Traps become important at

low illumination intensity, resulting in slow transport and a small diffusion coefficient. At higher light intensity, deep traps are filled, meaning that electron transport is faster and the diffusion coefficient is larger [18, 42]. An additional mechanism regarding the charge transport of TiO_2 films has been suggested, indicating that self-doping is occurring under illumination, which results in enhanced conductivity of the originally poorly conductive material [38]. Under illumination, a transient charging process is happening, and when carrier concentration of 10^{19} cm^{-3} is reached, the region of the film that is not illuminated undergoes the Mott (insulator-metal) transition, resulting in a significant increase in electrical conductivity [38, 43]. Modification of the TiO_2 layer has been attempted by various groups to improve its characteristics, including doping of TiO_2 with Zn, Al, Zr, Nb [39, 44, 45], or preparation of 1D nanostructures to enhance electron transport [46].

2.1.2. Liquid electrolytes

For efficient DSSCs, electrolytes must be chosen such that they can transport the charge carriers between anode and cathode successfully, considering the redox potential, regeneration of the dye and the electrolyte. Furthermore, it must ensure good contact with the mesoporous ETL, have minimal leakage and evaporation, as well as long-term stability. In addition, it should not result in dye degradation or desorption, and should not absorb a significant portion of visible light [47–50]. In a DSSC, the electrolyte is acting as a hole-transport medium, and is responsible for regenerating the oxidized dye, with the cycle completed after conversion of the triiodide to iodide at the counter electrode. Therefore, the counter electrode must be chosen to ensure low overpotential and rapid reaction [17, 47, 51]. Platinum (Pt) has been a good candidate for a counter electrode. In liquid electrolytes, ion diffusion occurs via ion hopping or liquid-like diffusion of ionic sub-lattice [47, 52]. However, when there is a high concentration of iodide, polyiodides are formed, resulting in an electron exchange mechanism to be responsible for carrier transportation [47, 53, 54]. In this case, electrons are transported via chemical bond exchanges [53, 55]. Overall, the diffusion process is controlled by the size of the redox species, the solvent viscosity, the redox medium concentration, and the separation between electrodes [47, 56].

In the first example of DSSC, a liquid electrolyte prepared with the iodide/triiodide couple in an organic solvent was used [14]. Liquid electrolytes offer several attractive characteristics: they can be prepared easily, they are highly conductive, they have low viscosity, and can achieve good interfacial contact with the counter electrode [47, 48, 56]. They remain the most common choice for hole transport, and were used in the most efficient DSSCs so far [16, 57]. The liquid electrolyte usually comprises of the solvent, the ionic conductor, and the additives. Good solvents must have melting points below −20 °C, and boiling points above 100 °C to prevent evaporation during cell operation, they must be chemically stable within the operating potential window of the device, have low viscosity to ensure that the redox species has high diffusion coefficient and high conductivity, it should not absorb incident light, it should not react with the sensitizer dye, not dissolve the sealant material, be non-toxic and cheap [47]. While polar organic solvents and ionic liquids are good candidates, a single solvent cannot satisfy all the conditions, therefore solvents are usually mixed. Water was initially used as a solvent in DSSCs, but the oxidation of iodide to iodate, which is not reduced by the counter electrode, prevented long-term operation of the device, whereas many dyes are sensitive to water [17, 47, 56, 58]. Acetonitrile is another good electrolyte as it has low viscosity, good chemical stability and solubility, and was used in the DSSC that achieved record efficiency of 13% [16, 47]. Nevertheless, it suffers from low boiling point and high toxicity, meaning it cannot be implemented in industrial devices. Methoxyacetonitrile and 3-methoxypropionitrile have been used in DSSCs, with the latter demonstrating particularly good stability, retaining 98% of the efficiency after 1000 h of accelerated heat tests under thermal stress [17, 47, 59]. Other common solvents include ethylene carbonate, propylene carbonate, γ-butyrolactone, and N-methyloxazolidinone, which are characterized by high boiling and melting points [47]. A DSSC prepared with γ-butyrolactone solvent has been shown to operate outdoors for almost 2.5 years [60]. It should be noted that basic solvents affect the TiO_2 surface, raising its flatband potential, and subsequently not only reducing the driving force for electron injection from the dye to the TiO_2, but additionally preventing electron recombination between the TiO_2 and the redox species [15, 47, 61]. This results in lower device photocurrent, but higher open circuit voltage.

Ionic liquids have also been incorporated in the electrolytes in DSSCs, as they possess good chemical and thermal stability and high ionic conductivity, while their viscosity can be tailored and they do not evaporate or leak as much [47]. Methyl-hexyl-imidazolium iodide was used in a device that demonstrated impressive stability in 1996 [53]. Later, an electrolyte made with $SeCN^-/(SeCN)_3^-$ and without any solvent was implemented, achieving high efficiency at the time (7.5%–8.3%) [62]. The good performance was attributed to the low viscosity, high conductivity, and low light absorption of the ionic liquid, but the stability of the device was not good. Though imidazolium-based ionic liquids are common, other materials that have been used in electrolytes include ionic liquids with sulfonium, guanidinium, ammonium, pyridinium, and phosphonium, but none of these has shown good efficiencies [63–68]. However, implementation of a tetrahydrothiophenium melt demonstrated that ionic liquids can also be used for high efficiency devices [69]. Pure ionic liquids are characterized by high viscosity and low ion mobility, which results in lower diffusion coefficient of the triiodide, in comparison to organic solvents [70]. Hence, in order to improve their performance, ionic liquids are often mixed with organic solvents, which produced devices of high efficiency

[71]. Ionic liquids have also been mixed with solid components to improve their conductivity [72]. Mixing with multi-walled carbon nanotubes resulted in significant improvement of device efficiency [73].

The iodide/triiodide redox couple has traditionally been used in DSSCs for dye regeneration, as it has a redox potential that matches that of the dye, thereby ensuring rapid dye regeneration and slow recombination. Furthermore, this redox couple is soluble, conductive, does not absorb as much visible light, has good stability, and can form good interfaces with the mesoporous ETL [47]. One of the issues of DSSC operation is the recombination of charge carriers at the interface between the ETL and the electrolyte, which can be suppressed by incorporation of a metal oxide blocking layer [74]. It can also be suppressed by introducing additives such as 4-tert-butylpyridine and guanidium thiocynate in the electrolyte [21, 47, 75–77]. Similarly, dyes that have hydrophobic chains also appear to prevent recombination by blocking the contact of the two materials [78], whereas other dyes have the reverse effect of increasing the amount of triiodide near the dye [79, 80]. In order to increase the rate at which the dye is regenerated, the concentration of iodide must be tailored depending on whether organic solvent or ionic liquid is used; higher concentration is needed for the latter due to its lower viscosity [81]. Even though the iodide/triiodide redox species has been used for a large number of DSSCs, it suffers from issues of encapsulation due to the high vapor pressure of iodide and corrosion of the sealant by the iodide, while the polyiodides absorb part of the incident light, limiting the photocurrent [47]. In addition, the mismatch between the redox potential of the dye and that of the redox species causes a reduction of the possible open circuit voltage that can be achieved [47, 82]. As a result, alternative complexes were pursued. These include bromide/tribromide [51], interhalogen redox systems [83], disulfide/thiolate [84], and most notably, cobalt complexes [16, 34, 57]. Cobalt complexes have been used in both devices that currently hold the efficiency record [16, 57] and are considered to be the most efficient redox species for DSSCs, with further improvements expected after tuning the redox potentials of the redox couple [47]. Other metal complexes that have been studied include Ni(III)/Ni(IV), Cu(I)/Cu(II), and ferrocene/ferrocenium [85–89].

Electrical additives are often included in the electrolyte to optimize device performance. As mentioned in sections 2.1.1, 4-tert-butylpyridine (tBP) is a common additive, which improves the open circuit voltage, by shifting the conduction band edge of TiO_2 to more negative values [47]. Additives with similar effects include various nitrogen-containing compounds, such as pyridine, alkylaminopyridine, alkylpyridine, benzimidazole, pyrzaole, quinolone, among others [47]. Another type of additive, also mentioned in the previous section, are lithium ions (Li^+) or guanidinium ions, which adsorb to the surface of TiO_2 and assist in electron injection from the dye and reduce electron recombination by attaching to the surface of the TiO_2 layer, thereby improving the device photocurrent. Both types of additives are often combined in devices in order to acquire benefits from each one: raising the conduction band of TiO_2 and minimizing recombination losses [90–92].

2.1.3. Solid-state hole transport materials (HTMs)

Liquid electrolytes suffer from instability and leakage issues under exposure to air and prolonged storage. Therefore, research focus shifted to developing solid-state HTMs to avoid such problems. The redox electrolytes discussed in section 2.1.2 can transport charge carriers via ion movement and can be essentially considered a hole-transport layer. Thus, they could be replaced by p-type semiconductors, which are also capable of hole-transport via hole hopping through neighboring molecules [47]. A good HTM must have its valence band maximum above the ground state energy level of the dye to allow for efficient hole transfer and should be characterized by good hole mobility [93–95]. Furthermore, it should not absorb visible light, or cause dye degradation. [96, 97] In addition, as sufficient pore filling of the mesoporous ETL is crucial, the HTM should allow for deposition in an amorphous state to ensure good contact between the various layers of the DSSC [98, 99]. Some of the first types of inorganic solid-state HTMs included copper compounds (CuI, CuBr, CuSCN) [100–103]. These materials allow for solution or vacuum deposition, and are characterized by good hole conductivity [97]. CuI was incorporated in a DSSC for the first time in 1995, with low efficiency, which was attributed to the rapid crystallization of CuI that prevented sufficient filling of the mesoporous ETL and hence, caused insufficient electrical contact [95, 100]. After addition of 1-methyl-3-ethylimidazolium thiocyanate (MEISCN), which acts as a growth inhibitor for CuI, improved pore filling was achieved, leading to increased device efficiency of 3.8% [104]. Nevertheless, devices based on CuI HTM decay rapidly, because of the formation of Cu_2O and CuO caused by the iodine molecules on the surface of CuI acting as hole trapping sites [47, 105–107]. Introduction of a MgO blocking layer increased device efficiency by preventing hole transfer from TiO_2 to CuI [108]. The low efficiency of these devices could also be attributed to the insufficient contact between the dye and the HTM. However, it was observed that dyes with thiocyanate ligands can be strongly bound to CuI films, improving contact and therefore, device efficiency [109]. Further modification of the CuI HTM and the counter electrode with guanidine thiocyanate enhanced device performance, reaching device efficiency of 7.4% [110, 111].

CuSCN was investigated as an alternative to CuI, as it could offer higher stability [47, 101]. However, CuSCN suffers from low hole conductivity which necessitates material engineering to improve its electrical characteristics. Doping with $(SCN)_2$ led to the formation of acceptor levels below the CuSCN band gap, whereas

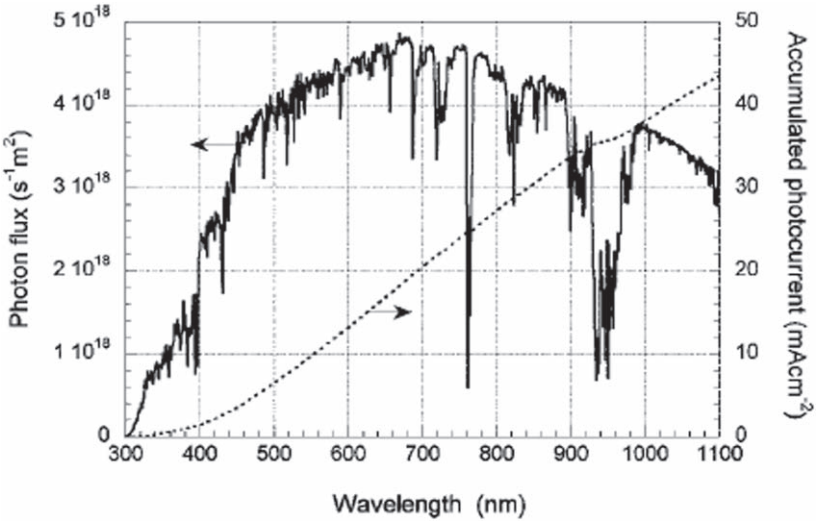

Figure 3. AM 1.5 G spectrum at 1000 W m^{-2} and accumulated photocurrent. Reprinted with permission from [17]. Copyright (2010) American Chemical Society.

inclusion of Cu(II) sites in CuSCN increased its hole conductivity, with both modifications resulting in improved device performance [112, 113]. Another promising solid-state HTM is cesium tiniodide ($CsSnI_3$), which demonstrates high hole conductivity and hole mobility, and a band gap of 1.3 eV [47]. Since $CsSnI_3$ can be prepared by solution processing, it allows for good pore filling of the mesoporous ETL, whereas its low band gap improves light absorption at longer wavelengths. Its incorporation in a DSSC resulted in device efficiency of 3.72% and doping of $CsSnI_3$ with SnF_2 raised the efficiency to 6.81% [47]. Through additional device engineering, $CsSnI_3$-based DSSCs reached efficiency of 10.2% [114]. Further modifications include use of Cs_2SnI_6 instead of $CsSnI_3$, which is stable in air and moisture, allowing for device fabrication in air [115].

Organic HTMs offer certain benefits over inorganic materials, such as abundancy, low cost, and facile preparation [47, 116]. and can be broadly classified into polymeric and molecular HTMs [116]. Polymeric HTM polypyrrole was first implemented in a DSSC in 1997, but it performed poorly due to absorption of visible light [117–119]. Polyaniline was also introduced as a potential HTM, but only reached device efficiency of 1.15% [120, 121]. Poly(3-hexylthiophene) (P3HT) and poly(3-octylthiophene) (P3OT) have dominated the polymeric HTM research landscape since then. While initial device efficiencies were low due to insufficient pore filling of the mesoporous TiO_2, device engineering boosted efficiency to 1.3% and demonstrated good stability after 3-month storage in air [122–125]. Device efficiencies were further enhanced by addition of bis (trifluoromethanesulfonyl)imide (LiTFSI) and tBP to P3HT reaching 2.7% [126, 127], as well as successful infiltration of P3HT into TiO_2 nanotubes [128]. Combination of P3HT with [6,6]-phenyl-C61-butyric acid methyl ester (PCBM) further increased device efficiency to 4.11% [129]. One of the most promising polymeric HTMs is poly(3,4-ethylenedioxythiophene) (PEDOT), which is characterized by minimal absorption in the visible part of the spectrum, good hole conductivity, and good stability at room temperature [47]. DSSCs incorporating PEDOT have reached efficiency of 6.8% [130]. Among molecular HTMs, 2,2′,7,7′-tetrakis(N,N-di-p-methoxyphenylamine)-9,9′-spirobifluorene (spiro-OMeTAD) is one that has shown remarkable results [47]. It initially resulted in device efficiency of 0.74% due to charge recombination at the spiro-OMeTAD/ETL interface [93], but through doping of the material with FK102 cobalt(III) complex that increased its hole mobility, and combination with Y123 sensitizer, device efficiency of 7.2% was achieved [131]. Even though solid state HTMs show better long-term stability, they still lag in device efficiency in comparison to their liquid-based counterparts, due to electrical contact issues with the rest of the device layers [47].

2.1.4. Progress on the main limitations of DSSCs

While significant improvements have been made in the materials incorporated in DSSCs, there are still issues to be resolved before the efficiency can be enhanced further. Extensive work has been done on understand and addressing each of these.

2.1.4.1. Absorption in the near-infrared spectral region

The first record efficiencies in DSSC research were achieved by implementation of the ruthenium N3, N719, and black N749 dyes. These dyes performed well as sensitizers in the visible part of the spectrum, but failed to absorb well in the near-infrared part of the spectrum, which, as shown in figure 3, is a significant portion of the solar

spectrum [17, 132]. Therefore, it is imperative to develop dyes with improved response in the region of the spectrum beyond 900 nm to achieve high power conversion efficiencies. To meet this requirement, various types of sensitizers for DSSCs have been developed. Metal complexes, including ruthenium, have been popular due to their broad absorption spectrum. These sensitizers consist of a metal ion and ancillary ligands with an anchoring group, with the absorption in the visible part of the spectrum associated with a metal to ligand charge transfer [17]. The ligands are tuned to modify the properties of the sensitizer to achieve higher device performance.

Ruthenium N3 dye has been commonly used due to its broad absorption in the visible part of the spectrum, leading to efficiencies of 10% [15]. By modifying the ligands to extend the absorption spectrum to the near-infrared region, the N749 'black dye' was designed, which successfully extended IPCE to 920 nm, and resulted in PCE of 10.4% [133, 134]. Other efforts include preparation of a ruthenium dye with a tetradentate ligand, which extended the absorption spectrum to 900 nm, resulting in efficiency of 5.9% [135]. Due to a modification of the HOMO and LUMO levels of the dye, improved spectral response was achieved, resulting in device efficiency of 8.7% [136]. Introduction of thiophene ligands was observed to alter the energy levels of the dye, red-shifting the absorption spectrum [17]. Therefore, this lead to a 10 nm red shift of the absorption, and a device efficiency of 9.5%, when the modified N719 was implemented [137]. Other metal complexes were also investigated in the efforts to achieve improved near-infrared absorption. By replacing the ruthenium ion with osmium, the IPCE spectrum was extended to 1100 nm, while maintaining good device performance [138].

Porphyrins are also of significant interest in the effort to achieve good absorption in the near-infrared part of the spectrum. They demonstrate strong absorption in the Soret band (400–450 nm) and the Q-band (500–700 nm) [139], indicating that they can operate as panchromatic sensitizers, with efforts made to enhance the Q-band. Porphyrin dyes with a donor-π-acceptor structure, with porphyrin as the donor, and cyanoacrylic acid as the acceptor, can be tuned through various thiophene derivatives which act as the π bridge and can be used to enhance the absorption of the dye [17, 140]. Such a dye was used to achieve record device efficiency of 13% with a single sensitizer, as addition of the proquinoidal benzothiadiazole resulted in broadening of the Soret and Q-band absorption, reaching 800 nm [16]. Phthalocyanines are another type of dye that demonstrate high absorption around 700 nm, and are thus candidates for good absorption in the near-infrared part of the spectrum [17]. Nevertheless, these dyes suffer from poor solubility and aggregation on the ETL surface, necessitating the use of a co-adsorber [17]. A Zn-phthalocyanine dye has demonstrated maximal IPCE in the near-infrared region, but the device efficiency was only 0.57% [141].

Extensive work has also been done on this front on organic dyes, as they also possess a donor-π-acceptor structure, which makes tuning of their absorption spectra easy [17]. Vinylene units were introduced into coumarin sensitizers to extend their absorption spectrum, producing dyes characterized by broad red-shifted absorption, due to a shift of the HOMO level to higher energy, and resulting in device efficiency of 6% [17, 142]. Device performance based on coumarin dyes was enhanced by introduction of thiophene units, as vinylene units proved problematic for dye aggregation, achieving efficiency of up to 8.1% [17, 143]. Furthermore, addition of more cyanate groups to the π bridge of the dye resulted in additional extension of the absorption spectrum [144]. Indoline dyes showed a broader absorption spectrum after incorporation of a rhodamine framework, reaching efficiency of 9.5% after optimization of the dye structure and accompanying ETL [145–147]. One of the highest near-infrared IPCE values for organic dyes of donor-π-acceptor structure was achieved using a tetrahydroquinoline dye, through modification to separate the anchoring and acceptor group, resulting in device efficiency of 3.7% [148]. The broadest IPCE spectrum of organic dye-based DSSCs reached 920 nm and was achieved by incorporation of a phenoxazine dye with a thienyl π bridge and a corhodanine acceptor [149]. Other organic dyes that have been engineered for red-shifted absorption include N,N-dialkylaniline dyes which reached 6.8% efficiency [150, 151], squaraine dyes which show good absorption in the near-infrared region [17, 152], and boradiazaindacene dye, which has a near-infrared absorption spectrum (600–800 nm) and produced a device of 1.7% efficiency [153].

Despite the extensive work that has been done on this aspect of DSSCs, an optimum sensitizer that can cover the entire solar spectrum has not been fabricated yet, although mixing of different sensitizers has been implemented in devices with impressive results [18, 57]. It has been estimated that by extending the absorption spectrum to 920 nm, PCE of 19% can be achieved [154].

2.1.4.2. Leakage in DSSCs

While the most efficient devices yet have been fabricated with liquid electrolytes [16, 57], the use of liquid electrolytes faces issues associated with leakage of the solvent and subsequent instability of the photovoltaic performance of the device, inhibiting commercialization of DSSCs [47]. This encouraged research into alternative materials for hole transport and dye regeneration, which resulted in solid-state DSSCs, but despite demonstrating good stability, they suffer from reduced efficiency due to low conductivity and poor pore filling, and therefore poor electrical contact, of the mesoporous ETL [47]. Work was also done to develop quasi-solid electrolytes, such as polymers [155, 156], and gels [157], but, like solid-state HTMs, they are also plagued by

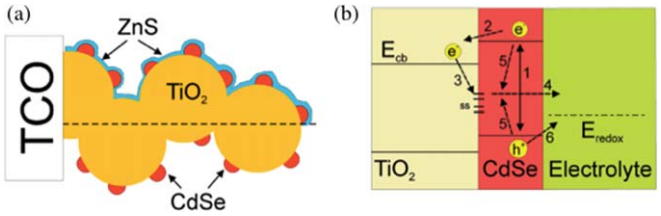

Figure 4. (a) QDs on TiO_2 nanoparticles, (b) operating principle of a QDSSC [165]. Common QD sensitizers include CdS, CdSe, CdTe, PbS. Reprinted with permission from [165]. Copyright (2009) American Chemical Society.

reduced transfer rates of the redox species because of the increased material viscosity and poor contact with the electrodes, meaning that device efficiency of devices incorporating quasi-solid electrolytes remains below (8%–9%) that of DSSCs prepared with liquid electrolytes [47, 158]. This issue has not been resolved yet, but advances are constantly being made towards achieving more stable DSSCs.

2.1.4.3. Photo-bleaching in DSSCs

DSSC stability is not only due to leakage and evaporation of the liquid electrolyte, but also limited by degradation of the electrolyte under long-term irradiation by sunlight, and in particular, ultraviolet (UV) light [51]. The ETL, commonly TiO_2, absorbs UV light to form excitons, and the photogenerated holes might react with any other component that is not the iodide, leading to a depletion of triiodide in the device, which hinders the proper operation of the device [159–161]. The lack of redox couples in the device has further implications on the dye stability. As the dye is not reduced, it could react with other elements in the device, producing new species are cannot be used for generation of charges [159]. This has been observed to lead to a significant drop in short-circuit current. Nevertheless, this effect is initially negligible in a full device until the concentration of redox species is significantly quenched, and only a reduction of open-circuit voltage is observed that is associated with reduction of redox species in the electrolyte [159]. Efforts to improve the stability of the electrolyte under UV irradiation include incorporation of UV filters [51, 162], as well as electrolyte additives which can enhance its stability, such as MgI_2 and CaI_2 [162]. MgI_2 appears to perform best for this purpose, and the mechanism behind the improvement is still unclear, although it could be the formation of a MgO surface layer which prevents the reactions between the ETL and the electrolyte, or the reduction of the holes in the ETL by the iodide [162]. Nevertheless, this is another key issue that needs to be addressed before DSSCs can reach the stability level suitable for commercial devices.

2.2. Quantum dot-sensitized solar cells

QDSSCs operate much like DSSCs. In these devices, the sensitizer layer now consists of quantum dots (QDs) instead of a dye, on a mesoporous semiconductor which serves as the ETL, such as TiO_2 or ZnO [163, 164]. The solar cell is completed by the electrolyte or HTM, and the counter electrode. As outlined in figure 4, when sunlight is incident on the QDSSC, the QDs will absorb light to generate electron–hole pairs. The electrons are then transferred from the conduction band of the QD to the conduction band of the ETL, and the holes are transferred to the electrolyte/HTM, which is typically made of polysulfides. The oxidized electrolyte is then reduced to its original state by electrons re-entering the cell from the external circuit [163, 165]. The open-circuit voltage is determined by the difference between the fermi level of the QD/ETL system and the redox potential of the electrolyte, whereas the produced current is controlled by the sensitizing ability of the QDs and the efficiency of electron separation and extraction [163, 166]. QDSSCs have become an attractive alternative to DSSCs due to ease of fabrication, tunable spectral properties allowing for tandem architectures, improved stability over DSSCs as they can form better junctions with solid state HTMs, and the potential of multiple exciton generation by impact ionization that could increase the theoretical limit in efficiency to 44% [163–165, 167–169]. The current best efficiency recorded for QDSSCs is 11.61% [170], and while significant enhancements have been achieved in the past few years, the record efficiency is still below the record efficiency of DSSCs [165].

2.2.1. Size tunable properties

Implementation of QDs offers a variety of benefits over dyes as sensitizers in a solar cell. Perhaps their biggest benefit is the ability to tune their spectral properties easily by varying the diameter of the QD, due to quantization effects present. By modifying the energy levels of the QDs, light absorption and electron injection can be tailored to match the needs of the solar cell [171, 172], whereas generation of multiple excitons by a single photon and hot electrons offer new possibilities for enhancement of device performance [171, 173].

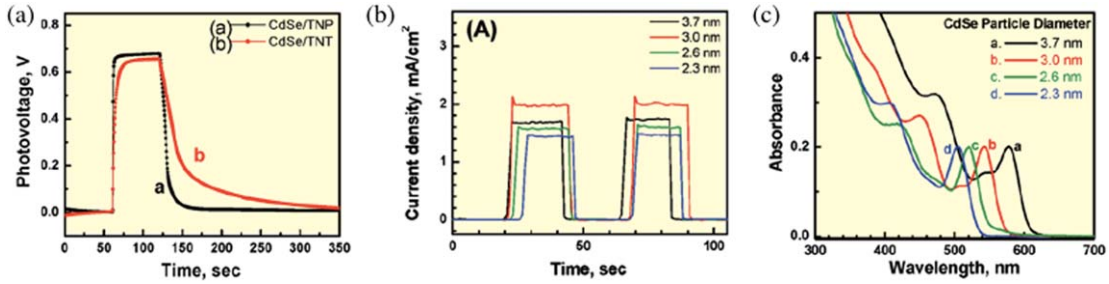

Figure 5. (a) Open-circuit voltage for TiO_2 nanoparticles/3 nm CdSe QDs and TiO_2 nanotubes/3 nm CdSe QDs, (b) photocurrent of TiO_2 nanoparticles/CdSe QDs of various sizes, (c) absorption spectra of CdSe QDs of various sizes. Reprinted with permission from [171]. Copyright (2008) American Chemical Society.

Good QDSSC operation requires that the conduction band of the QD sensitizer be higher than the conduction band of the ETL for efficient electron transfer between the two, as the offset provides the driving force for charge transfer [163, 171]. While the open circuit voltage of the device is independent of the size of the QDs used in the sensitizer, as demonstrated in figure 5(a), the device photocurrent is directly correlated to the properties of the QDs [171]. It has been observed that smaller QDs result in higher photocurrent due to the higher conduction band as shown in figure 5(b), implying that a larger driving force will be available for electron injection to the ETL [171, 174]. However, decreasing QD size is also associated with more limited response in the visible part of the spectrum as shown in figure 5(c) [171].

The emission decay of CdSe/TiO_2 electrodes was used to estimate electron transfer constants through measurement of the recombination rate constants [170, 171]. Exponential decay models were implemented to extract emission lifetimes, and it was observed that for smaller nanoparticles, shorter electron transfer constants are obtained [171]. Furthermore, there was no apparent difference between the QDs on TiO_2 nanoparticles and TiO_2 nanotubes, indicating that the morphology of the ETL does not influence the charge injection process. This further supports the evidence that photocurrent is dominated by QD properties. IPCE was also seen to improve with smaller QDs, establishing that since they possess a more energetic excited state, their electron injection rate is higher. The morphology of the ETL becomes important where open-circuit voltage is concerned. As seen in figure 5(a), the photo-voltage of the solar cell decays more slowly after illumination stops for the TiO_2 nanotube substrate, which is direct indication that the electrons injected in the TiO_2 have a longer lifetime before recombination, hence the tubular structure can be used to minimize losses at grain boundaries [163, 171]. Therefore, both smaller and larger QDs offer different benefits for the solar cell and its operation. Thus, a tandem structure ('rainbow' configuration) has been proposed for QDSSCs, which would leverage benefits from both small and large QDs [163, 171]. A gradient assembly of QDs of various sizes could be used, in which small QDs would absorb light of higher energy, allowing longer wavelengths to be transmitted and eventually be absorbed by larger QDs below them. This would utilize the fast electron injection of small QDs and high absorption of large QDs at the same time [171].

This concept has also encouraged research into alloyed QDs which would combine the beneficial properties of various materials to fabricate QDs that are most suitable for QDSSCs [163, 175]. This has led to the preparation of the champion device with 11.61% certified efficiency, which used 4 nm Zn-Cu-In-Se QDs as sensitizers and combined absorption onset of 1000 nm and fast electron injection rate of $9.1 \times 10^{10}\ s^{-1}$ [170].

2.2.2. Stability improvement

Another major benefit of QD sensitizers is the potentially higher stability of QDs in oxygen and water, in comparison to molecular dyes [176]. While originally the iodide/triiodide couple was implemented in QDSSCs as well, it was observed to be detrimental to QDs which were unstable in this electrolyte [163, 165]. Instead, the sulfide/polysulfide system was implemented as redox couple, with good results [177]. Nevertheless, this has shown issues with low open-circuit voltage due to the high redox potential of the polysulfide electrode, and various techniques to address this issue have been used, including adjusting the concentration of the redox couple, changing the solvent composition, and incorporating additives [178–181]. However, the inability of the polysulfide electrolyte to scavenge holes from QDs efficiently has been a source of device instability, as the QDs oxidize and subsequently degrade [175]. This has encouraged research into alternative electrode materials, which resulted in improved device fill factor and enhanced stability [165, 175, 182]. Such materials include Cu_2S or Au, instead of the typical Pt. Furthermore, QDs with enhanced stability have been engineered to address this

issue. Alloyed QDs are observed to demonstrate increased stability in the polysulfide environment in comparison to QDs prepared with the constituent materials [175, 183].

Like DSSCs, QDSSCs also face instability issues due to leakage of the liquid electrolyte [170]. Research efforts to implement quasi-solid and solid-state electrolytes in QDSSCs, such as ionic liquids, gels, hydrogels, spiro-OMeTAD, and P3HT have met with great success [184–188]. QDSSC with a gel electrolyte combined with $CdSe_xTe_{1-x}$ QDs has demonstrated power efficiency of 9.21% [189], whereas a device with CuS QDs and P3HT has produced PCE of 8.07% [190]. QD-sensitized ETLs appear to form better junctions with solid-state electrolytes as compared to dye-sensitized ETLs, as the thinner layer of sensitizer alleviates the issue of insufficient penetration of the solid-state electrolyte into the sensitizer/ETL structure that is commonly seen in DSSCs [164, 191]. Consequently, more stable solid-state devices are feasible when QDs are used as the light harvesting medium, instead of dyes.

2.2.3. Loading on mesoporous ETLs

Another bottleneck QDSSCs must overcome before the PCE can be enhanced is the poor loading of QDs on the mesoporous or nanostructured ETL. This has been associated with enhanced recombination of photogenerated excitons in QDs at the interface, thereby limiting device efficiency [191, 192]. Different techniques to prepare and deposit QDs on the ETL have been developed, including techniques that QDs are grown *in situ* and *ex situ* [193–195]. The former encompasses techniques such as chemical bath deposition, which is a fast and easy process [163, 193], as well as successive ionic layer adsorption and reaction (SILAR), which allows easy tuning of QD sizes [163, 194]. QDs grown *ex situ* are deposited onto the ETL with the aid of molecular linkers to enable attachment of the QDs to the metal oxide ETL [163, 195]. Other methods include electrodeposition [196], spray pyrolysis deposition [197], and pulsed layer deposition [198].

Work has been done to optimize these techniques and find experimental conditions for optimum loading of QDs on the ETL. In the case of QDs grown *ex situ*, mercaptopropionic acid (MPA) and cysteine have been identified as good molecular linkers for attachment to metal oxides [199, 200]. It was observed that as coverage of the ETL increased, the IPCE was initially enhanced, before reaching some threshold value after which it started decreasing, which was attributed to enhanced recombination of photogenerated charge carriers brought on by aggregation of QDs as the electrons must now transfer across QD/QD interfaces before reaching the metal oxide [200]. However, the amount of QDs that cause the decline in IPCE is dependent on the molecular linker used, indicating that the choice of linker is influencing the electron transfer process [200, 201]. Similar trends have also been observed in samples with QDs deposited by SILAR or CBD [202–205]. These deposition methods also result in the growth of larger QDs as the quantity of QDs increases. Atomic layer deposition (ALD) has been suggested as an alternative method for *in situ* growth of QDs that does not suffer from the same problem [192]. This is another aspect in which smaller QDs appear to be superior. The QDSSC with record PCE was obtained with 4 nm QDs, and the authors have attributed the high efficiency partially to the improved coverage of the TiO_2 ETL due to the small QD size [170]. The small diameter QDs reduce the blocking effect observed otherwise, allowing the QDs to penetrate through the ETL [175, 206, 207].

2.2.4. Quantum yield of charge injection

Another common issue observed in QDSSCs is poor quantum yield of electron and hole injection into the respective adjacent layers. This has been associated with trap state defects in QDs which result in charge recombination [170, 206, 208, 209]. It has been found that deposition of a 2–3 nm thin ZnS layer on the photoanode improved device performance as it passivated surface traps and prevented electron injection to the HTM [165, 204, 210], whereas alloyed QDs could be engineered to minimize the amount of surface traps [170, 211, 212]. The choice of passivating ligands on QD-sensitized metal oxides has enhanced internal quantum efficiency of photon-to-electron conversion to ~100%, matching that of DSSCs [213]. Furthermore, use of small QDs increases the difference between excited state of QD and ETL conduction band, providing a larger driving force for electron injection, and leading to higher IPCE [171]. Deposition on nanostructured TiO_2 (nanotubes) was also observed to enhance electron injection as it reduced recombination losses observed at grain boundaries of TiO_2 nanoparticles [171]. QDSSCs additionally offer the potential of leveraging impact ionization occurring in QDs, which would result in two or more excitons forming with a single photon, as well as hot electron transfer [163, 214, 215]. Work done on this front has resulted in impressive outcomes, with absorbed photon-to-current efficiency of PbS QD-sensitized TiO_2 exceeding 100% [214].

2.3. Colloidal QD solar cells

The first example of a solar cell employing colloidal QDs for both light harvesting and charge transport was made in 2005, using a mixture of PbS QDs and a conjugated polymer poly[2-methoxy-5-(2′-ethylhexyloxy-p-phenylenevinylene)] (MEH-PPV), which served as HTM [215]. However, the efficiency of these devices was limited by poor electron transport and after significant enhancements in the conductivity of QD films, the active

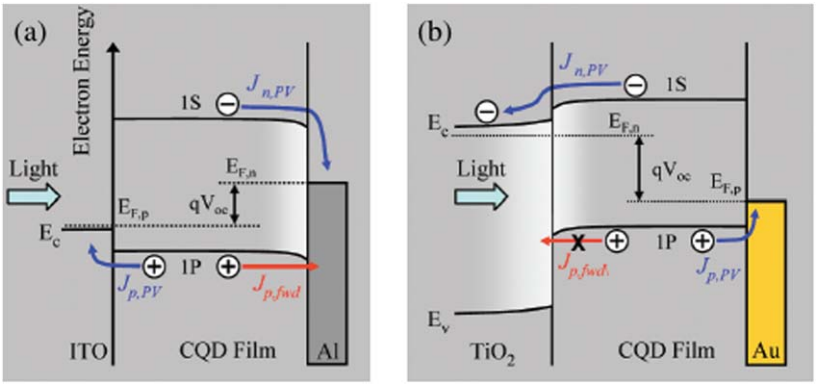

Figure 6. Device operation of: (a) Schottky colloidal QD solar cell, and (b) depleted heterojunction colloidal QD solar cell. Reprinted with permission from [220]. Copyright (2010) American Chemical Society.

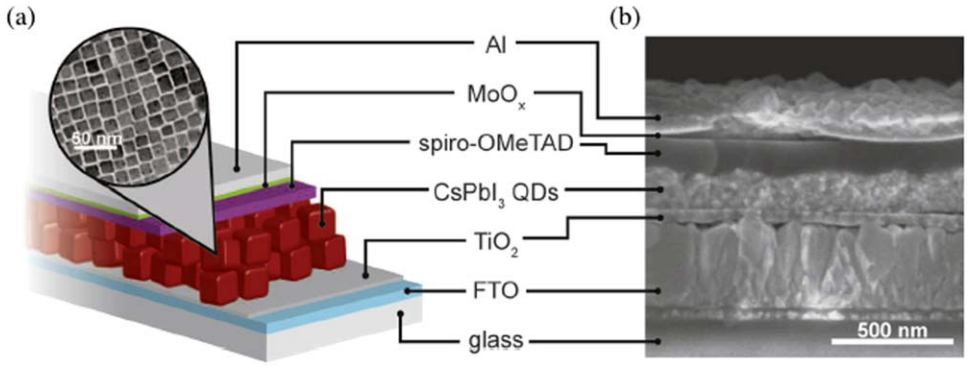

Figure 7. (a) Schematic of the solar cell structure, (b) scanning electron microscopy images of the device. Reprinted/adapted from [221]. © The Authors, some rights reserved; exclusive licensee American Association for the Advancement of Science. Distributed under a Creative Commons Attribution NonCommercial License 4.0. (CC BYNC).

layer was prepared by PbS QDs only, which was found to enhance charge carrier extraction from the active layer [216]. These devices were built as Schottky cells, as the semiconducting active layer (PbS) formed a rectifying junction with a low work function metal and the operating procedure is outlined in figure 6(a) [217]. Metals used for this purpose included aluminum, calcium, magnesium, silver, and gold. The best device efficiency achieved with such an architecture was 5.2% [218]. Nevertheless, the device performance is limited by the Fermi level at the interface which limits the open-circuit voltage, whereas illumination from the non-rectifying side of the device was required, which meant that internal quantum efficiency was low as this was far from the junction [217, 219].

These limitations led to the development of depleted heterojunction colloidal QD solar cells, in which a p-type monolayer of colloidal QDs is deposited on a wide band gap semiconductor, typically n-type, with TiO_2 and ZnO being common choices [217, 220]. The device was completed with deposition of a doped metal oxide HTM and a metal contact, and the device operation is shown in figure 6(b). This device architecture allowed illumination close to the interface, and charge carriers in the colloidal QD monolayer are driven by drift currents. This device structure yielded record device efficiency of 13.43% with use of $CsPbI_3$ QDs in the device structure shown in figures 7(a) and (b) [217, 221]. The performance of these devices is limited by short charge carrier transport lengths in the QD film, as enough thickness is necessary for light absorption, with adverse effects on charge carrier transport.

This limitation encouraged the development of bulk heterojunction colloidal QD solar cells, in which the n-type semiconductor and the colloidal QD film are combined in an interpenetrating layer to ensure that photogenerated excitons are formed close to the interface [217]. Unfortunately, this suffered from increased recombination, reducing the photo-voltage. More work is being done to enhance the performance of colloidal QD solar cells, which ranges from material and ligand modifications, to band engineering and passivation, as will be discussed below.

2.3.1. Pb-based QD solar cells

Pb-based QDs, in particular PbS and PbSe, have been very popular choices as sensitizers in colloidal QD solar cells. PbS QDs were used both in the first case of colloidal QD solar cells, as well as high efficiency colloidal QD solar cells reaching 8.55%, because of their excellent absorption properties, which can be tuned from 800 to

2000 nm [222–224]. Furthermore, PbS QDs demonstrate good air stability, which has been a challenge for colloidal QD solar cells. PbSe QDs have also been implemented in solar cells with impressive results, and both PbS and PbSe have demonstrated multiple exciton generation resulting in internal quantum efficiency that exceeded 100%, proving that QD-based solar cells could reach high efficiencies, beyond that of DSSCs [214, 225]. Hot electron transfer from PbSe QD films to TiO_2 has also been observed, which can be additionally leveraged for high efficiency devices [226].

Since one of the major limitations of colloidal QD solar cells is charge transport within the QD layer, the conduction characteristics of materials such as PbSe, PbS, and CdSe QD films were investigated to elucidate the processes occurring during device operation. It was found that after exciton dissociation, charge carrier transport occurs through phonon-assisted hopping between the energy levels in QDs, contrary to earlier claims of band-like conductivity [227, 228]. PbS and PbSe QD films have been shown to possess good electrical properties, with PbSe QD films reaching mobilities of 7 $cm^2 V^{-1} s^{-1}$ after treatment with passivation and infilling [229], which will be re-visited in the next sections.

2.3.2. Improving drift of carriers

The charge carriers inside the QD film are driven by drift currents generated by the electric field in the device [217]. Since carrier transport is below optimal, improvements are needed to enhance the drift of carriers. Efforts have been focused on band engineering and ligand modification to improve charge transport.

Ligand modification has proven key in controlling the electrical properties of QD films. Use of ethanedithiol (EDT) molecules to assist in film fabrication has demonstrated improvement in carrier mobility, associated with reduced inter-particle spacing [230, 231]. But owing to the vulnerability of organic ligands, inorganic ligands were developed to enhance electronic transport and passivate surface defects [232]. Metal chalcogenide complexes were found to result in electron mobilities of 16 $cm^2 V^{-1} s^{-1}$ in CdSe QDs [233], whereas atomic ligand passivation produced a PbS QD device with efficiency of 6% in the first attempt to fabricate a photovoltaic device with inorganic ligands [232]. In this device, the PbS QDs were capped with oleic acid ligands when synthesized, with thiol treatments removing the oleic acid and passivating the QDs through a Pb–-S bond [232, 234]. The PbS QDs were then treated in $CdCl_2$, tetradecylphosphonic acid (TDPA), and oleylamine (OLA), which improved sized distribution, stability, and reduced defects. Finally, the film was treated with either cetyltrimethylammonium bromide (CTAB), hexadecyltrimethylammonium chloride (HTAC), or tetrabutylammonium iodide (TBAI) to generate halide-passivated PbS QD films.

Apart from ligand modification, band engineering has also been very useful in improving electrical transport in colloidal QD solar cells, involving tuning of the band alignment between the colloidal QD film and the ETL to favor electron injection into the ETL [217]. This has also led to the concept of quantum funnels, essentially the preparation of graded band gap using five QD layers and leveraging the fact that carriers will end up in the layer with the smallest band gap. This has resulted in improved fill factor, open-circuit voltage, and short-circuit current [217, 235, 236]. In addition, graded doping architectures have been used to improve device efficiency [237]. The dopant can be used to tune the conduction band edge and band bending at interfaces, with ligands such as 3-mercaptobutyric acid and EDT used to dope PbS QD films, showing impressive results and leading to record efficiencies [224, 235]. Other efforts have included doping of the metal oxide used as ETL, incorporating impurities in TiO_2 and magnesium doping of ZnO, to achieve optimal band offset [238, 239].

2.3.3. Infilling

Another approach to address the limited mobility and conductivity demonstrated by colloidal QD films is infilling with metal oxides. Deposition of Al_2O_3 and ZnO via ALD to fill the pores of PbSe QD films was observed to reduce the inter-QD tunnel barriers, enhancing carrier mobility [240, 241]. Enhanced conductivity and carrier mobility was also observed after infilling of CdSe QD films with ZnO [242]. ALD appears to be the optimum technique for deposition of the infilling material as it can uniformly coat structures characterized by high aspect ratio, and in work done on infilling a PbSe QD film with amorphous Al_2O_3, high charge mobility was achieved (7 $cm^2 V^{-1} s^{-1}$), due to passivation of the QD surface trap states, as well as strong electronic coupling of the sodium sulfide ligands [229]. Furthermore, infilling of a PbSe QD film with Al_2O_3 or Al_2O_3/ZnO was observed to result in multiple exciton generation in the QDs, which was not observed in the non-filled films, providing additional motivation for infilling [243]. This is a consequence of the enhanced charge mobility in the infilled films which reduces the possibility of Auger recombination of charges.

2.3.4. Surface passivation

Since the presence of defects hinders charge carrier transport through the QD film and enhances the possibility of charge recombination before they reach their respective contacts, surface passivation to eliminate these trap states can be a useful tool in improving device performance [227]. This can be achieved through different techniques, with ligand passivation being a common method. It was observed that PbS QD films that were treated with

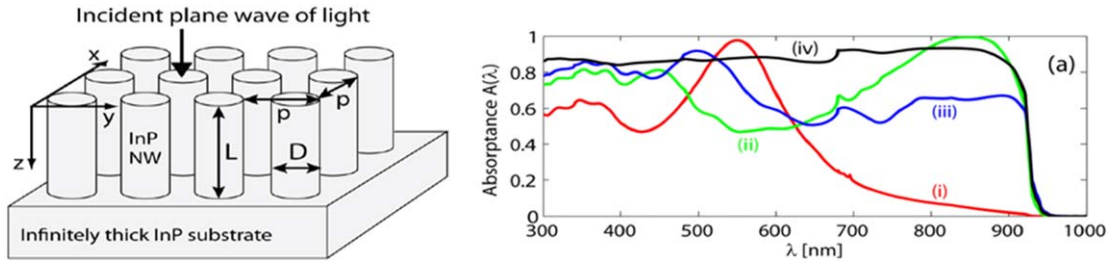

Figure 8. Schematic of the simulation setup used by Anttu *et al* for InP nanowires. The substrate is of infinite thickness and the space between the wire is filled with air (a) Absorbance spectra for nanowires of pitch 680 nm and length 2000 nm and diameter—100 nm (i), 177 nm (ii), 221 nm (iii), and 441 nm (iv). The light is incident normal to the surface. Reproduced with permission from [274], OSA.

3-mercaptopropionic acid (MPA) demonstrated improved device performance as compared to oleic acid or EDT, associated with superior passivation of defects, leading to higher mobility and minority carrier transport [244]. Infilling is also used to yield improved device stability which is achieved through surface passivation, as it prevents oxidation and photothermal degradation of QDs exposed to ambient conditions [229, 240, 243].

Surface passivation is achieved by exposure of PbSe QDs to chlorine gas, as it results in a thin $PbCl_2$ layer which passivates the QDs and prevents oxidation [245]. $PbCl_2$ can also be used as a precursor for PbSe QDs to create a passivating thin $PbCl_2$ layer [246, 247], or alternatively, treatment of PbSe QDs with NH_4Cl can produce a thin $PbCl_2$ layer [248]. In addition, cation exchange techniques have been used to introduce metal cations post-synthesis and enable implementation of techniques used for Cd structures to be used in Pb structures that can ultimately be used to improve carrier transport and reduction of trap states [249, 250] which has been used to passivate PbSe QD films and eventually produce air-stable devices [250].

While many improvements are needed in terms of device stability, conductivity, and performance, colloidal QD solar cells have demonstrated impressive improvements in efficiency since their inception in 2005, reaching efficiencies close to those of DSSCs [221], showing that they are a very promising photovoltaic technology.

2.4. Nanowires

Among nanostructures being actively researched for solar cells, nanowires (NWs) with high aspect ratios and length of 100 nm or more have shown remarkable improvement in PCE compared to their bulk counterparts. Solar cells based on NWs have seen rapid increase in efficiency with PCE values as high as 17% [251, 252], while keeping production costs low. NWs are passive towards impurities present in the bulk, and hence can be fabricated from bulk materials with lower purity, reducing the cost [253]. They help in efficient light management in solar cells through two main methods: (a) by providing spectrally selective improved scattering of light and increased absorption through resonant modes [254–261] and (b) by enhancing charge carrier dynamics through increased efficiency of charge carrier generation and collection [253, 262]. Further, theoretical limit for NW solar cells can reach up to 42% [263], though some have argued that such high performance cannot be attained due to contact and surface recombination [264]. Silicon [258, 265–267] and III–V materials [251, 268–271] are the most commonly studied solar cells possessing NW morphology, although other materials have been studied as well [272]. However, they still have PCE significantly lower than their bulk counterparts and are far from reaching large scale production capabilities. Here, we discuss some key concepts of NW solar cells.

2.4.1. Efficient light management

Scattering of light in NWs is described in terms of wave optics and depends on NW diameter, length, pitch and slant angle [270, 273, 274]. By warrying these parameters it is possible to improve scattering and absorption within a material compared to its bulk counterpart. It is also important to remember that the dependence of these parameters vary with different materials due to differences in their electronic band structure and dielectric properties. Li *et al* used simulations based on full wave finite element method to show that the hexagonally arranged Si nanopillars with pitch and diameter lying close to 600 nm and 500 nm respectively has increased absorption compared to thin films with the same amount of material [275].

Apart from light scattering, the presence of guided leaky resonant modes are also responsible for increased absorption in nanowires [274, 276]. Multiple studies using analytical waveguide theory have shown that the resonance position of these modes are minimally perturbed from a single NW to sparsely spaced III–V NW array [274, 277], while near field coupling between neighboring NWs is significant in Si NWs [278, 279]. Calculation from Anttu *et al* showed that these modes had strong diameter dependence and weak dependence on pitch and length in InP NWs with minimal absorption below 100 nm diameter and maximum at 170 and 410 nm respectively [274]. The increase in absorption at these diameters is due to the strong excitation of HE_{11} (170 nm)

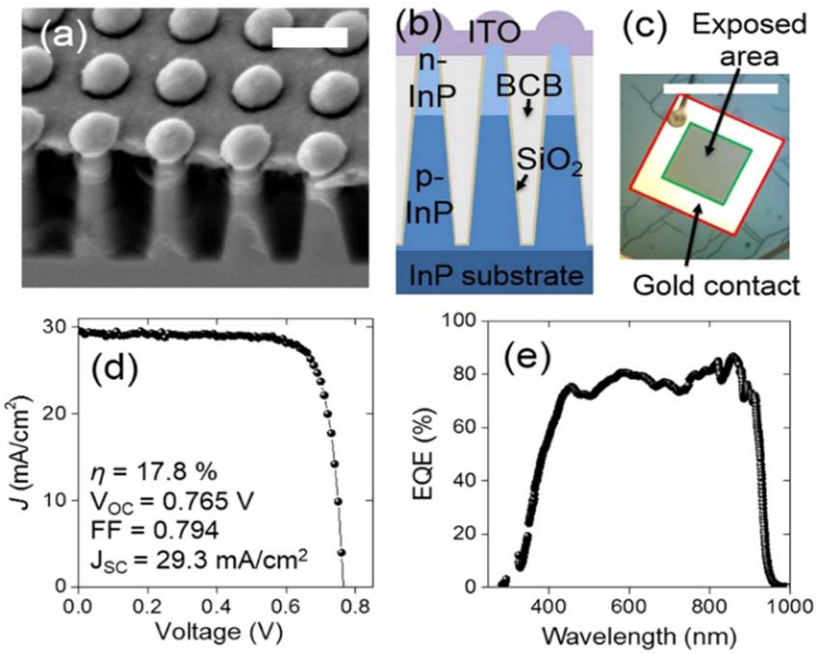

Figure 9. (a) SEM image of the solar cell device. Scale bar 500 nm (b) Schematic representation of the nanowire solar cell device showing different parts of the device (c) Optical microscope image of the solar cell. Scale bar 0.5 mm. The red and the green boxes represent the full device and active area respectively. (d) *J–V* characteristics of the device at 1 Sun (AM 1.5G) showing PCE, V_{oc}, fill factor and J_{sc}. The external quantum efficiency spectra of the device from 2250 to 1000 nm [251]. Reprinted with permission from [251]. Copyright (2016) American Chemical Society.

and HE_{22} (410 nm) modes by incident light followed by strong absorption by the NWs. The design of the simulation along with results of which are shown in figure 8. In addition, Dhindsa *et al* reported that smaller NWs have low absorption at longer wavelengths irrespective of packing density [280], further confirming the dependence of nanowire diameter on performance.

2.4.2. Charge carrier dynamics

Another important property of NWs is the ability to separate charge carriers near the p–n junction. NWs have significant advantages over bulk materials as the charge carries have to transverse much smaller distances compared to their diffusion lengths, minimizing losses due to scattering and radiative recombination [281, 282]. Some of the important parameters that determine electrical properties of NW solar cells are doping concentration, geometry and surface passivation. In III–V NWs, crystal structure also seem to play an important role in charge separation [264]. Since III–V's can exist in zinc blend and wurzite crystal structure or predominantly as a mixture of the two, such two phase systems can act as scatterers and trap states for radiative recombination [283, 284].

Incorporation of dopants during the growth step on nanowires to create p and n type semiconductor is another important parameter determining the electrical properties of nanowires [285]. In vapor–liquid–solid (VLS), which is the most common growth method for Si NWs, the dopants are introduced as vapor precursors [285]. While the effective incorporation of dopants during growth is still being investigated, the present understanding is that the dopants enter via the seed particle-nanowire interface [285]. In 2009, Nduwimana *et al* used first principle density functional theory to show charge carrier densities in p and n type doped Si nanowires [286]. Further, Murthy *et al* used time resolved measurements to show efficient charge carrier separation in Si NWs by having a radial doping gradient [287]. Similar ultrafast charge carrier dynamics studies were also done on GaAs [288] and InP [288, 289] NWs to understand the effect of doping. Some of the recent research on the properties of NWs include charge separation in VLS grown axial nanowires [290], effect of Nb doping and oxygen vacancy centers in TiO_2 [291] and ZnO [291–294] respectively.

2.4.3. Device measurements

Due to limitations in fabrication, even with extensive theoretical and experimental study on nanowire optical enhancements and electric properties, it was tough to achieve similar results with device performance [295]. But towards the second half of the last decade, multiple experimental groups have made progress in fabricating structures with results in agreement with theoretical predictions. An image of a working device along with its *J–V* characteristics are shown in figure 9.

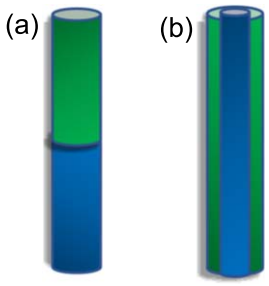

Figure 10. Schematic representation of axial (a) and radial (b) p–n junction geometries in nanowire solar cells.

Some of the nanowire fabricating techniques will be discussed in brief in the following section, prior to which we need to look the two designs in which we can fabricate a nanowire p–n junction. p–n junction nanowires can be fabricated in both radial and axial direction as shown in figure 10.

In 2012, it was shown experimentally that radial designs are much less prone to surface defect compared to axial designs though both are capable of maintaining a V_{oc} greater than 0.7 V [296]. It was further confirmed that axial designing of GaAs exhibits large leakage current under backward bias [297]. A radial p–n junction is also ideal for orthogonalization of light absorption and charge carrier collection [281]. However, fabricating a radial NW heterostructure requires precise lattice matching steps and brings up the production costs, while axial designs are passive to any such lattice mismatch strains. Some of the earlier work on coaxial nanowires in 2007 achieved a quantum efficiency of 12% at 690 nm incident light [265] and a PCE of 3.4% in a coaxial p–i–n coaxial silicon solar cell [258]. However, one of the first radial p–n junction solar cells reported a PCE of 12.2% [298] followed by a current density of 40 mA cm^{-2} in radial Si p–i–n nanowire solar cell [299]. More recently, a hybrid solar cell of Si nanowires and PEDOT:PSS showed a PCE of 13.2% [300]. Apart from Si, there have been various experimental realizations of III–V nanowire solar cells. In 2013, radial GaAs nanopillar solar cells with 70% quantum efficiencies and 63% fill factors were reported [301]. Even though axial design has a disadvantage over radial design, some of the highest recorded efficiencies have been reported for axial nanowires. Axial GaAs nanowire solar cells in 2015 demonstrated a record efficiency of 15.3% [269] in well over the previous highest value of 13.8% in InP nanowire solar cells [302]. This value was exceeded in coaxial InP NWs with the help of self-aligned nanoparticles which helped in improved absorption, with a reported a PCE value of 17.8% [251]. Similar high performance solar cells have also been reported for CdS [303–305], ZnO [306, 307], Cu_2O [306] and more recently, for perovskite nanowires [271]. Research has also begun into tapered NW structures like nanocones [308] and dual-diameter tandem NW solar cells [309]. Such structures help reduce reflectance while maximizing effective absorption.

2.4.4. Fabrication techniques

For the realization of efficient light management and enhanced PCE in nanowire solar cells, it is of paramount importance to develop low cost, precise and reproducible fabrication routes. In the section we will look at different growth methods employed for nanowires (mostly Si and III–V's). Since several detailed reviews on nanowire growths are available [310–313], the discussion is intended as a brief overview with some recent advances made.

VLS method is a growth mechanism in 1D materials known for than more than 50 years [314] and is the most common technique used for the growth of Si and other semiconductor nanowires. They are cheap and can grow single crystal nanowires with high crystallinity [281, 282]. The process involves passing a vapor of the precursors on a substrate with a solid seed nanoparticle, generally gold, at very high temperatures (500 °C–1000 °C) [315, 316] in the presence of a liquid catalyst. The liquid catalyst is formed during the initial phase, when the precursors dissociate to form a metal-nanoparticle droplet, that on further addition of dissociated precursor, leads to nucleation sites at its surface. SiH_4, disilane, SiH_2 and $SiCl_4$ are the most commonly used source gasses for Si [317]. In 2009, growth of GaAs nanowires was demonstrated via VLS in a gas source molecular beam epitaxial system [295]. Another advantage of VLS is the ease of growing p–n heterostructures by passing different doping gases along with the source gases. One of the earlier uses of VLS growth mechanism was to grow Si nanowires using chemical vapor deposition (CVD) technique [316]. They further demonstrated patterned growth of nanowires using Au colloidal seed particles. CVD [315, 316] and molecular beam epitaxy techniques [318, 319] are two of the common fabrication routes that uses VLS mechanism for aligned single crystalline growth of nanowires. The 17.8% efficiency reported in nanowires were grown using VLS [251]. However, it must be noted that multiple other factors like plasmonic enhancement played an important role in the high efficiency reported.

Metal organic chemical vapor epitaxy (*MOVPE*) is predominantly used for III–V nanowire growth as initial results of GaAs nanowire solar cell grown using VLS showed very low efficiencies, less than 1% [295]. Though

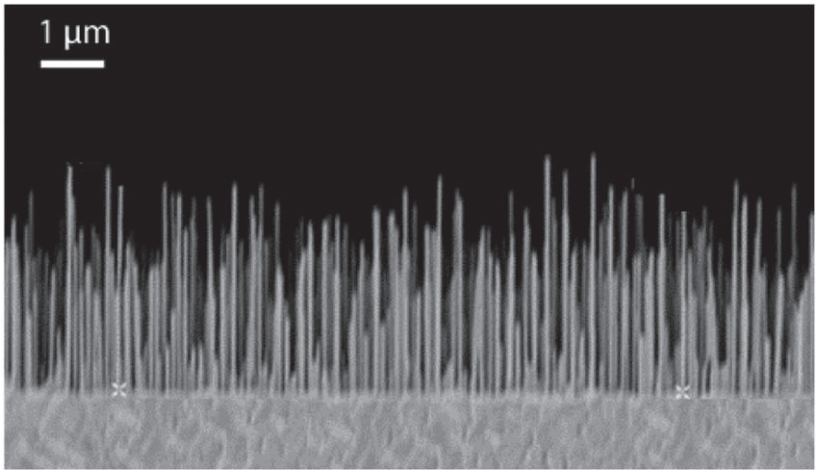

Figure 11. SEM image of MOVPE grown lnAs nanowires. Reprinted with permission from [323]. Copyright (2013) American Chemical Society.

multiple reports on InP nanowire growth using MOVPE existed [320–323], the first InP nanowire solar cell, based on the method was reported in 2009, and showed an impressive PCE of 3.37% [324]. In the case of GaAs, it was not until 2012, that an impressive PCE of 2.54% was reported in densely packed uniform GaAs nanowires [301]. Further, the same group improved on the efficiency to 6.63% in 2013 [325] by making use of surface passivation techniques. Since then, multiple reports showing high efficiencies in GaAs [252, 268] InP [251, 302] have been reported. The MOCVE technique involves a combination of electron beam lithography and vapor epitaxy to grow nanowires of uniform thickness and shape [301]. The first step involves deposition of lithographically patterned SiO_2 mask with an array of holes onto a p-type substrate of the nanowire material. This is followed by chemical vapor epitaxial growth of the nanowire though the etched out holes, followed by growing the n-type shell on the p-type nanowires, by varying the growth conditions. The process involves elevated temperatures in the range of 600 °C–800 °C. Figure 11 shows InAs nanowires gown using MOVPE.

Most of the growth techniques mentioned above are based on bottom-up methods. Many top down synthesis routes also exist for the fabrication of nanowires, although, challenges exist due to the need for high precision and throughput production. In 2005 a growth technique was developed for single Si nanowire using aqueous electroless etching method, involving etching a Si wafer using HF acid followed by deposition of a-Si using disilane gas at 450 °C [326, 327]. This synthesis technique was made use of to test a Si nanowire solar cell which reported a low efficiency of 0.5% [328]. The most common type of wet etching—metal assisted chemical (MAC) etching involves a noble metal nanoparticle covering the Si wafer followed by reaction with an etchant [329–331]. The etchant facilitates oxidation of the Si wafer beneath the metal and as the process progresses, the Si beneath the metal nanoparticle is etched away forming Si nanowires [282]. This method is cheap, and can be used for mass production of isotropic nanowires. The etching technique was further improved upon with the addition of template assisted MAC etching [327, 332] as shown in figure 12. This technique offers better control over density, shape and length of the nanowires. MAC technique is still popular for the growth of nanowires and results have shown comparable solar cell efficiencies [333, 334]. Apart from wet etching, a number of dry etching techniques such as laser ablation [335], reactive iron etching [336], plasma etching [337] and chemical assisted ion beam etching [338] also exist for nanowire growth.

The above discussed methods are the common techniques for growth of nanowires, but there have also been reports of various improvements on existing techniques to show high efficiencies. MOCVD was used to report a PCE of 8.8% in graphene/single nanowire Schottky junction solar cell [339, 340]. Nanowire solar cells with efficient light management has the capability to outperform their bulk counterparts both in efficiency and cost. Due to fabrications limitations, material quality and poor design they are yet to achieve efficiencies close to their theoretical predictions. But the last few years have seen substantial improvement in nanowire solar cells and shows great promise to improve further in the next few years.

3. Photon management

In the previous section we discussed how different types of active materials can help to enhance efficiencies in solar cell technologies. Improvements of even a few percentages are considered respectful when it comes to photovoltaics. Hence, scientists over the past few decades have started to look beyond materials improvements

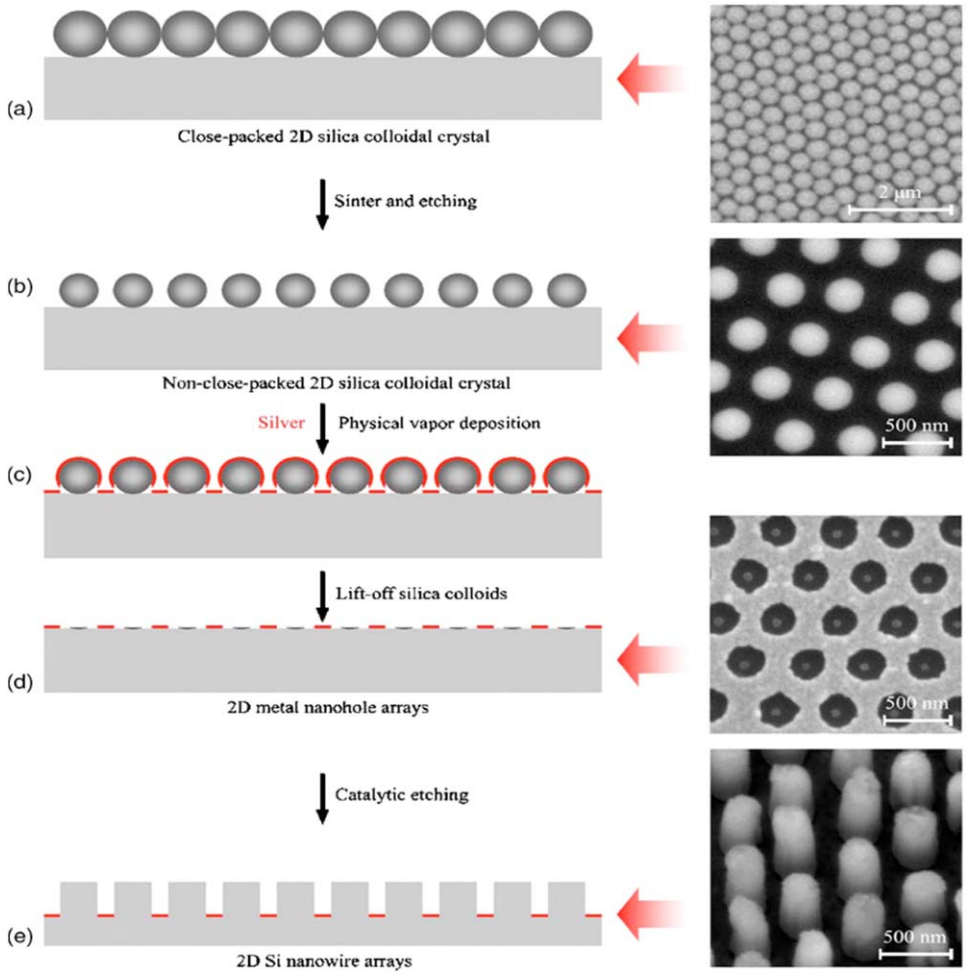

Figure 12. Schematic and corresponding SEM images of ordered nanowires arrays formed through metal assisted chemical etching. (a) A mono layer of silica colloidal crystal is deposited on the silicon substrate. (b) Silica crystal template is then sintered at 1273 K for 80 min followed by etching using 50:1 HF to form 2D array of non-close packed silica colloidal crystal. (c) Silver is deposited on the silica through conventional vacuum vapor deposition. (d) silver coated silica is then lifted through ultra-sonication for 2–3 min to form a 2D metal arrays of silver. (e) The ordered array of SI nanowires is formed from etching using HF. The corresponding SEM mage of each step is shown on the right side of the figure. Reprinted from [332], with the permission of AIP Publishing.

and focused a substantial effort on improvements through incorporation of plasmonic nanostructures [341–343], and up- and down-conversion materials with the PV medium. Enhancement in solar cell performance can occur either through improved light management such as absorption due to localized electric fields, or by efficient use of the solar spectrum via hot electron injection and up/down conversion (UC/DC). In this section, we will briefly review the role of plasmonics and UC/DC materials in photovoltaic enhancement.

Plasmons are quasiparticle excitations of electrons in metals due to interaction with electromagnetic waves. Such excitations are not observed within the bulk of the material where the plasmon and photon dispersion curve do not intersect, however propagating plasmons are possible near the surface of the metal and are aptly called surface plasmon resonances. Metal nanoparticles having a size much smaller than the wavelength of visible light, allowing electric fields to propagate within the volume and resulting in plasmon excitations that are localized on the nanoparticle, producing waves of collective electron oscillations called Localized surface plasmon resonances (LSPR). LSPR have finite lifetimes and decay either radiatively or non-radiatively. The radiative decay leads to near and far filed scattering effects, while non-radiative decay leads to hot carrier generation and plasmon resonance energy transfer (PRET). A number of reviews detailing theoretical and experimental reviews on plasmon resonance on metal nanoparticles such as Au and Ag are available [344–348], hence in this section we will not be dwelling on the details of LSPR theory, but rather focus on its use in enhancing PV performance.

Though surface plasmons have been studied since the 1950s [349], it was only towards the end of the 20th century that it got a major boost in materials science due to improved fabrication techniques. In 2000, the term 'plasmonics' was coined, predicting a new class of devices based on surface plasmons [350]. Around 2004, multiple groups in parallel demonstrated charge transfer from metal nanoparticles to semiconductors using

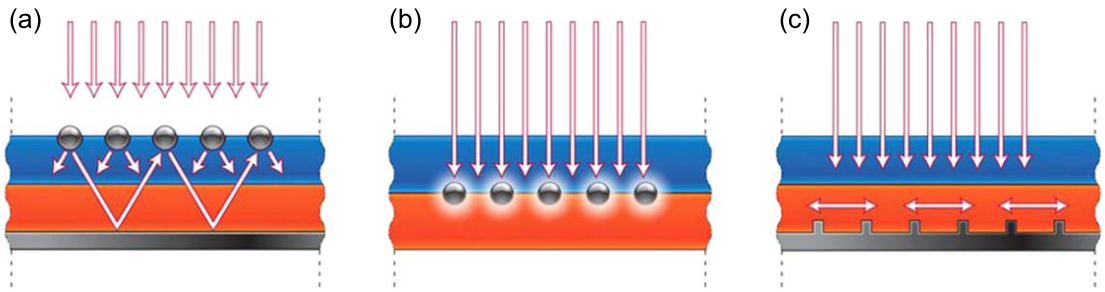

Figure 13. Schematic representation of different designs of plasmonic solar cells. (a) nanoparticle on the front of the solar cell using far field scattering to enhance absorption (b) PNs are incorporated into the active material for near field scattering effects and non-radiative plasmonic processes like HEI and PRET. For PRET, the PNs will have a dielectric coating to prevent interfacial recombination. (c) Patterned back metal contacts for propagating surface plasmons at the metal semiconductor interface for efficient light absorption. [341] (2010) Copyright © 2010, Springer Nature. With permission of Springer.

LSPR [351–353]. This led to a major boom in the field of plasmonics with extensive research being carried out on the use of this aspect in photo catalysis [354–356], drug delivery [357, 358], nanoscale wave guides [358, 359], circuits [360–362], optical emitters and antennas [363–365]. Almost immediately, plasmonic nanostructures (PNs) were tested for improving existing high efficiency photovoltaic technologies including silicon [366–370], DSSC [369–373], GaAs [374, 375], and recently, even perovskite solar cells [376, 377].

3.1. Plasmonic nanoparticles based solar cells

There has been a steady increase in published work on PN-based solar cells since 2006 [378]. Improvements in performance of DSSC, Si and perovskite solar cells on incorporation of PNs have been reported. Au and Ag are the most commonly used nanostructures in plasmonic solar cells, as their plasmon resonance wavelength lies within the solar spectrum. Their high stability and relative ease in synthesizing anisotropic structures also aid in incorporating them into different sensitizer materials. Materials like Ti [379], Al [380], and Cu [381, 382] have also been tested with reasonable success. In photovoltaics, PNs are mainly used in different configurations alongside the active material of a solar cell as shown in figure 13 [341]. They improve the performance of the solar cell through (a) enhanced absorption due to multiple scattering mechanisms (b) enhancement charge carrier separation from localized high electric fields (c) Plasmon assisted hot electron injection and (d) PRET between the active material using plasmonic nanostructures. The schematics of these mechanisms can be seen in figure 14 [342]. We will discuss these mechanisms in detail in the following subsections.

3.1.1. Enhanced scattering in plasmonic solar cells

3.1.1.1. Far field scattering

For enhanced far-field scattering, the metal nanoparticle is generally placed in the front side of the device, at the interface between air/dielectric and the active material. Mertz *et al* had shown that although light scattering is symmetrical in a uniform medium, when placed at an interface, there is preferential scattering towards the material with higher permittivity [383]. This in turn increases the optical path length of solar radiation due to angular dispersion and total internal reflection resulting in enhanced absorption. Additionally, the scattered light can encounter nearby nanostructures, additionally increasing the percentage of trapped light. It is also important to note that the scattering cross section of the nanoparticle can be much bigger than its physical cross section, thus reducing the amount of nanoparticle required [341].

Shape, size and dielectric medium are key factors that lets you tune scattering cross section and LSPR frequency of the metal nanoparticle [373, 384–386]. Since scattering cross section scale as the square of the volume, and ohmic losses is proportion to the volume, larger Ag and Au nanoparticles are preferred for large field scattering. The most common morphology utilized for achieving far field scattering in solar cells is by distributing the nanoparticle on top of the thin film. In 2006, 100 nm Au nanoparticles were used on top of amorphous Silicon solar cells, and an 8.1% increase in short circuit current was observed [387]. A similar increase in short circuit current was observed in GaAs solar using 110 nm Ag nanoparticles [369]. Catchpole and Polman numerically calculated the amount of light scattered for different nanoparticles and reported higher scattering for a cylinder or a hemisphere over spherical particles [388]. They further saw that the scattering cross section can be tuned effectively by adding a spacer above the substrate. A 45% enhancement in short circuit current was achieved by using metallic arrays on top of thin films [389]. Fabricating a plasmonic layer in front of

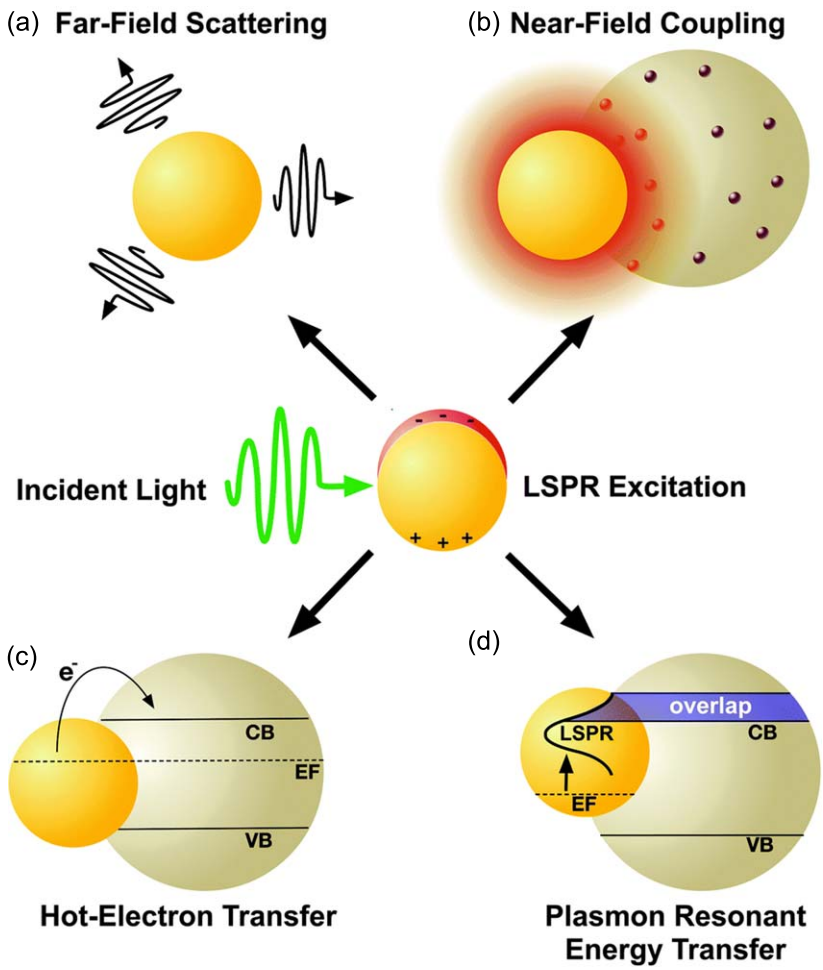

Figure 14. Schematic representation of different plasmon enhancement mechanisms used in solar cells. (a) and (b) are near and far field scattering respectively. (c) and (d) represent non-radiative coupling using hot electron transfer and PRET. Reproduced from [342]. CC BY 3.0.

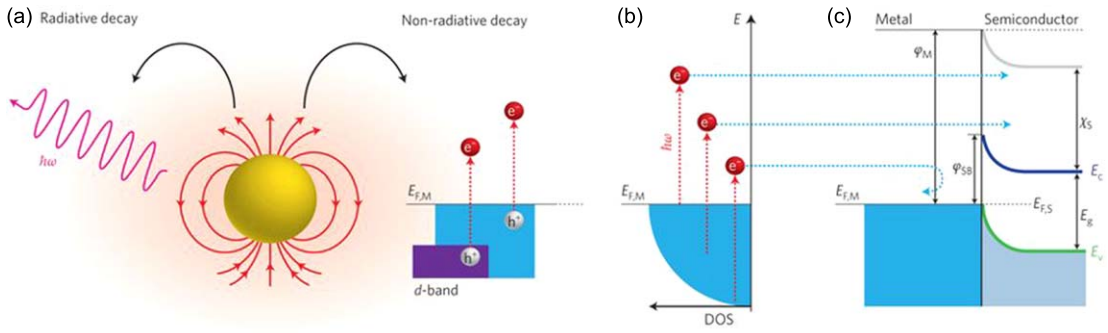

Figure 15. Schematic representation of hot electron transfer mechanism. (a) Excited plasmons decaying via radiative emission of photons or non-radiatively by exiting hot electrons in the metal. Localized surface plasmons can decay radiatively via re-emitted photons or non-radiatively via excitation of hot electrons in the conduction band. (b)Hot electron having energy above the Fermi level (c) Hot electrons can be transferred to the semiconductor if the electrons have energy greater than the Schottky barrier of the metal-semiconductor junction. φ_M is the work function of the metal and χ_S is the electron affinity of the semiconductor. [343] (2014) Copyright © 2014, Springer Nature. With permission of Springer.

the device for far field scattering is relatively straightforward, as a result encouraging such a design for plasmonic solar cells. However, the improvements observed are relatively below par. Consequently, for plasmonic solar cells to demonstrate significant improvement, multiple plasmonic enhancement mechanisms must occur in parallel.

3.1.1.2. Localized field scattering

Absorption is also enhanced within the local vicinity of the plasmonic nanoparticle due to near field enhancement of electric fields resulting from localized surface plasmons. In such plasmonic solar cell designs, metal nanoparticles are embedded into the active material as shown in figure 14(b). At resonance, the electric field around the nanoparticle can be orders of magnitude higher than the incident electromagnetic spectrum, thereby creating a small region of concentrated photon flux than can be absorbed by the semiconductor, creating an additional fraction of electron hole pairs [341, 342, 390, 391]. These effects become prominent near the LSPR frequency, which can be tuned by adding a dielectric spacer between the nanoparticle and the active material. For example, in 2009 an increased absorption in Si solar cells was observed with the use of Ag nanoparticles whose resonance could be tuned up to 200 nm with the use of dielectrics SiO_2, TiO_2 and Si_3N_4 [392]. Further, FDTD simulations have showed that structures with sharp edges enhance electric fields much more than smooth surfaces [393–396], hence anisotropic structures such as rods [397], cones [398], bowties [390], etc have been tested extensively for enhanced near field effects.

Several groups have reported enhancement in PV performance based on incorporation of plasmonic nanoparticles into the active material of the device. It must be noted that these enhancements also have significant contributions from non-radiative effects. In 2008, electrodeposited Ag nanoparticles were used which resulted in an improvement in PCE of organic solar cells [399]. A similar improvement in polymer heterojunction solar cells was observed using Au nanoparticles [400]. Both these results primarily originated from the concentration of electric fields near the nanoparticles. Multiple reports of enhancements in DSSC by integrating metal nanoparticles with the mesoporous TiO_2 layer have been reported [401–405] as well. A systematic study of the effect of size of Au nanoparticle on DSSC performance found a maximum efficiency using 36 nm Au [406]. Similar enhancements were reported for perovskite solar cells in which a core shell Au nanoparticle was incorporated with the perovskite thin film [407]. They argued that a reduction in exciton binding energy as a result of coupling with the LSPR was responsible for the improved efficiency. Another technique to improve absorption is using the back metal surface that facilitates the propagation of surface plasmons at the metal-semiconductor interface. Since these do not closely lie within the scope of this article, we will not be discussing it in detail.

3.1.2. Non-radiative effects

3.1.2.1. Hot electron injection (HEI)

In addition to enhancement through efficient absorption, recent investigations proved that it is possible for plasmonic nanostructures to transfer hot electrons from the metal directly into the conduction band of the semiconductor [164]. Hot electrons refer to electrons that have gained kinetic energy from an external electric field and are no longer in thermal equilibrium with the atom, hence are described by Fermi statistics with an elevated temperature. Schematic and band diagram of hot electron transfer is shown in figure 15 [343]. Many existing PV technologies such as DSSC, quantum dot solar cells and quantum dot-sensitized solar cells have previously utilized HEI to further improve their power conversion efficiencies [164, 408, 409]. Around 2004–2005, several groups reported on the ability of plasmonic nanostructures to generate 'hot electrons' under illumination, and these led to major progress in photo-catalysis and photovoltaics [346–348]. Hot electrons in metal nanoparticles are generated as a result of non-radiative decay of localized surface plasmons. LSPR excitation decay occurs on a time scale of femtoseconds with the emission of radiation or non-radiatively by transferring the energy to hot electrons, which can undergo photoemission, if its energy exceeds the work function of the material. A fraction of the energy is also lost as heat, but as mentioned above, ohmic losses are lower in Au and Ag. Probabilistically, majority of excited electrons originate from intraband excitations within the conduction band compared to interband excitations, as the *d* band energy levels lie 2.4 and 4 eV below Fermi level in Au and Ag, respectively [343].

The excited hot electrons can thus escape the nanoparticle and can be injected into the conduction band of the semiconductor by forming a Schottky junction. Note that this mechanism becomes efficient only if the energy needed for such injection is lower than the band gap of the active material. Even with a perfectly absorbing plasmonic nanostructure, the PCE enhancement through HEI is limited to $<8\%$ [411]. However, modifying the electronic density of states of the donor and acceptor could help improve upon this value.

One of the first comprehensive studies of HEI came from observation of photo-induced electron transfer between Au and thin film and nonporous TiO_2 [346]. Shortly afterward, multiple results observing electron diffusion between metal nanoparticles and TiO_2 were published [412–415]. Some of the recent results of HEI in PV include using HEI in sandwiched TiO_x–Au–$TiO_x$to improve efficiency in perovskite solar cells [416], improving NIR absorption in Si solar cells using Ag nano arrays [417], independent plasmonic solar cell with 0.2% PCE [418] and solid state ITO|Au-NPs|TiO_2 solar cell with 5.84% photon to electron conversion rate at

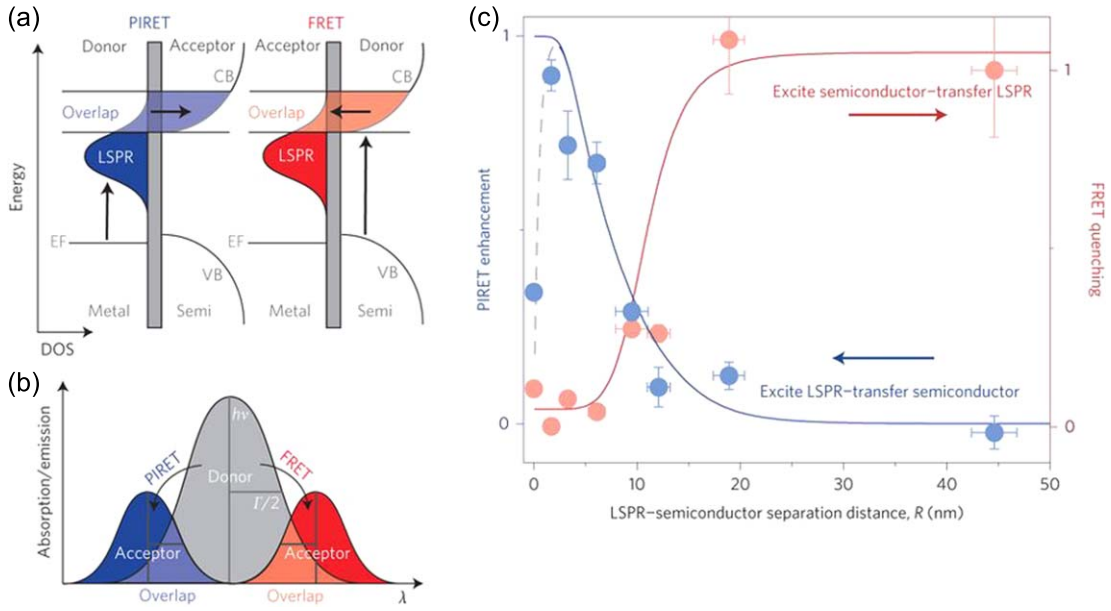

Figure 16. (a) Band diagram comparing FRET and PRET mechanisms along with the direction of energy transfer in both (b) spectral overlap between donor and acceptor in FRET and PRET. (c) Distance dependent dipole–dipole interaction in FRET and PRET. 1 in FRET means no energy transfer from semiconductor to metal and 0 means the semiconductor is fully quenched. 1 in PRET refers to full energy transfer between the plasmon and the semiconductor while 0 means no energy is transferred. [410] (2015) Copyright © 2015, Springer Nature. With permission of Springer.

700 nm incidence [419]. HEI using plasmonics have shown the ability to increase population of electron hole pairs in solar cells, but their performance have been limited by the fraction of the hot carriers having energy to cross the Schottky barrier and various hot electron relaxation pathways [420].

3.1.2.2. Plasmon resonance energy transfer

PRET or plasmon induced energy transfer, is the non-radiative energy transfer between a plasmonic nanoparticle and a semiconducting material via dipole–dipole coupling. Upon illumination of resonant light, the excited plasmon decays by transferring energy to the semiconducting material, thus creating extra electron hole pairs near its conduction band edge [410]. The metal and the semiconductor is separated by an insulating layer such as SiO_2 to prevent interfacial recombination or losses due to hot electron transfer. The large dipole moment in plasmons arise from coherent oscillation of the conducting electrons. An efficient PRET system can improve the performance of solar cells by utilizing light below the band gap. A major drawback of PRET is that it competes with Forster resonance energy transfer (FRET), i.e. an efficient FRET system implies an inefficient PRET system. The two competing energy transfer mechanisms are shown in figure 16 [410]. The efficiency of either system is determined by the dephasing time of the plasmons, versus that of excitons, in the semiconductor. When the excitons have a lower dephasing time, energy is transferred to the semiconductor from the plasmonic particle (PRET), while the reverse energy transfer (FRET) is favored when the plasmon has a low dephasing time. It was experimentally demonstrated in the same study that in $Au@SiO_2@Cu_2O$, a separation of greater than 10 nm between the Au and Cu_2O results in no PRET [410].

Most studies on PRET are fairly recent, and have been focused on understanding plasmon dephasing times using optical spectroscopic techniques such as interferometric frequency resolved optical gating [421]. Over the last 3 years, PRET has found application in sensing, photo catalysis and photovoltaics [351, 422–424]. High photocurrent density was reported in $Ag@Ag_2S$ sensitized thin film solar cells, attributed to both PRET and HEI mechanisms [425]. It is quite possible that while PRET has been delved into only recently, earlier enhancements reported had contributions from PRET, particularly in the near field scattering designs. Over the last decade, rapid development in plasmonics have shown promising results in photovoltaics. Though, initially plasmonic nanostructures made their foray into solar cells for their improved scattering capability, recent findings have presented their ability to non-radiatively couple to semiconducting materials, presenting a case for additional enhancements. Nevertheless, further improvements in plasmonic solar cells demands parallel designing of novel nanostructures as well as their integration of them into the solar cells.

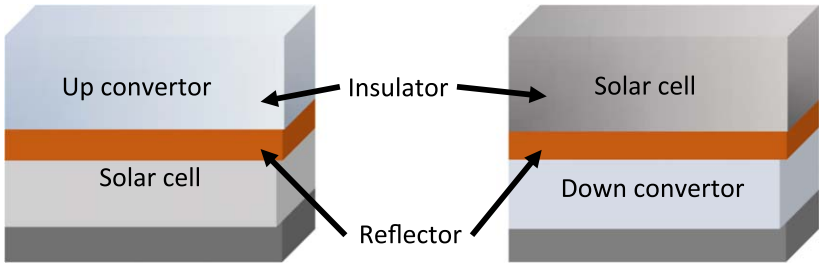

Figure 17. Schematic representation of the solar cell with up and down conversion layers added on them.

3.2. UC and DC materials

In order to exceed the Shockley–Queisser limit for single junction solar cells, two other possible methods commonly employed are UC and DC processes. This is achieved by reducing losses due to transparency and lattice thermalization, two major loss mechanisms in single junction solar cells. Transparency is where any photon of lower energy than the band gap is not absorbed by the material, whereas lattice thermalization is when a photon of higher energy than the band gap is absorbed to create and electron–hole pair with the excess energy is released as lattice vibrations to the material. Both UC and DC are non-linear optical process that convert two photons to a single photon and a single photon to two photons respectively.

The multiple forms of energy losses in a single junction PV include '(1) Non absorption of light with energy lower than the band gap (2) Energy loss due to lattice thermalization (3) Junction loss (4) Contact loss and (5) loss due to recombination' [426]. Other major mechanisms leading to losses in solar cells are radiative losses from recombination of electrons and holes and from voltage drop across junctions and contacts [427–429]. One of the major advantages of the UC and DC methods of improving PV efficiency is that it can be implemented to existing single junction PV, without adding any additional fabrication techniques to avoid current mismatch losses as in the case of tandem device [430, 431]. These UC and DC layers are optically passive, while current collection architecture remains the same as in a single junction PV device. In the case of UP the layer is added to the rear end of the device to convert two low energy photons to a higher energy such that the emitted photon has an energy greater than the band gap of the material [432, 433], while in DC, the optical layer is at the front of the device as they convert a higher energy photon to lower energy. The effectiveness of UC and DC depends on the band gap of the material used in the solar cell. For example, crystalline silicon (c-Si) has a short band gap of 1.12 eV and can utilize a large portion of the long wavelength region of the solar spectrum, while hydrogenated amorphous silicon (a-Si:H) has a larger band gap of 1.7 eV and makes use of the shorter wavelength in the spectrum, while being transparent to most near infra-red light [427]. It is easy to see that UC will be more beneficial for a-Si:H compared to c-Si. The schematic of an upconverter and a downconverter solar cell is shown in figure 17.

3.2.1. Up conversion materials

UC is an anti-Stokes process, can be done at low power, does not require highly coherent light and can be achieved even using Xenon or Halogen lamps [434–436]. The underlying principle of up conversion can be understood from figure 18. Energy is absorbed from the ground state and electrons are carried to their first exited state. The first exited state is a metastable state and require a relatively long lifetime for the UC process to work. Consequently, another photon is absorbed and now the highly populated metastable state is exited to the higher energy state, followed by radiative recombination to the lowest energy state [429, 437]. During the whole process two photons of lower energy were absorbed and a photon of higher energy was emitted.

The most common materials used for up conversion processes are lanthanide nanoparticle based luminescence [427–430] and triplet triple annihilation based on organic molecules [427, 439]. In this article, we will focus on the lanthanide nanomaterials for up conversion. Although the basic energy scheme remains the same, there are multiple ways to achieve up conversions and the most effective way is to use an energy transfer up converison, in which a host material is responsible for transferring energy to the activator nanophore. The first energy transfer excites the activator to the metastable state, this can either be followed by another energy transfer or the activator absorbs the next photon to reach the excited state [440, 441]. Similarly, there are other pathways to achieve such energy transfers [442, 443]. The advantage of using energy transfer up conversion is that we do not require a high concentration of activator ions [440].

The host is generally an inorganic molecule with minimum non-radiative losses. Researchers have studied various host matrices including fluorides [444–446], other halides [447], oxides [448, 449], and phosphates [450, 451] etc. For lanthanide nanoparticles, $NaYbF_4$ is the most common used host. However, using Gd_2O_2S

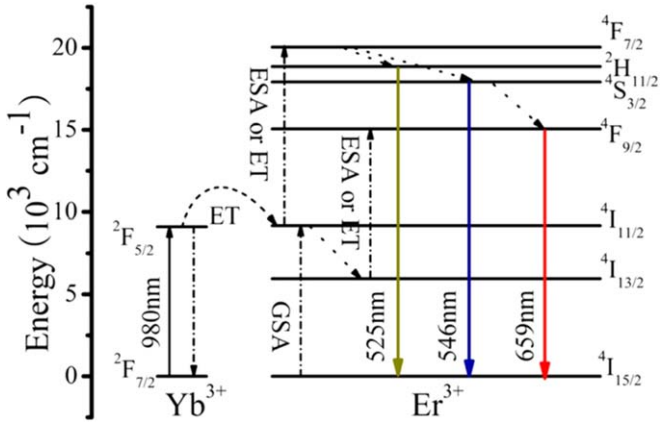

Figure 18. Schematic representation of energy level diagram in NaYF4:Yb^{3+},Er^{3+} nanoparticles. The arrows indicate the up conversion process. Reprinted with permission from [438]. Copyright (2014) American Chemical Society.

[452–454], BaY_2F_8 [455, 456] and fluorozirconate glass [457, 458] as host material is also common. Er^{3+} [431, 434, 445, 452, 454–456, 459], Tm^{3+} [447, 450, 460], and Ho^{3+} [460, 461] ions, with their appropriate *f* electron configurations, nearly evenly spaced energy levels and long excitation lifetime, are commonly used as the activator material. The three step UC in Er^{3+} energy levels are shown in figure 18 [438]. The larger absorption cross sectional area in Yb^{3+} ions compared to activator along with their convenient relaxation energy, which resonates with the excitation energies of activator ions are major factors in improving the efficiency of the energy transfer UC [436].

The first proposed use of UC was in 1982 using terbium-doped lanthanum fluoride and thulium-doped calcium tungstate [437], followed by the first demonstration in 1996 of an improvement in GaAs solar cell performance using co-doped Er^{3+} and Yb^{3+} [462]. Over the years, different solar calls have been tested using various lanthanides as dopants. In 2002, a theoretical prediction was made of a PCE of 47.6% in c-Si solar cells using sub-band gap light, considerably higher than the Shockley–Quessier limit [463]. Erbium-doped sodium yttrium fluoride ($NaYF_4$:Er^{3+}) as the host-activator matrix achieved an internal quantum efficiency of 3.8% in c-Si solar cells at laser excitation of 1523 nm [459]. In 2009, $Gd_2(Mo0_4)_3$:Er^{3+} was proposed as an up conversion phosphor for Si solar cells [464], but it was only in 2010, that UC was finally tested in organic and DSSCs, with the use of Er^{3+},Yb^{3+} co-doped LaF_3-TiO_2 nanocomposites as a middle layer in DSSC to produce an improved PCE of 2.69% [465]. Yttrium fluoride host doped with erbium in P_3HT:PCBM solar cell showed a four-fold increase in photocurrent at 975 nm illumination [466]. With silicon solar cells, some of the recent works involve improved external quantum efficiencies at long wavelength irradiance and approaches into NIR broadband UCs [467, 468].

Some of the recent works on up conversion in PV are summarized in table 1.

3.2.2. DC materials

Losses due to thermalization can be reduced with the use of DC materials that help in generation of multiple electron–hole pairs for incident photons of energy greater than twice the band gap of the material. Hence, DC is more beneficial for solar cells with smaller band gaps as it converts a photon of higher energy to two photons of lower energy, implying an external quantum efficiency of 200%. Although a DC layer is typically applied to the front surface of a solar cell, it is possible to add a rear layer in the case of bifacial solar cells [427, 428]. It was theoretically predicted that a conversion efficiency of 38.6% can be achieved in c-Si solar cells attached to an ideal DC convertor under un-concentrated light, by increasing the available spectral irradiance by 32% [475].

DC works in materials with an intermediate state between their bands. It was shown that in such materials, under low light intensity such as concentrate light, absorption occurs via band to band transition, while radiative recombination occurs with the help of an intermediate level [475]. However, another way to achieve such DC is through cooperative energy transfer between ions, achieved through co-doping two different ionic systems in a material [476, 477].

In 2005, a cooperative energy transfer efficiency of 88% was reported in $(Yb_xY_{1-x})PO_4$ doped with 1% Tb^{3+} upon excitation using a Xe lamp [478]. As expected, the energy transfer in DC occurs opposite to that of UC, that is, from two Tb^{3+} to one Yb^{3+} ion. Around the same time, multiple groups also reported improved PCE and short current density in c-Si solar cells with the use DC materials [478]. Broadband DC of UV light resulting in emission of NIR photons upon excitation using was reported in 2008 with a high energy transfer efficiency of

Table 1. Recent studies on up converison materials for improved solar cell performance.

Material	Comments	Year
$NaYF_4$:Yb/Er up conversion nanoparticles	PCE in Perovskite solar cells increased from 17.8% to 18.1% upon NIR irradiation	2016 [469]
Er^{3+}-doped β-$NaYF_4$	Si solar cells—internal and external PL quantum yield of 10.7% and 6.6% at 980 nm	2014 [470]
BaY_2F_8:30% Er^{3+}	Si solar cells—external quantum yield 8% at 1520 nm and 0.55% relative efficiency increase	2015 [471]
$NaYF_4$:Yb,Er/Li-Ag@SiO_2	Co-enhancing effect between up converison and LSPR.	2017 [472]
$NaYF_4$:Yb^{3+}, Er^{3+}@SiO_2,@Au,@TiO_2	Enhanced up converison efficiencies in $NaYF_4$:Yb^{3+}, Er^{3+} prisms due to LSPR in Au nanoparticles	2016 [364]
Er^{3+}-Yb^{3+}-Li^{+} tri-doped TiO_2	PCE in Perovskite solar cell increased from 14% to 16.5%	2018 [473]
Cylamine sensitized $NaYF_4$:Yb,Er nanoparticles	Broadband NIR up conversion. Up conversion efficiency enhanced by a factor of ~3300	2012 [474]

Table 2. Recent studies on down conversion materials for improved solar cell performance.

Material	Comments	Year
ZnO: Eu^{3+}, Dy^{3+}	<200% improvement in current density and PCE in DSSC compared to using TiO2 alone	2014 [406]
Eu and Tb coordination complexes	On spin coating DC coordination complexes onto Si solar cell, a maximum relative increase in PCE by 8%	2016 [407]
Lanthanide ions doped into Metal organic frameworks	PL, absorption and NIR emission enhancement	2018 [408]
Graphene quantum dots	Improved fill factors and short circuit current, achieving a PCE of 16.55% in Si heterojunction solar cells	2016 [409]
Ce and Yb doped Perovskite quantum dots—$CsPbCl_{1.5}Br_{1.5}$:Yb^{3+}, Ce^{3+}	PCE improved from 18.1 to 21.5% in Si solar cells	2017 [164]
$CuInS_2$/ZnS core shell quantum dots	10.5% relative PCE improvement in Si solar cells	2014 [411]

74% between Ce^{3+} and Yb^{3+} ions co-doped in borated glasses [479]. Further, they reported a DC of visible light at 475 nm in a co-doped system of Yb^{3+} doped oxyfluoride glass ceramics with precipitated TbF^3 nanocrystals [480]. Other commonly used materials for down conversion are CdO nanotips [481], ZnO:Er^{3+}/Yb^{3+} [482], $GdAl_3(BO_3)_4(Pr,Tb)_{3+}$,$Yb^{3+}$ [483], YF_3 doped with Pr^{3+} Yb^{3+} [484], Gd_2O_2S:Tm^{3+} [485], and lanthanide ion doped glasses [486]. Many groups have reported improved performance in solar cells with DC materials, and some of the recent results are shown in table 2.

Over the last decade active research on UC and DC materials have helped in improving the efficiencies of solar cells. However, the reported values are still low and demands testing new materials and better fabrication techniques. Researchers have also tested plasmonic and photonic materials as efficient UC/DC materials [487, 488]. These materials have additional benefits of enhanced scattering and other plasmonic effects described earlier. Another approach is the use of concentrated light source [427, 489]. UC/DC are yet to achieve substantial improvements that can be implemented into existing commercial devices. However, over the last decade, encouraging results with an increasing trend in efficiencies is visible.

4. Nanomaterials beyond PV

The properties of nanomaterials that make them well-suited as active materials in photovoltaic devices (broadband absorption, high quantum yield, etc) also make them ideal candidates for LSCs. These devices also harvest solar energy, but instead of directly allowing charge generation, they act as down converters for other PV cells. LSCs are economically more viable than PVs and have the additional advantage in that they may be incorporated in to existing PV modules to improve performance. Further, they are far better candidates as building incorporated photovoltaic (BIPV) platforms, given they function under both direct and diffuse light. We will review dye, thin film, and quantum dot based LSCs that have garnered a lot of attention in recent years as these devices face a resurgence given the advances in materials science and engineering which have led to novel QDs and hybrid semiconductors.

LSCs are usually made from some transparent layer, typically a polymer thin film, which is doped with a fluorescent species, such as dye molecules or quantum dots, among others, that are responsible for absorbing

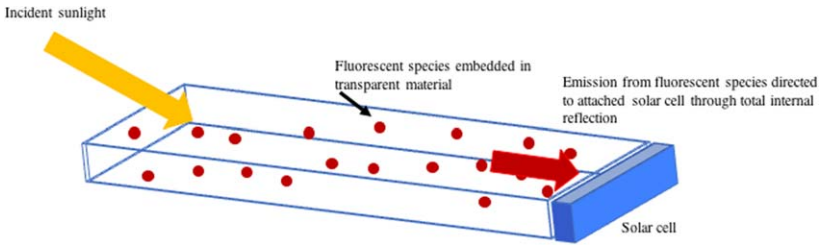

Figure 19. Operating principle of LSCs.

sunlight and re-emitting at a longer wavelength [490, 491]. The emitted light is then trapped in the LSC due to the high refractive index of the transparent layer and via total internal reflection it is waveguided to the edges of the LSC, where an attach solar cell converts the light to electricity, as shown in figure 19. Therefore, a good LSC material should demonstrate a broad absorption spectrum, minimal overlap in its absorption and emission spectra (i.e. minimal Stokes' shift) to prevent re-absorption of the emitted light, high quantum yield, and emission should match the absorption of the attached solar cell [490]. In the effort to optimize all aspects of the LSC, various materials were investigated as possible fluorophores.

4.1. Organic dye-based LSCs

Organic dyes were considered in the original design and used as the fluorophore in the first LSCs, as they offer good solubility in solvents, high quantum yield, and good absorption spectra [490, 492–494]. Since then, extensive work on various types of dyes has yielded a large amount of potential dyes. These include dicyano methylenes, lactones, bipyridines, coumarins, rhodamines, porphyrins, phtalocyanines, and perylenes, as well as many others, among which coumarines, rhodamines, and perylenes have been particularly popular [490]. Rhodamines were used since early work on LSCs due to their high quantum yield, but suffer from small Stokes' shift, which results in significant losses due to high re-absorption [492, 495]. Furthermore, the Rhodamine 6G fluorescence was reduced after incorporation in a polymer [496], whereas various rhodamine dyes demonstrate poor photostability [497, 498]. This encouraged investigation of alternative dyes. Coumarins show a larger Stokes' shift and quantum yields of up to 98% have been observed [498–500]. Furthermore, they exhibit superior stability, although they are still lagging in comparison to other dyes. Perylene dyes are characterized by bright fluorescence and good stability after modification with cyano side groups, reaching quantum yield of 91% [501]. Perylene derivatives, such as perylene bismides, show very bright fluorescence and good stability, but suffer from low solubility, which is improved by addition of ortho-alkylated aromatic bulky groups [490, 502]. Moreover, perylene dyes have been engineered to demonstrate Stokes' shift of up to 300 meV [503]. As perylene dyes show such good properties, multiple dyes can be combined in LSCs to achieve good absorption and quantum yield simultaneous [504]. Dicyano methylene dyes have also shown good properties for implementation in LSCs. DCM (4-(dicyanomethylene)-2-methyl-6-(p-dimethylaminostyryl)-4H-pyran) possesses a broad absorption spectrum and large Stokes' shift, while its quantum yield can reach 80%, but it suffers from poor photostability [490, 496, 499]. DCJTB (4-(dicyanomethylene)-2-t-butyl-6-(1,1,7,7-tetramethyljulolidyl-9-enyl)-4H-pyran) combined with a platinum-porphyrin dye yielded a device with efficiency 6.8% when attached to a GaAs solar cell [505].

Other well performing dyes include CRS 040 yellow (coumarine dye) and Lumogen red (perylene dye) [506, 507]. Combination of these two dyes in a LSC attached to a GaAs solar cell has generated the highest PCE using an LSC to date, reaching 7.1% [508]. Due to the limited absorption of organic dyes, combination of dyes, either in a single device, or in a stack of devices, can be used to leverage the absorption spectra of multiple dyes [490]. In addition, multiple efforts to improve stability of organic dyes have encompassed introduction of UV absorbers to prevent degradation under UV light, and use of copolymers to improve photostability [490, 509].

4.2. Quantum dot based LSCs

Due to the issues faced by dyes, such as rapid degradation and limited absorption by a single dye, QDs have risen as a potential alternative to dyes as fluorophores in LSCs, since the absorption spectrum of QDs can be easily manipulated to match that of the solar spectrum [510], whereas their composition of mostly inorganic semiconductors prevents rapid degradation [511]. Moreover, by appropriate combination of QDs of different sizes, LSCs with significant Stokes' shift can be fabricated [512, 513].

Common colloidal QDs that have been used in LSCs include CdS, CdSe/CdS, CdSe/ZnS, and PbS/CdS, among others [490, 491]. Work has been done to understand how each of these behaves in a LSC and how they can be optimized. Comparison between the properties of PbS QDs and CdSe/ZnS QDs in solution has shown

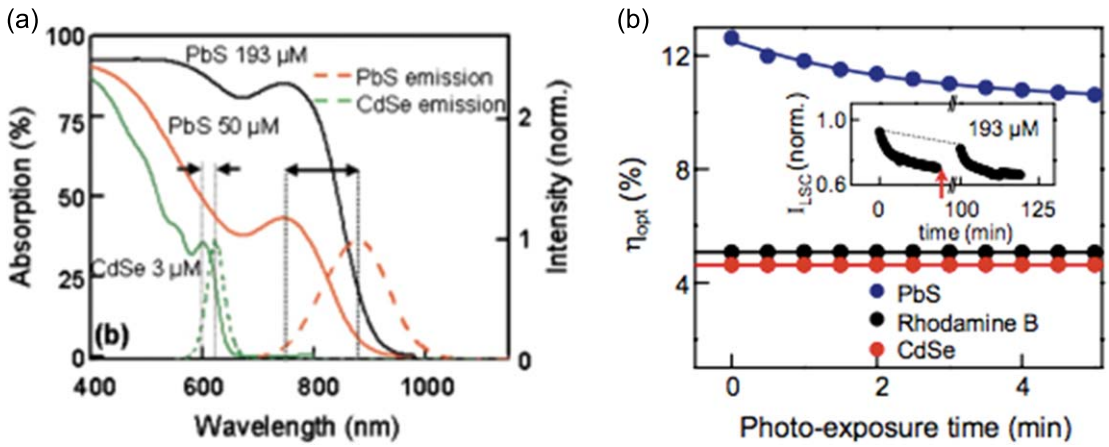

Figure 20. (a) Absorption and emission curves for CdSe/ZnS and PbS QDs with Stoke's shift indicated by double headed arrows, (b) optical efficiency of LSCs as a function of exposure time for PbS, CdSe, and Rhodamine B fluorophores, (inset) Reversal of photodarkening of PbS based LSC. Reprinted from [514], with the permission of AIP Publishing.

that PbS QDs demonstrate a much larger Stokes' shift of 122 nm, as compared to 23 nm for the CdSe/ZnS system, as shown in figure 20(a) [514]. Nevertheless, PbS QDs are found to possess a much lower extinction coefficient than CdSe/ZnS. On the other hand, a study on Cd-based QDs has indicated that despite the decreased absorption coefficient for NIR-absorbing QDs, they still have a better absorption efficiency compared to QDs that only absorb in the visible part of the spectrum [515]. Similarly, PbS QDs exhibit better absorption efficiency than CdSe/ZnS QDs, while their quantum yield is lower, leading to better devices as demonstrated in figure 20(b) [514]. A comparative study of CdSe/ZnS QD-based LSC and a Lumogen Red F 300 LSC has demonstrated that QD-based LSC shows device performance 42% lower than that of the dye-based LSC [516]. Furthermore, a study comparing CdSe/ZnS QD-LSCs with LSCs fabricated with Rhodamine B, Lumogen Red F, and laser dyes LDS698 and LDS821, has concluded that the optical efficiency of the QD-based LSC is only 10% of that of the LSCs prepared with Rhodamine B and Lumogen Red F, and was comparable to that of the LSCs prepared with the LDS laser dyes [517]. In all cases, the lower device performance of the QD-based LSCs was attributed to the lower quantum yield of the QDs, indicating that QDs with high quantum yields must be fabricated for QD-based LSCs to be competitive with dye-based LSCs. While core/shell QD structures were originally implemented to achieve high extinction ratios, higher ratios have been achieved with doped systems, such as ZnSe and $CsPbCl_3$ perovskite QDs doped with manganese, which have shown high extinction ratios and very low re-absorption, opening a route for high efficiency LSCs [518, 519]. In addition, manganese and copper doped CdSe QDs have exhibited increased photoluminescence quantum yield, with copper doped CdSe QD-LSCs outperforming the traditional CdSe/CdS structure [520].

Concerns over the toxicity of the materials used in LSCs have led to the search for QDs that do not require any heavy metals [490, 491]. Therefore, devices with $CuInS_2$, $AgInS_2$, and CuInSeS were developed with promising results [521–524]. In particular, $CuInSe_xS_{2-x}$ QDs in poly(lauryl methacrylate) have produced a colorless LSC, and the low reabsorption and high emission of the QDs allowed for optical power efficiency of 3.2% in a $12 \times 12 \times 0.3$ cm^3 large area LSC, making the possibility of LSC windows more realistic [524]. Moreover, Si QDs embedded in a polymerized acrylic matrix of area 144 cm^2 have achieved PCE of 2.85%, while maintaining a transmittance of 70% [525]. Simulations showed that efficiency could exceed 5%, whereas flexible LSCs were fabricated, and along with simulation results, it was observed that the curvature of the device does not affect the performance. These results strongly encourage the potential implementation of LSCs in BIPV platforms.

4.3. Thin film based LSCs

While dyes and QDs are often implemented along with transparent polymer thin films in devices, work on opaque thin film based LSCs has not been as extensive due to the likelihood of increased self-absorption of the emitted light by the thin film itself, as well as the motivation for transparent LSCs as windows. Nevertheless, although opaque thin films might not be suitable for use as windows, they offer the potential of use in structures that require shading, such as bus stops [490].

QD-based LSCs suffer from limited quantum yield of the fluorophore, whereas dye-based LSCs suffer from photostability issues, hence alternative materials with more suitable properties are sought after. Hybrid organic–inorganic perovskites (PVSK) are in the forefront of photovoltaic research due to their excellent properties and

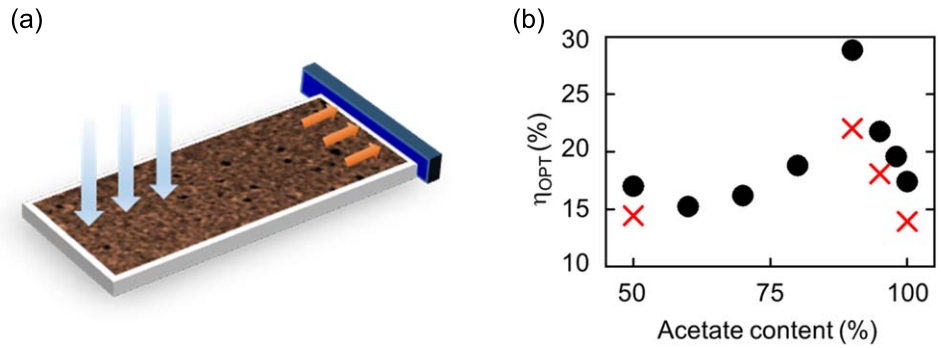

Figure 21. (a) Schematic of PVSK thin film LSC with Silicon PV attached at the end, (b) Optical efficiency of PVSK thin film LSCs: black dots represent initial optical efficiency, red crosses show the optical efficiency after 4 weeks of storage in ambient conditions. [531] John Wiley & Sons. Copyright © 2016, John Wiley and Sons.

have been used to fabricate high efficiency solar cells [526]. PVSKs can be prepared easily, using solution processing [527], and are characterized by broad absorption spectra, high quantum yield reaching 80% for thin films [527, 528], and refractive index of 2.5 that surpasses that of glass and polymer films [529, 530], both of which are necessary characteristics for a good LSC material. Recent work on PVSK-based LSCs, as shown in figure 21(a), has shown that despite the increased self-absorption shown by thin film LSCs, the use of materials with very high photoluminescence quantum yields and high absorption could make up for the self-absorption losses exhibited [531]. The devices reached optical efficiency of 29%, and were operational after seven weeks of storage in ambient conditions, as demonstrated in figure 21(b), demonstrating that while electrical properties of PVSK degrade quickly, the optical properties of PVSK are far more stable and can be leveraged for optical devices. This reveals that development of possible thin film materials with favorable optical properties can yield high efficiency thin film-based LSCs, a device architecture that has not been thoroughly explored in the past.

5. Conclusions and future outlook

The foray into nanostructured photovoltaics has been driven by the dual need for less expensive and more efficient PV devices. The encouraging trends and substantial progress summarized in the previous sections, combined with the wide variety of nanomaterials that are suited to serve as the active media, in combination with the many different designs and additives possible, has enlarged the scope of this field, making it all the more probable that a solution may be found. A summary of this field will, however, remain inadequate without some discussion of the shortcomings and concerns that are common to these materials.

The first and most obvious drawback is the fact that the device efficiencies remain, on average, lower than the traditional first and second-generation PVs. This is the reason that nanostructured PVs remain an 'emergent' technology, not yet ready to be integrated in to the grid in the form of modules. One of the causes that contribute to this is the inherent high surface-to-volume ratio of nanomaterials. This exacerbates the contribution of surface defects and trap states, which increase recombination losses and hinder the transport of photogenerated charge carriers. Mitigation of this particular issue requires increased focus on suitable architecture of nanostructures, such as one-dimensional materials, and surface ligands that allow improved charge conduction. Another fundamental problem that may also be addressed through suitable surface functionalization and modification of nanostructures is the matter of stability. Again, owing to the susceptibility of surface states, ambient environmental factors such as exposure to light and humidity can cause degradation of optical and electronic properties of nanomaterials. Dyes tend to photo bleach while semiconducting nanostructures are prone to photo-oxidation and darkening. The option of encapsulating and hermetically sealing the entire device is not an attractive one, as that adds to material costs.

On the topic of expenses, it is worth mentioning that to be truly cost-effective and achieve grid parity, the fabrication processes currently used for nano-synthesis will need to be scaled up for large scale production, allowing for roll-to-roll processing on industrial levels. Additionally, most of the nanomaterials used in PVs currently use heavy metals and other components that would not stand up to safe long-term use. Incorporating non-toxic elements, especially in the semiconducting nanomaterials will be imperative for future use.

ORCID iDs

Sayantani Ghosh https://orcid.org/0000-0003-3440-7194

References

[1] IEA. World Energy Outlook 2017 Organization for Economic Co-operation and Development, OECD, 2017 https://www.iea.org/weo2017/
[2] Lewis N S and Crabtree G W 2005 *Basic Research Needs for Solar Energy Utilization Report of the Basica Energy Sciences Workshop on Solar Energy Utilization (April 18–21)* US Department of Energy pp 1–24
[3] Mints P SPV market research, photovoltaic manufacturer shipments: capacity, price & revenues 2017/2018, Report SPV-Supply 6, April 2018
[4] Gallagher B US PV system pricing H2 2017: forecasts and breakdowns, gtmresearch, http://caiso.com/informed/Pages/ManagingOversupply.aspx
[5] U.S. Energy Information Administration https://www.eia.gov/
[6] Green M A 2015 The passivated emitter and rear cell (PERC): from conception to mass production *Sol. Energy Mater. Sol. Cells* **143** 190–7
[7] Beard Matthew C, Luther Joseph M and Nozik Arthur J 2014 *Nat. Nanotechnol.* **9** 951–4
[8] NREL Research Cell Efficiency Records https://www.nrel.gov/
[9] Algora C, Ortiz E, Rey-Stolle I, Diaz V, Peña R, Andreev V M, Khvostikov V and Rumyantsev V D 2001 A GaAs solar cell with an efficiency of 26.2% at 1000 suns and 25.0% at 2000 suns *IEEE Trans. Electron Devices* **48** 840–4
[10] King R R, Law D C, Edmondson K M, Fetzer C M, Kinsey G S, Yoon H, Sherif R A and Karam N H 2007 40% efficient metamorphic GaInP/GaInAs/Ge multijunction solar cells *Appl. Phys. Lett.* **90** 183516
[11] William S and Queisser Hans J 1961 Detailed balance limit of efficiency of p–n junction solar cells *J. Appl. Phys.* **32** 510–9
[12] Roduner E 2006 Size matters: why nanomaterials are different *Chem. Soc. Rev.* **35** 583–92
[13] Chen X and Mao S Titanium dioxide nanomaterials: synthesis, properties, modifications, and applications *Chem. Rev.* **107** 2891–959
[14] O'Regan B and Gratzel M 1991 A low-cost, high-efficiency solar-cell based on dye-sensitized colloidal TiO_2 films *Nature* **353** 737–40
[15] O'Regan B C and Durrant J R 2009 Kinetic and energetic paradigms for dye sensitized solar cells: moving from the ideal to the real *Acc. Chem. Res.* **42** 1799–808
[16] Mathew S, Yella A, Gao P, Humphry-Baker R, Curchod B F E, Ashari-Astani N, Tavernelli I, Rothlisberger U, Nazeeruddin M K and Grätzel M 2014 Dye-sensitized solar cells with 13% efficiency achieved through the molecular engineering of porphyrin sensitizers *Nat. Chem.* **6** 242–7
[17] Hagfeldt A, Boschloo G, Sun L, Kloo L and Pettersson H 2010 Dye-sensitized solar cells *Chem. Rev.* **110** 6595–663
[18] Hagfeldt A and Grätzel M 2000 Molecular photovoltaics *Acc. Chem. Res.* **33** 269–77
[19] Kallioinen J, Benkö G, Sundström V, Korppi-Tommola J E I and Yartsev A P 2002 Electron transfer from the singlet and triplet excited states of $Ru(dcbpy)_2(NCS)_2$ into nanocrystalline TiO_2 thin films *J. Phys. Chem.* B **106** 4396–404
[20] Hagfeldt A and Graetzel M 1995 Light-induced redox reactions in nanocrystalline systems *Chem. Rev.* **95** 49–68
[21] Nazeeruddin M K, Kay A, Rodicio I, Humphry-Baker R, Mueller E, Liska P, Vlachopoulos N and Graetzel M 1993 Conversion of light to electricity by cis-X_2bis(2,2′-bipyridyl-4,4′-dicarboxylate)ruthenium(II) charge-transfer sensitizers (X = Cl-, Br-, I-, CN-, and SCN-) on nanocrystalline titanium dioxide electrodes *J. Am. Chem. Soc.* **115** 6382–90
[22] Asbury J B, Hao E, Wang Y, Ghosh H N and Lian T 2001 Ultrafast electron transfer dynamics from molecular adsorbates to semiconductor nanocrystalline thin films *J. Phys. Chem.* B **105** 4545–57
[23] Tachibana Y, Moser J E, Grätzel M, Klug D R and Durrant J R 1996 Subpicosecond interfacial charge separation in dye-sensitized nanocrystalline titanium dioxide films *J. Phys. Chem.* **100** 20056–62
[24] Asbury J B, Ellingson R J, Ghosh H N, Ferrere S, Nozik A J and Lian T 1999 Femtosecond IR study of excited-state relaxation and electron-injection dynamics of $Ru(dcbpy)_2(NCS)_2$ in solution and on nanocrystalline TiO_2 and Al_2O_3 thin films *J. Phys. Chem.* B **103** 3110–9
[25] Durrant J R, Tachibana Y, Mercer I P, Moser J E, Grätzel M and Klug D R 1999 The excitation wavelength and solvent depdence of the kinmatics of electron injection in $Ru(dcbpy)_2(NCS)_2$ sensitized nanocrystalline TiO_2 films *Z. Phys. Chem.* **212** 93–8
[26] Tachibana Y, Haque S A, Mercer I P, Durrant J R and Klug D R 2000 Electron injection and recombination in dye sensitized nanocrystalline titanium dioxide films: a comparison of ruthenium bipyridyl and porphyrin sensitizer dyes *J. Phys. Chem.* B **104** 1198–205
[27] Kallioinen J, Lehtovuori V, Myllyperkiö P and Korppi-Tommola J 2001 Transient absorption studies of the $Ru(dcbpy)_2(NCS)_2$ excited state and the dye cation on nanocrystalline TiO_2 film *Chem. Phys. Lett.* **340** 217–21
[28] Tachibana Y, Haque S A, Mercer I P, Moser J E, Klug D R, Durrant J R and Fe Ä P 2001 Modulation of the rate of electron injection in dye-sensitized nanocrystalline TiO_2 films by externally applied bias *J. Phys. Chem.* B **105** 7424–31
[29] Moser J E and Grätzel M 1993 Observation of temperature independent heterogeneous electron transfer reactions in the inverted Marcus region *Chem. Phys.* **176** 493–500
[30] Koops S E, O'Regan B C, Barnes P R F and Durrant J R 2009 Parameters influencing the efficiency of electron injection in dye-sensitized solar cells *J. Am. Chem. Soc.* **131** 4808–18
[31] Kusama H, Orita H and Sugihara H 2008 DFT investigation of the TiO_2 band shift by nitrogen-containing heterocycle adsorption and implications on dye-sensitized solar cell performance *Sol. Energy Mater. Sol. Cells* **92** 84–7
[32] Nakade S, Kanzaki T, Kubo W, Kitamura T, Wada Y and Yanagida S 2005 Role of electrolytes on charge recombination in dye-sensitized TiO_2 solar cell (1): the case of solar cells using the I^-/I^{3-} redox couple *J. Phys. Chem.* B **109** 3480–7
[33] Redmond G and Fitzmaurice D 1993 Spectroscopic determination of flatband potentials for polycrystalline titania electrodes in nonaqueous solvents *J. Phys. Chem.* **97** 1426–30
[34] Yella A, Lee H-W, Tsao H N, Yi C, Chandiran A K, Nazeeruddin M K, Diau E W-G, Yeh C-Y, Zakeeruddin S M and Grätzel M 2011 Porphyrin-sensitized solar cells with cobalt (II/III)-based redox electrolyte exceed 12 percent efficiency *Science* **334** 629–34
[35] Kay A and Graetzel M 1993 Artificial photosynthesis: I. Photosensitization of titania solar cells with chlorophyll derivatives and related natural porphyrins *J. Phys. Chem.* **97** 6272–7
[36] Boschloo G K and Goossens A 1996 Electron trapping in porphyrin-sensitized porous nanocrystalline TiO_2 electrodes *J. Phys. Chem.* **3654** 19489–94
[37] Kalyanasundaram K, Vlachopoulos N, Krishnan V, Monnier A and Graetzel M 1987 Sensitization of titanium dioxide in the visible light region using zinc porphyrins *J. Phys. Chem.* **91** 2342–7
[38] Wahl A and Augustynski J 1998 Charge carrier transport in nanostructured anatase TiO_2 films assisted by the self-doping of nanoparticles *J. Phys. Chem.* B **102** 7820–8

[39] Lü X, Mou X, Wu J, Zhang D, Zhang L, Huang F, Xu F and Huang S 2010 Improved-performance dye-sensitized solar cells using Nb-doped TiO_2 electrodes: efficient electron injection and transfer *Adv. Funct. Mater.* **20** 509–15
[40] O'Regan B, Moser J, Anderson M and Graetzel M 1990 Vectorial electron injection into transparent semiconductor membranes and electric field effects on the dynamics of light-induced charge separation *J. Phys. Chem.* **94** 8720–6
[41] Haque S A, Tachibana Y, Klug D R and Durrant J R 1998 Charge recombination kinetics in dye-sensitized nanocrystalline titanium dioxide films under externally applied bias *J. Phys. Chem.* B **102** 1745–9
[42] Cao F, Oskam G, Meyer G J and Searson P C 1996 Electron transport in porous nanocrystalline TiO_2 photoelectrochemical cells *J. Phys. Chem.* **100** 17021–7
[43] Tang H, Prasad K, Sanjinès R, Schmid P E and Lévy F 1994 Electrical and optical properties of TiO_2 anatase thin films *J. Appl. Phys.* **75** 2042–7
[44] Okuya M, Nakade K and Kaneko S 2002 Porous TiO_2 thin films synthesized by a spray pyrolysis deposition (SPD) technique and their application to dye-sensitized solar cells *Sol. Energy Mater. Sol. Cells* **70** 425–35
[45] Imahori H, Hayashi S, Umeyama T, Eu S, Oguro A, Kang S, Matano Y, Shishido T, Ngamsinlapasathian S and Yoshikawa S 2006 Comparison of electrode structures and photovoltaic properties of porphyrin-sensitized solar cells with TiO_2 and Nb, Ge, Zr-added TiO_2 composite electrodes *Langmuir* **22** 11405–11
[46] Mor G K, Shankar K, Paulose M, Varghese O K and Grimes C A 2006 Use of highly-ordered TiO_2 nanotube arrays in dye-sensitized solar cells *Nano Lett.* **6** 215–8
[47] Wu J, Lan Z, Lin J, Huang M, Huang Y, Fan L and Luo G 2015 Electrolytes in dye-sensitized solar cells *Chem. Rev.* **115** 2136–73
[48] Wu J, Lan Z, Hao S, Li P, Lin J, Huang M, Fang L and Huang Y 2008 Progress on the electrolytes for dye-sensitized solar cells *Pure Appl. Chem.* **80** 2241–58
[49] Ardo S and Meyer G J 2009 Photodriven heterogeneous charge transfer with transition-metal compounds anchored to TiO_2 semiconductor surfaces *Chem. Soc. Rev.* **38** 115–64
[50] Nogueira A F, Longo C and De Paoli M-A 2004 Polymers in dye sensitized solar cells: overview and perspectives *Coord. Chem. Rev.* **248** 1455–68
[51] Boschloo G, Hagfeldt A and Spectus C O N 2009 Characteristics of the iodide/triiodide redox mediator in dye-sensitized solar cells *Acc. Chem. Res.* **42** 1819–26
[52] Ratner M A and Shriver D F 1988 Ion transport in solvent-free polymers *Chem. Rev.* **88** 109–24
[53] Papageorgiou N, Athanassov Y, Armand M, Bonhôte P, Pettersson H, Azam A and Grätzel M 1996 The performance and stability of ambient temperature molten salts for solar cell applications *J. Electrochem. Soc.* **143** 3099
[54] Kubo W, Murakoshi K, Kitamura T, Yoshida S, Haruki M, Hanabusa K, Shirai H, Wada Y and Yanagida S 2001 Quasi-solid-state dye-sensitized TiO_2 solar cells: effective charge transport in mesoporous space filled with gel electrolytes containing iodide and iodine *J. Phys. Chem.* B **105** 12809–15
[55] Ghosh B D, Lott K F and Ritchie J E 2005 Conductivity dependence of PEG content in an anhydrous proton conducting sol-gel electrolyte *Chem. Mater.* **17** 661–9
[56] Yu Z, Vlachopoulos N, Gorlov M and Kloo L 2011 Liquid electrolytes for dye-sensitized solar cells *Dalt. Trans.* **40** 10289
[57] Kakiage K, Aoyama Y, Yano T, Oya K, Fujisawa J and Hanaya M 2015 Highly-efficient dye-sensitized solar cells with collaborative sensitization by silyl-anchor and carboxy-anchor dyes *Chem. Commun.* **51** 15894–7
[58] Tributsch H 2004 Dye sensitization solar cells: a critical assessment of the learning curve *Coord. Chem. Rev.* **248** 1511–30
[59] Grätzel M 2003 Dye-sensitized solar cells *J. Photochem. Photobiol.* C **4** 145–53
[60] Kato N, Takeda Y, Higuchi K, Takeichi A, Sudo E, Tanaka H, Motohiro T, Sano T and Toyoda T 2009 Degradation analysis of dye-sensitized solar cell module after long-term stability test under outdoor working condition *Sol. Energy Mater. Sol. Cells* **93** 893–7
[61] Hong J S, Joo M, Vittal R and Kim K-J 2002 Improved photocurrent-voltage characteristics of Ru(II)-dye sensitized solar cells with polypyrrole-anchored TiO[sub 2] films *J. Electrochem. Soc.* **149** E493
[62] Wang P, Zakeeruddin S M, Moser J-E, Humphry-Baker R and Grätzel M 2004 A solvent-free, $SeCN^-/(SeCN)_3^-$ based ionic liquid electrolyte for high-efficiency dye-sensitized nanocrystalline solar cells *J. Am. Chem. Soc.* **126** 7164–5
[63] Paulsson H, Hagfeldt A and Kloo L 2003 Molten and solid trialkylsulfonium iodides and their polyiodides as electrolytes in dye-sensitized nanocrystalline solar cells *J. Phys. Chem.* B **107** 13665–70
[64] Paulsson H, Kloo L, Hagfeldt A and Boschloo G 2006 Electron transport and recombination in dye-sensitized solar cells with ionic liquid electrolytes *J. Electroanal. Chem.* **586** 56–61
[65] Paulsson H, Berggrund M, Svantesson E, Hagfeldt A and Kloo L 2004 Molten and solid metal-iodide-doped trialkylsulphonium iodides and polyiodides as electrolytes in dye-sensitized nanocrystalline solar cells *Sol. Energy Mater. Sol. Cells* **82** 345–60
[66] Ramírez R E and Sánchez E M 2006 Molten phosphonium iodides as electrolytes in dye-sensitized nanocrystalline solar cells *Sol. Energy Mater. Sol. Cells* **90** 2384–90
[67] Ramírez R E, Torres-González L C and Sánchez E M 2007 Electrochemical aspects of asymmetric phosphonium ionic liquids *J. Electrochem. Soc.* **154** B229
[68] Santa-Nokki H, Busi S, Kallioinen J, Lahtinen M and Korppi-Tommola J 2007 Quaternary ammonium polyiodides as ionic liquid/soft solid electrolytes in dye-sensitized solar cells *J. Photochem. Photobiol.* A **186** 29–33
[69] Xi C, Cao Y, Cheng Y, Wang M, Jing X, Zakeeruddin S M, Grätzel M and Wang P 2008 Tetrahydrothiophenium-based ionic liquids for high efficiency dye-sensitized solar cells *J. Phys. Chem.* C **112** 11063–7
[70] Gorlov M and Kloo L 2008 Ionic liquid electrolytes for dye-sensitized solar cells *Dalton Trans.* **0** 2655
[71] Sauvage F, Chhor S, Marchioro A, Moser J-E and Graetzel M 2011 Butyronitrile-based electrolyte for dye-sensitized solar cells *J. Am. Chem. Soc.* **133** 13103–9
[72] Yang S C, Yoon H G, Lee S-S and Lee H 2009 Roles of layered titanates in ionic liquid electrolytes for quasi-solid state dye-sensitized solar cells *Mater. Lett.* **63** 1465–7
[73] Neo C Y and Ouyang J 2012 Functionalized carbon nanotube-induced viscosity reduction of an ionic liquid and performance improvement of dye-sensitized solar cells *Electrochim. Acta* **85** 1–8
[74] Cameron P J, Peter L M and Hore S 2005 How important is the back reaction of electrons via the substrate in dye-sensitized nanocrystalline solar cells? *J. Phys. Chem.* B **109** 930–6
[75] Huang S Y, Schlichthörl G, Nozik A J, Grätzel M and Frank A J 1997 Charge recombination in dye-sensitized nanocrystalline TiO_2 solar cells *J. Phys. Chem.* B **101** 2576–82
[76] Boschloo G, Häggman L and Hagfeldt A 2006 Quantification of the effect of 4-tert-butylpyridine addition to I-/I3- redox electrolytes in dye-sensitized nanostructured TiO_2 solar cells *J. Phys. Chem.* B **110** 13144–50

[77] Kopidakis N, Neale N R and Frank A J 2006 Effect of an adsorbent on recombination and band-edge movement in dye-sensitized TiO_2 solar cells: evidence for surface passivation *J. Phys. Chem.* B **110** 12485–9
[78] Mori S N, Kubo W, Kanzaki T, Masaki N, Wada Y and Yanagida S 2007 Investigation of the effect of alkyl chain length on charge transfer at TiO_2/dye/electrolyte interface *J. Phys. Chem.* C **111** 3522–7
[79] Miyashita M, Sunahara K, Nishikawa T, Uemura Y, Koumura N, Hara K, Mori A, Abe T, Suzuki E and Mori S 2008 Interfacial electron-transfer kinetics in metal-free organic dye-sensitized solar cells: combined effects of molecular structure of dyes and electrolytes *J. Am. Chem. Soc.* **130** 17874–81
[80] O'Regan B C, Walley K, Juozapavicius M, Anderson A, Matar F, Ghaddar T, Zakeeruddin S M, Klein C and Durrant J R 2009 Structure/function relationships in dyes for solar energy conversion: a two-atom change in dye structure and the mechanism for its effect on cell voltage *J. Am. Chem. Soc.* **131** 3541–8
[81] Wang P, Wenger B, Humphry-Baker R, Moser J E, Teuscher J, Kantlehner W, Mezger J, Stoyanov E V, Zakeeruddin S M and Grätzel M 2005 Charge separation and efficient light energy conversion in sensitized mesoscopic solar cells based on binary ionic liquids *J. Am. Chem. Soc.* **127** 6850–6
[82] Wang M, Grätzel C, Zakeeruddin S M and Grätzel M 2012 Recent developments in redox electrolytes for dye-sensitized solar cells *Energy Environ. Sci.* **5** 9394
[83] Gorlov M, Pettersson H, Hagfeldt A and Kloo L 2007 Electrolytes for dye-sensitized solar cells based on interhalogen ionic salts and liquids *Inorg. Chem.* **46** 3566–75
[84] Wang M, Chamberland N, Breau L, Moser J-E, Humphry-Baker R, Marsan B, Zakeeruddin S M and Grätzel M 2010 An organic redox electrolyte to rival triiodide/iodide in dye-sensitized solar cells *Nat. Chem.* **2** 385–9
[85] Bai Y, Yu Q, Cai N, Wang Y, Zhang M and Wang P 2011 High-efficiency organic dye-sensitized mesoscopic solar cells with a copper redox shuttle *Chem. Commun.* **47** 4376
[86] Gregg B A, Pichot F, Ferrere S and Fields C L 2001 Interfacial recombination processes in dye-sensitized solar cells and methods to passivate the interfaces *J. Phys. Chem.* B **105** 1422–9
[87] Hamann T W, Farha O K and Hupp J T 2008 Outer-sphere redox couples as shuttles in dye-sensitized solar cells. performance enhancement based on photoelectrode modification via atomic layer deposition *J. Phys. Chem.* C **112** 19756–64
[88] Feldt S M, Cappel U B, Johansson E M J, Boschloo G and Hagfeldt A 2010 Characterization of surface passivation by poly (methylsiloxane) for dye-sensitized solar cells employing the ferrocene redox couple *J. Phys. Chem.* C **114** 10551–8
[89] Daeneke T, Kwon T-H, Holmes A B, Duffy N W, Bach U and Spiccia L 2011 High-efficiency dye-sensitized solar cells with ferrocene-based electrolytes *Nat. Chem.* **3** 211–5
[90] Lewis N S 2007 Toward cost-effective solar energy use *Science* **315** 798–801
[91] Shi D, Pootrakulchote N, Li R, Guo J, Wang Y, Zakeeruddin S M, Grätzel M and Wang P 2008 New efficiency records for stable dye-sensitized solar cells with low-volatility and ionic liquid electrolytes *J. Phys. Chem.* C **112** 17046–50
[92] Bai Y, Cao Y, Zhang J, Wang M, Li R, Wang P, Zakeeruddin S M and Grätzel M 2008 High-performance dye-sensitized solar cells based on solvent-free electrolytes produced from eutectic melts *Nat. Mater.* **7** 626–30
[93] Grätzel M, Bach U, Lupo D, Comte P, Moser J E, Weissörtel F, Salbeck J and Spreitzer H 1998 Solid-state dye-sensitized mesoporous TiO_2 solar cells with high photon-to-electron conversion efficiencies *Nature* **395** 583–5
[94] Zhang W, Cheng Y, Yin X and Liu B 2011 Solid-state dye-sensitized solar cells with conjugated polymers as hole-transporting materials *Macromol. Chem. Phys.* **212** 15–23
[95] Li D, Qin D, Deng M, Luo Y and Meng Q 2009 Optimization the solid-state electrolytes for dye-sensitized solar cells *Energy Environ. Sci.* **2** 283–91
[96] Li B, Wang L, Kang B, Wang P and Qiu Y 2006 Review of recent progress in solid-state dye-sensitized solar cells *Sol. Energy Mater. Sol. Cells* **90** 549–73
[97] Smestad G P, Spiekermann S, Kowalik J, Grant C D, Schwartzberg A M, Zhang J, Tolbert L M and Moons E 2003 A technique to compare polythiophene solid-state dye sensitized TiO_2 solar cells to liquid junction devices *Sol. Energy Mater. Sol. Cells* **76** 85–105
[98] Kroeze J E, Hirata N, Schmidt-Mende L, Orizu C, Ogier S D, Carr K, Grätzel M and Durrant J R 2006 Parameters influencing charge separation in solid-state dye-sensitized solar cells using novel hole conductors *Adv. Funct. Mater.* **16** 1832–8
[99] Schmidt-Mende L and Grätzel M 2006 TiO_2 pore-filling and its effect on the efficiency of solid-state dye-sensitized solar cells *Thin Solid Films* **500** 296–301
[100] Tennakone K, Kumara G R R A, Kumarasinghe A R, Wijayantha G U and Sirimanne P M 1995 A dye-sensitized nano-porous solid-state photovoltaic cell *Semicond. Sci. Technol.* **10** 1689–93
[101] Kumara G R R, Konno A, Senadeera G K, Jayaweera P V, De Silva D B R and Tennakone K 2001 Dye-sensitized solar cell with the hole collector p-CuSCN deposited from a solution in n-propyl sulphide *Sol. Energy Mater. Sol. Cells* **69** 195–9
[102] Tennakone K, Senadeera G K R, De Silva D B R A and Kottegoda I R M 2000 Highly stable dye-sensitized solid-state solar cell with the semiconductor 4CuBr $3S(C_4H_9)_2$ as the hole collector *Appl. Phys. Lett.* **77** 2367
[103] O'Regan B and Schwartz D T 1998 Large enhancement in photocurrent efficiency caused by UV illumination of the dye-sensitized heterojunction TiO_2/RuLL'NCS/CuSCN: initiation and potential mechanisms *Chem. Mater.* **10** 1501–9
[104] Meng Q B, Takahashi K, Zhang X T, Sutanto I, Rao T N, Sato O, Fujishima A, Watanabe H, Nakamori T and Uragami M 2003 Fabrication of an efficient solid-state dye-sensitized solar cell *Langmuir* **19** 3572–4
[105] Tennakone K, Perera V P S, Kottegoda I R M, De Silva L A A, Kumara G R R A and Konno A 2001 Dye-sensitized solid-state photovoltaic cells: suppression of electron–hole recombination by deposition of the dye on a thin insulating film in contact with a semiconductor *J. Electron. Mater.* **30** 992–6
[106] Zhang X-T, Liu H-W, Taguchi T, Meng Q-B, Sato O and Fujishima A 2004 Slow interfacial charge recombination in solid-state dye-sensitized solar cell using Al_2O_3-coated nanoporous TiO_2 films *Sol. Energy Mater. Sol. Cells* **81** 197–203
[107] Perera V P S and Tennakone K 2003 Recombination processes in dye-sensitized solid-state solar cells with CuI as the hole collector *Sol. Energy Mater. Sol. Cells* **79** 249–55
[108] Kumara G R A, Okuya M, Murakami K, Kaneko S, Jayaweera V V and Tennakone K 2004 Dye-sensitized solid-state solar cells made from magnesiumoxide-coated nanocrystalline titanium dioxide films: enhancement of the efficiency *J. Photochem. Photobiol.* A **164** 183–5
[109] Tennakone K, Kumara G R R A, Kottegoda I R M, Wijayantha K G U and Perera V P S 1998 A solid-state photovoltaic cell sensitized with a ruthenium bipyridyl complex *J. Phys. D: Appl. Phys.* **31** 1492–6
[110] Sakamoto H, Igarashi S, Niume K and Nagai M 2011 Highly efficient all solid state dye-sensitized solar cells by the specific interaction of CuI with NCS groups *Org. Electron.* **12** 1247–52

[111] Sakamoto H, Igarashi S, Uchida M, Niume K and Nagai M 2012 Highly efficient all solid state dye-sensitized solar cells by the specific interaction of CuI with NCS groups: II. Enhancement of the photovoltaic characteristics *Org. Electron.* **13** 514–8
[112] Perera V P S, Senevirathna M K I, Pitigala P K D D P and Tennakone K 2005 Doping CuSCN films for enhancement of conductivity: application in dye-sensitized solid-state solar cells *Sol. Energy Mater. Sol. Cells* **86** 443–50
[113] Premalal E V, Dematage N, Kumara G R R A, Rajapakse R M G, Shimomura M, Murakami K and Konno A 2012 Preparation of structurally modified, conductivity enhanced-p-CuSCN and its application in dye-sensitized solid-state solar cells *J. Power Sources* **203** 288–96
[114] Chung I, Lee B, He J, Chang R P H and Kanatzidis M G 2012 All-solid-state dye-sensitized solar cells with high efficiency *Nature* **485** 486–9
[115] Lee B, Stoumpos C C, Zhou N, Hao F, Malliakas C, Yeh C-Y, Marks T J, Kanatzidis M G and Chang R P H 2014 Air-Stable molecular semiconducting iodosalts for solar cell applications: Cs_2SnI_6 as a hole conductor *J. Am. Chem. Soc.* **136** 15379–85
[116] Yanagida S, Yu Y and Manseki K 2009 Iodine/iodide-free dye-sensitized solar cells *Acc. Chem. Res.* **42** 1827–38
[117] Murakoshi K, Kogure R, Wada Y and Yanagida S 1997 Solid state dye-sensitized TiO_2 solar cell with polypyrrole as hole transport layer *Chem. Lett.* **26** 471–2
[118] Murakoshi K, Kogure R, Wada Y and Yanagida S 1998 Fabrication of solid-state dye-sensitized TiO_2 solar cells combined with polypyrrole *Sol. Energy Mater. Sol. Cells* **55** 113–25
[119] Kitamura T, Maitani M, Matsuda M, Wada Y and Yanagida S 2001 Improved solid-state dye solar cells with polypyrrole using a carbon-based counter electrode *Chem. Lett.* **30** 1054–5
[120] Tan S X, Zhai J, Wan M X, Jiang L and Zhu D B 2003 Polyaniline as hole transport material to prepare solid solar cells *Synth. Met.* **137** 1511–2
[121] Tan S, Zhai J, Wan M, Meng Q, Li Y, Jiang L and Zhu D 2004 Influence of small molecules in conducting polyaniline on the photovoltaic properties of solid-state dye-sensitized solar cells *J. Phys. Chem.* B **108** 18693–7
[122] Kudo N, Honda S, Shimazaki Y, Ohkita H, Ito S and Benten H 2007 Improvement of charge injection efficiency in organic–inorganic hybrid solar cells by chemical modification of metal oxides with organic molecules *Appl. Phys. Lett.* **90** 183513
[123] Zafer C, Karapire C, Serdar Sariciftci N and Icli S 2005 Characterization of N, N′-bis-2-(1-hydoxy-4-methylpentyl)-3, 4, 9, 10-perylene bis (dicarboximide) sensitized nanocrystalline TiO_2 solar cells with polythiophene hole conductors *Sol. Energy Mater. Sol. Cells* **88** 11–21
[124] Lancelle-Beltran E, Prené P, Boscher C, Belleville P, Buvat P, Lambert S, Guillet F, Marcel C and Sanchez C 2008 Solid-state organic/inorganic hybrid solar cells based on poly(octylthiophene) and dye-sensitized nanobrookite and nanoanatase TiO_2 electrodes *Eur. J. Inorg. Chem.* 903–10
[125] Lancelle-Beltran E, Prené P, Boscher C, Belleville P, Buvat P and Sanchez C 2006 All-solid-state dye-sensitized nanoporous TiO_2 hybrid solar cells with high energy-conversion efficiency *Adv. Mater.* **18** 2579–82
[126] Zhu R, Jiang C-Y, Liu B and Ramakrishna S 2009 Highly efficient nanoporous TiO_2-polythiophene hybrid solar cells based on interfacial modification using a metal-free organic dye *Adv. Mater.* **21** 994–1000
[127] Jiang K-J, Manseki K, Yu Y-H, Masaki N, Suzuki K, Song Y and Yanagida S 2009 Photovoltaics based on hybridization of effective dye-sensitized titanium oxide and hole-conductive polymer P3HT *Adv. Funct. Mater.* **19** 2481–5
[128] Mor G K, Kim S, Paulose M, Varghese O K, Shankar K, Basham J and Grimes C A 2009 Visible to near-infrared light harvesting in TiO_2 nanotube array-P3HT based heterojunction solar cells *Nano Lett.* **9** 4250–7
[129] Yue G, Wu J, Lin J, Huang M, Yao Y, Fan L and Xiao Y 2011 Application of poly (3, 4-ethylenedioxythiophene): polystyrenesulfonate counter electrode in polymer heterojunction dye-sensitized solar cells *Front. Optoelectron. China* **4** 369–77
[130] Kim J, Koh J K, Kim B, Ahn S H, Ahn H, Ryu D Y, Kim J H and Kim E 2011 Enhanced performance of I2-free solid-state dye-sensitized solar cells with conductive polymer up to 6.8% *Adv. Funct. Mater.* **21** 4633–9
[131] Burschka J, Dualeh A, Kessler F, Baranoff E, Cevey-Ha N-L, Yi C, Nazeeruddin M K and Grätzel M 2011 Tris(2-(1*H*-pyrazol-1-yl) pyridine)cobalt(III) as p-type dopant for organic semiconductors and its application in highly efficient solid-state dye-sensitized solar cells *J. Am. Chem. Soc.* **133** 18042–5
[132] Grätzel M 2009 Recent advances in sensitized mesoscopic solar cells *Acc. Chem. Res.* **42** 1788–98
[133] Nazeeruddin M K, Péchy P and Grätzel M 1997 Efficient panchromatic sensitization of nanocrystalline TiO_2 films by a black dye based on a trithiocyanato–ruthenium complex *Chem. Commun.* **0** 1705–6
[134] Nazeeruddin M K *et al* 2001 Engineering of efficient panchromatic sensitizers for nanocrystalline TiO_2-based solar cells *J. Am. Chem. Soc.* **123** 1613–24
[135] Barolo C *et al* 2006 Synthesis, characterization, and DFT-TDDFT computational study of a ruthenium complex containing a functionalized tetradentate ligand *Inorg. Chem.* **45** 4642–53
[136] Klein C, Nazeeruddin M K, Liska P, Di Censo D, Hirata N, Palomares E, Durrant J R and Gratzel M 2005 Engineering of a novel ruthenium sensitizer and its application in dye-sensitized solar cells for conversion of sunlight into electricity *Inorg. Chem.* **44** 178–80
[137] Jiang K-J, Masaki N, Xia J, Noda S and Yanagida S 2006 A novel ruthenium sensitizer with a hydrophobic 2-thiophen-2-yl-vinyl-conjugated bipyridyl ligand for effective dye sensitized TiO_2 solar cells *Chem. Commun.* **23** 2460
[138] Altobello S, Argazzi R, Caramori S, Contado C, Da Fré S, Rubino P, Choné C, Larramona G and Bignozzi C A 2005 Sensitization of nanocrystalline TiO_2 with black absorbers based on Os and Ru polypyridine complexes *J. Am. Chem. Soc.* **127** 15342–3
[139] Lammi R K, Wagner R W, Ambroise A, Diers J R, Bocian D F, Holten D and Lindsey J S 2001 Mechanisms of excited-state energy-transfer grating in linear versus branched multiporphyrin arrays *J. Phys. Chem.* B **105** 5341–52
[140] Liu Y, Xiang N, Feng X, Shen P, Zhou W, Weng C, Zhao B and Tan S 2009 Thiophene-linked porphyrin derivatives for dye-sensitized solar cells *Chem. Commun.* **18** 2499
[141] Eu S, Katoh T, Umeyama T, Matano Y and Imahori H 2008 Synthesis of sterically hindered phthalocyanines and their applications to dye-sensitized solar cells *Dalton Trans.* **40** 5476
[142] Hara K, Sato T, Katoh R, Furube A, Ohga Y, Shinpo A, Suga S, Sayama K, Sugihara H and Arakawa H 2003 Molecular design of coumarin dyes for efficient dye-sensitized solar cells *J. Phys. Chem.* B **107** 597–606
[143] Hara K, Wang Z S, Sato T, Furube A, Katoh R, Sugihara H, Dan-Oh Y, Kasada C, Shinpo A and Suga S 2005 Oligothiophene-containing coumarin dyes for efficient dye-sensitized solar cells *J. Phys. Chem.* B **109** 15476–82
[144] Wang Z-S, Cui Y, Dan-oh Y, Kasada C, Shinpo A and Hara K 2008 Molecular design of coumarin dyes for stable and efficient organic dye-sensitized solar cells *J. Phys. Chem.* C **112** 17011–7
[145] Horiuchi T, Miura H, Sumioka K and Uchida S 2004 High efficiency of dye-sensitized solar cells based on metal-free indoline dyes *J. Am. Chem. Soc.* **126** 12218–9

[146] Ito S et al 2006 High-efficiency organic-dye- sensitized solar cells controlled by nanocrystalline-TiO_2 electrode thickness *Adv. Mater.* **18** 1202–5
[147] Ito S, Miura H, Uchida S, Takata M, Sumioka K, Liska P, Comte P, Péchy P and Grätzel M 2008 High-conversion-efficiency organic dye-sensitized solar cells with a novel indoline dye *Chem. Commun.* **41** 5194
[148] Hao Y, Yang X, Cong J, Tian H, Hagfeldt A and Sun L 2009 Efficient near infrared D–π–a sensitizers with lateral anchoring group for dye-sensitized solar cells *Chem. Commun.* **27** 4031
[149] Tian H, Yang X, Chen R, Hagfeldt A and Sun L 2009 A metal-free 'black dye' for panchromatic dye-sensitized solar cells *Energy Environ. Sci.* **2** 674
[150] Hara K, Kurashige M, Ito S, Shinpo A, Suga S, Sayama K and Arakawa H 2003 Novel polyene dyes for highly efficient dye-sensitized solar cells *Chem. Commun.* **2** 252
[151] Hara K et al 2005 Novel conjugated organic dyes for efficient dye-sensitized solar cells *Adv. Funct. Mater.* **15** 246–52
[152] Zhao W, Jun Hou Y, Song Wang X, Wen Zhang B, Cao Y, Yang R, Bo Wang W and Rui Xiao X 1999 Study on squarylium cyanine dyes for photoelectric conversion *Sol. Energy Mater. Sol. Cells* **58** 173–83
[153] Erten-Ela S, Yilmaz M D, Icli B, Dede Y, Icli S and Akkaya E U 2008 A panchromatic boradiazaindacene (BODIPY) sensitizer for dye-sensitized solar cells *Org. Lett.* **10** 3299–302
[154] Hardin B E, Snaith H J and McGehee M D 2012 The renaissance of dye-sensitized solar cells *Nat. Photon.* **6** 162–9
[155] Wu J H, Hao S C, Lan Z, Lin J M, Huang M L, Huang Y F, Fang L Q, Yin S and Sato T 2007 A thermoplastic gel electrolyte for stable quasi-solid-state dye-sensitized solar cells *Adv. Funct. Mater.* **17** 2645–52
[156] Wu J H, Lan Z, Lin J M, Huang M L, Hao S C, Sato T and Yin S 2007 A novel thermosetting gel electrolyte for stable quasi-solid-state dye-sensitized solar cells *Adv. Mater.* **19** 4006–11
[157] Benedetti J E, Gonçalves A D, Formiga A L B, De Paoli M-A, Li X, Durrant J R and Nogueira A F 2010 A polymer gel electrolyte composed of a poly(ethylene oxide) copolymer and the influence of its composition on the dynamics and performance of dye-sensitized solar cells *J. Power Sources* **195** 1246–55
[158] Ye M, Wen X, Wang M, Iocozzia J, Zhang N, Lin C and Lin Z 2015 Recent advances in dye-sensitized solar cells: from photoanodes, sensitizers and electrolytes to counter electrodes *Mater. Today* **18** 155–62
[159] Cester A, Wrachien N, Bon M, Meneghesso G, Bertani R, Tagliaferro R, Casolucci S, Brown T M, Reale A and Di Carlo A 2015 Degradation mechanisms of dye-sensitized solar cells: light, bias and temperature effects *2015 IEEE Int. Reliability Physics Symp.* (Piscataway, NJ: IEEE) p 1–3E
[160] Grünwald R and Tributsch H 1997 Mechanisms of instability in Ru-based dye sensitization solar cells *J. Phys. Chem.* B **101** 2564–75
[161] Hara K, Wang Z-S, Cui Y, Furube A and Koumura N 2009 Long-term stability of organic–dye-sensitized solar cells based on an alkyl-functionalized carbazole dye *Energy Environ. Sci.* **2** 1109
[162] Hinsch A, Kroon J M, Kern R, Uhlendorf I, Holzbock J, Meyer A and Ferber J 2001 Long-term stability of dye-sensitised solar cells *Prog. Photovolt., Res. Appl.* **9** 425–38
[163] Ye M, Gao X, Hong X, Liu Q, He C, Liu X and Lin C 2017 Recent advances in quantum dot-sensitized solar cells: insights into photoanodes, sensitizers, electrolytes and counter electrodes *Sustain Energy Fuels* **1** 1217–31
[164] Nozik A J 2002 Quantum dot solar cells *Physica* E **14** 115–20
[165] Mora-Sero I, Giménez S, Fabregat-Santiago F, Gómez R, Shen Q, Toyoda T and Bisquert J 2009 Recombination in quantum dot sensitized solar cells *Acc. Chem. Res.* **42** 1848–57
[166] Hwang I and Yong K 2015 Counter electrodes for quantum-dot-sensitized solar cells *Chem. Electron. Chem.* **2** 634–53
[167] Klimov V I 2006 Mechanisms for photogeneration and recombination of multiexcitons in semiconductor nanocrystals: implications for lasing and solar energy conversion *J. Phys. Chem.* B **110** 16827–45
[168] Schaller R D, Sykora M, Pietryga J M and Klimov V I 2006 Seven excitons at a cost of one: redefining the limits for conversion efficiency of photons into charge carriers *Nano Lett.* **6** 424–9
[169] Trinh M T, Houtepen A J, Schins J M, Hanrath T, Piris J, Knulst W, Goossens A P L M and Siebbeles L D A 2008 In spite of recent doubts carrier multiplication does occur in PbSe nanocrystals *Nano Lett.* **8** 1713–8
[170] Du J et al 2016 Zn–Cu–In–Se quantum dot solar cells with a certified power conversion efficiency of 11.6% *J. Am. Chem. Soc.* **138** 4201–9
[171] Kongkanand A, Tvrdy K, Takechi K, Kuno M and Kamat P V 2008 Quantum dot solar cells. Tuning photoresponse through size and shape control of CdSe-TiO_2 architecture *J. Am. Chem. Soc.* **130** 4007–15
[172] Vogel R, Hoyer P and Weller H 1994 Quantum-sized PbS, CdS, Ag_2S, Sb_2S_3, and Bi_2S_3 particles as sensitizers for various nanoporous wide-bandgap semiconductors *J. Phys. Chem.* **98** 3183–8
[173] Ross R T and Nozik A J 1982 Efficiency of hot-carrier solar energy converters *J. Appl. Phys.* **53** 3813–8
[174] Robel I, Kuno M and Kamat P V 2007 Size-dependent electron injection from excited CdSe quantum dots into TiO_2 nanoparticles *J. Am. Chem. Soc.* **129** 4136–7
[175] Pan Z, Zhao K, Wang J, Zhang H, Feng Y and Zhong X 2013 Near infrared absorption of $CdSe_x Te_{1-x}$ alloyed quantum dot sensitized solar cells with more than 6% efficiency and high stability *ACS Nano* **7** 5215–22
[176] Lee H J, Wang M, Chen P, Gamelin D R, Zakeeruddin S M, Gratzel M and Nazeeruddin M K 2009 Efficient CdSe quantum dot-sensitized solar cells prepared by an improved successive ionic layer adsorption and reaction process *Nano Lett.* **9** 4221–7
[177] Duan J, Zhang H, Tang Q, He B and Yu L 2015 Recent advances in critical materials for quantum dot-sensitized solar cells: a review *J. Mater. Chem.* A **3** 17497–510
[178] Hod I and Zaban A 2014 Materials and interfaces in quantum dot sensitized solar cells: challenges, advances and prospects *Langmuir* **30** 7264–73
[179] Liao Y, Zhang J, Liu W, Que W, Yin X, Zhang D, Tang L, He W, Zhong Z and Zhang H 2015 Enhancing the efficiency of CdS quantum dot-sensitized solar cells via electrolyte engineering *Nano Energy* **11** 88–95
[180] Chou C-Y, Lee C-P, Vittal R and Ho K-C 2011 Efficient quantum dot-sensitized solar cell with polystyrene-modified TiO_2 photoanode and with guanidine thiocyanate in its polysulfide electrolyte *J. Power Sources* **196** 6595–602
[181] Li L, Yang X, Gao J, Tian H, Zhao J, Hagfeldt A and Sun L 2011 Highly efficient CdS quantum dot-sensitized solar cells based on a modified polysulfide electrolyte *J. Am. Chem. Soc.* **133** 8458–60
[182] Giménez S, Mora-Seró I, Macor L, Guijarro N, Lana-Villarreal T, Gómez R, Diguna L J, Shen Q, Toyoda T and Bisquert J 2009 Improving the performance of colloidal quantum-dot-sensitized solar cells *Nanotechnology* **20** 295204
[183] Gopi C V V M, Venkata-Haritha M, Kim S-K and Kim H-J 2015 Improved photovoltaic performance and stability of quantum dot sensitized solar cells using Mn–ZnSe shell structure with enhanced light absorption and recombination control *Nanoscale* **7** 12552–63

[184] Jovanovski V, González-Pedro V, Giménez S, Azaceta E, Cabañero G, Grande H, Tena-Zaera R, Mora-Seró I and Bisquert J 2011 A sulfide/polysulfide-based ionic liquid electrolyte for quantum dot-sensitized solar cells *J. Am. Chem. Soc.* **133** 20156–9
[185] Feng W, Li Y, Du J, Wang W and Zhong X 2016 Highly efficient and stable quasi-solid-state quantum dot-sensitized solar cells based on a superabsorbent polyelectrolyte *J. Mater. Chem.* A **4** 1461–8
[186] Huo Z, Tao L, Wang S, Wei J, Zhu J, Dong W, Liu F, Chen S, Zhang B and Dai S 2015 A novel polysulfide hydrogel electrolyte based on low molecular mass organogelator for quasi-solid-state quantum dot-sensitized solar cells *J. Power Sources* **284** 582–7
[187] Roelofs K E, Brennan T P, Dominguez J C, Bailie C D, Margulis G Y, Hoke E T, McGehee M D and Bent S F 2013 Effect of Al_2O_3 recombination barrier layers deposited by atomic layer deposition in solid-state CdS quantum dot-sensitized solar cells *J. Phys. Chem.* C **117** 5584–92
[188] Qian J, Liu Q-S, Li G, Jiang K-J, Yang L-M and Song Y 2011 P3HT as hole transport material and assistant light absorber in CdS quantum dots-sensitized solid-state solar cells *Chem. Commun.* **47** 6461
[189] Feng W, Zhao L, Du J, Li Y and Zhong X 2016 Quasi-solid-state quantum dot sensitized solar cells with power conversion efficiency over 9% and high stability *J. Mater. Chem.* A **4** 14849–56
[190] Park J P, Heo J H, Im S H and Kim S-W 2016 Highly efficient solid-state mesoscopic PbS with embedded CuS quantum dot-sensitized solar cells *J. Mater. Chem.* A **4** 785–90
[191] Rühle S, Shalom M and Zaban A 2010 Quantum-dot-sensitized solar cells *ChemPhysChem* **11** 2290–304
[192] Roelofs K E, Brennan T P, Trejo O, Xu J, Prinz F B and Bent S F 2013 Effects of QD surface coverage in solid-state PbS quantum dot-sensitized solar cells *2013 IEEE 39th Photovoltaic Specialists Conf. (PVSC)* (Piscataway, NJ: IEEE) pp 1080–3
[193] Choi Y, Seol M, Kim W and Yong K 2014 Chemical bath deposition of stoichiometric CdSe quantum dots for efficient quantum-dot-sensitized solar cell application *J. Phys. Chem.* C **118** 5664–70
[194] Tubtimtae A, Lee M-W and Wang G-J 2011 Ag_2Se quantum-dot sensitized solar cells for full solar spectrum light harvesting *J. Power Sources* **196** 6603–8
[195] Liu F *et al* 2014 *Ex situ* CdSe quantum dot-sensitized solar cells employing inorganic ligand exchange to boost efficiency *J. Phys. Chem.* C **118** 214–22
[196] Yu X-Y, Liao J-Y, Qiu K-Q, Kuang D-B and Su C-Y 2011 Dynamic study of highly efficient CdS/CdSe quantum dot-sensitized solar cells fabricated by electrodeposition *ACS Nano* **5** 9494–500
[197] Zhu G, Lv T, Pan L, Sun Z and Sun C 2011 All spray pyrolysis deposited CdS sensitized ZnO films for quantum dot-sensitized solar cells *J. Alloys Compd.* **509** 362–5
[198] Dai Q, Sabio E M, Wang W and Tang J 2014 Pulsed laser deposition of Mn doped CdSe quantum dots for improved solar cell performance *Appl. Phys. Lett.* **104** 183901
[199] Robel I, Subramanian V, Kuno M and Kamat P V 2006 Quantum dot solar cells. Harvesting light energy with CdSe nanocrystals molecularly linked to mesoscopic TiO_2 films *J. Am. Chem. Soc.* **128** 2385–93
[200] Guijarro N, Lana-Villarreal T, Mora-Seró I, Bisquert J and Gómez R 2009 CdSe quantum dot-sensitized TiO_2 electrodes: effect of quantum dot coverage and mode of attachment *J. Phys. Chem.* C **113** 4208–14
[201] Mora-Seró I, Giménez S, Moehl T, Fabregat-Santiago F, Lana-Villareal T, Gómez R and Bisquert J 2008 Factors determining the photovoltaic performance of a CdSe quantum dot sensitized solar cell: the role of the linker molecule and of the counter electrode *Nanotechnology* **19** 424007
[202] Vogel R, Pohl K and Weller H 1990 Sensitization of highly porous polycrystalline TiO_2 electrodes by quantum size CdS *Chem. Phys. Lett.* **174** 241
[203] Toyoda T, Sato J and Shen Q 2003 Effect of sensitization by quantum-sized CdS on photoacoustic and photoelectrochemical current spectra of porous TiO_2 electrodes *Rev. Sci. Instrum.* **74** 297–9
[204] Shen Q, Kobayashi J, Diguna L J and Toyoda T 2008 Effect of ZnS coating on the photovoltaic properties of CdSe quantum dot-sensitized solar cells *J. Appl. Phys.* **103** 084304
[205] Toyoda T, Kobayashi J and Shen Q 2008 Correlation between crystal growth and photosensitization of nanostructured TiO_2 electrodes using supporting Ti substrates by self-assembled CdSe quantum dots *Thin Solid Films* **516** 2426–31
[206] Pan Z, Mora-Seró I, Shen Q, Zhang H, Li Y, Zhao K, Wang J, Zhong X and Bisquert J 2014 High-efficiency 'green' quantum dot solar cells *J. Am. Chem. Soc.* **136** 9203–10
[207] Li W and Zhong X 2015 Capping ligand-induced self-assembly for quantum dot sensitized solar cells *J. Phys. Chem. Lett.* **6** 796–806
[208] McDaniel H, Fuke N, Makarov N S, Pietryga J M and Klimov V I 2013 An integrated approach to realizing high-performance liquid-junction quantum dot sensitized solar cells *Nat. Commun.* **4** 2887
[209] Panthani M G, Stolle C J, Reid D K, Rhee D J, Harvey T B, Akhavan V A, Yu Y and Korgel B A 2013 $CuInSe_2$ quantum dot solar cells with high open-circuit voltage *J. Phys. Chem. Lett.* **4** 2030–4
[210] Kim J-Y, Yang J, Yu J H, Baek W, Lee C-H, Son H J, Hyeon T and Ko M J 2015 Highly efficient copper–indium–selenide quantum dot solar cells: suppression of carrier recombination by controlled ZnS overlayers *ACS Nano* **9** 11286–95
[211] Regulacio M D and Han M-Y 2010 Composition-tunable alloyed semiconductor nanocrystals *Acc. Chem. Res.* **43** 621–30
[212] Zhong X, Han M, Dong Z, White T J and Knoll W 2003 Composition-tunable $Zn_xCd_{1-x}Se$ nanocrystals with high luminescence and stability *J. Am. Chem. Soc.* **125** 8589–94
[213] Fuke N, Hoch L B, Koposov A Y, Manner V W, Werder D J, Fukui A, Koide N, Katayama H and Sykora M 2010 CdSe quantum-dot-sensitized solar cell with ~100% internal quantum efficiency *ACS Nano* **4** 6377–86
[214] Sambur J B, Novet T and Parkinson B A 2010 Multiple exciton collection in a sensitized photovoltaic system *Science* **330** 63–6
[215] Nozik A J, Beard M C, Luther J M, Law M, Ellingson R J and Johnson J C 2010 Semiconductor quantum dots and quantum dot arrays and applications of multiple exciton generation to third-generation photovoltaic solar cells *Chem. Rev.* **110** 6873
[216] Maria A, Cyr P W, Klem E J D, Levina L and Sargent E H 2005 Solution-processed infrared photovoltaic devices with >10% monochromatic internal quantum efficiency *Appl. Phys. Lett.* **87** 213112
[217] Carey G H, Abdelhady A L, Ning Z, Thon S M, Bakr O M and Sargent E H 2015 Colloidal quantum dot solar cells *Chem. Rev.* **115** 12732–63
[218] Piliego C, Protesescu L, Bisri S Z, Kovalenko M V and Loi M A 2013 5.2% efficient PbS nanocrystal Schottky solar cells *Energy Environ. Sci.* **6** 3054
[219] Henry C H 1980 Limiting efficiencies of ideal single and multiple energy gap terrestrial solar cells *J. Appl. Phys.* **51** 4494–500
[220] Pattantyus-Abraham A G, Kramer I J, Barkhouse A R, Wang X, Konstantatos G, Debnath R, Levina L, Raabe I, Nazeeruddin M K and Gratzel M 2010 Depleted-heterojunction colloidal quantum dot solar cells *ACS Nano* **4** 3374–80
[221] Sanehira E M, Marshall A R, Christians J A, Harvey S P, Ciesielski P N, Wheeler L M, Schulz P, Lin L Y, Beard M C and Luther J M 2017 Enhanced mobility $CsPbI_3$ quantum dot arrays for record-efficiency, high-voltage photovoltaic cells *Sci. Adv.* **3** eaao4204

[222] Mcdonald S A, Konstantatos G, Zhang S, Cyr P W, Klem E J D, Levina L and Sargent E H 2005 Solution-processed PbS quantum dot infrared photodetectors and photovoltaics *Nat. Mater.* **4** 138–42
[223] Hines M A and Scholes G D 2003 Colloidal PbS nanocrystals with size-tunable near-infrared emission: observation of post-synthesis self-narrowing of the particle size distribution *Adv. Mater.* **15** 1844–9
[224] Chuang C-H M, Brown P R, Bulović V and Bawendi M G 2014 Improved performance and stability in quantum dot solar cells through band alignment engineering *Nat. Mater.* **13** 796–801
[225] Semonin O E, Luther J M, Choi S, Chen H Y, Gao J, Nozik A J and Beard M C 2011 Peak external photocurrent quantum efficiency exceeding 100% via MEG in a quantum dot solar cell *Science* **334** 1530–3
[226] Tisdale W A, Williams K J, Timp B A, Norris D J, Aydil E S and Zhu X-Y 2010 Hot-electron transfer from semiconductor nanocrystals *Science* **328** 1543–7
[227] Gao J, Zhang J, van de Lagemaat J, Johnson J C and Beard M C 2014 Charge generation in PbS quantum dot solar cells characterized by temperature-dependent steady-state photoluminescence *ACS Nano* **8** 12814–25
[228] Guyot-Sionnest P 2012 Electrical transport in colloidal quantum dot films *J. Phys. Chem. Lett.* **3** 1169–75
[229] Liu Y, Tolentino J, Gibbs M, Ihly R, Perkins C L, Liu Y, Crawford N, Hemminger J C and Law M 2013 PbSe quantum dot field-effect transistors with air-stable electron mobilities above 7 $cm^2 V^{-1} s^{-1}$ *Nano Lett.* **13** 1578–87
[230] Klem E J D, Shukla H, Hinds S, MacNeil D D, Levina L and Sargent E H 2008 Impact of dithiol treatment and air annealing on the conductivity, mobility, and hole density in PbS colloidal quantum dot solids *Appl. Phys. Lett.* **92** 212105
[231] Gao J, Luther J M, Semonin O E, Ellingson R J, Nozik A J and Beard M C 2011 Quantum dot size dependent $J-V$ characteristics in heterojunction ZnO/PbS quantum dot solar cells *Nano Lett.* **11** 1002–8
[232] Tang J *et al* 2011 Colloidal-quantum-dot photovoltaics using atomic-ligand passivation *Nat. Mater.* **10** 765–71
[233] Lee J-S, Kovalenko M V, Huang J, Chung D S and Talapin D V 2011 Band-like transport, high electron mobility and high photoconductivity in all-inorganic nanocrystal arrays *Nat. Nanotechnol.* **6** 348–52
[234] Tang J *et al* 2010 Quantum dot photovoltaics in the extreme quantum confinement regime: the surface-chemical origins of exceptional air- and light-stability *ACS Nano* **4** 869–78
[235] Kramer I J, Levina L, Debnath R, Zhitomirsky D and Sargent E H 2011 Solar cells using quantum funnels *Nano Lett.* **11** 3701–6
[236] Adinolfi V, Ning Z, Xu J, Masala S, Zhitomirsky D, Thon S M and Sargent E H 2013 Electric field engineering using quantum-size-effect-tuned heterojunctions *Appl. Phys. Lett.* **103** 011106
[237] Yuan M *et al* 2013 Doping control via molecularly engineered surface ligand coordination *Adv. Mater.* **25** 5586–92
[238] Liu H *et al* 2011 Electron acceptor materials engineering in colloidal quantum dot solar cells *Adv. Mater.* **23** 3832–7
[239] Hoye R L Z *et al* 2014 Improved open-circuit voltage in ZnO–PbSe quantum dot solar cells by understanding and reducing losses arising from the ZnO conduction band tail *Adv. Energy Mater.* **4** 1301544
[240] Liu Y, Gibbs M, Perkins C L, Tolentino J, Zarghami M H, Bustamante J and Law M 2011 Robust, functional nanocrystal solids by infilling with atomic layer deposition *Nano Lett.* **11** 5349–55
[241] Luther J M, Law M, Song Q, Perkins C L, Beard M C and Nozik A J 2008 Structural, optical, and electrical properties of self-assembled films of PbSe nanocrystals treated with 1,2-ethanedithiol *ACS Nano* **2** 271–80
[242] Pourret A, Guyot-Sionnest P and Elam J W 2009 Atomic layer deposition of ZnO in quantum dot thin films *Adv. Mater.* **21** 232–5
[243] Ten Cate S, Liu Y, Suchand Sandeep C S, Kinge S, Houtepen A J, Savenije T J, Schins J M, Law M and Siebbeles L D A 2013 Activating carrier multiplication in PbSe quantum dot solids by infilling with atomic layer deposition *J. Phys. Chem. Lett.* **4** 1766–70
[244] Jeong K S *et al* 2012 Enhanced mobility-lifetime products in PbS colloidal quantum dot photovoltaics *ACS Nano* **6** 89–99
[245] Bae W K, Joo J, Padilha L A, Won J, Lee D C, Lin Q, Koh W, Luo H, Klimov V I and Pietryga J M 2012 Highly effective surface passivation of PbSe quantum dots through reaction with molecular chlorine *J. Am. Chem. Soc.* **134** 20160–8
[246] Moreels I, Justo Y, De Geyter B, Haustraete K, Martins J C and Hens Z 2011 Size-tunable, bright, and stable PbS quantum dots: a surface chemistry study *ACS Nano* **5** 2004–12
[247] Zhang J, Gao J, Miller E M, Luther J M and Beard M C 2014 Diffusion-controlled synthesis of PbS and PbSe quantum dots with *in situ* halide passivation for quantum dot solar cells *ACS Nano* **8** 614–22
[248] Woo J Y, Ko J-H, Song J H, Kim K, Choi H, Kim Y-H, Lee D C and Jeong S 2014 Ultrastable PbSe nanocrystal quantum dots via *in situ* formation of atomically thin halide adlayers on PbSe(100) *J. Am. Chem. Soc.* **136** 8883–6
[249] Hughes B K, Luther J M and Beard M C 2012 The subtle chemistry of colloidal, quantum-confined semiconductor nanostructures *ACS Nano* **6** 4573–9
[250] Zhang J, Gao J, Church C P, Miller E M, Luther J M, Klimov V I and Beard M C 2014 PbSe quantum dot solar cells with more than 6% efficiency fabricated in ambient atmosphere *Nano Lett.* **14** 6010–5
[251] van Dam D, van Hoof N J J, Cui Y, van Veldhoven P J, Bakkers E P A M, Gómez Rivas J and Haverkort J E M 2016 High-efficiency nanowire solar cells with omnidirectionally enhanced absorption due to self-aligned indium-tin-oxide mie scatterers *ACS Nano* **10** 11414–9
[252] Han N, Yang Z, Wang F, Dong G, Yip S, Liang X, Hung T F, Chen Y and Ho J C 2015 High-performance GaAs nanowire solar cells for flexible and transparent photovoltaics *ACS Appl. Mater. Interfaces* **7** 20454–9
[253] Kayes B M, Atwater H A and Lewis N S 2005 Comparison of the device physics principles of planar and radial p–n junction nanorod solar cells *J. Appl. Phys.* **97** 114302
[254] Garnett E and Yang P 2010 Light trapping in silicon nanowire solar cells *Nano Lett.* **10** 1082–7
[255] Hu L and Chen G 2007 Analysis of optical absorption in silicon nanowire arrays for photovoltaic applications *Nano Lett.* **7** 3249–52
[256] Lin C and Povinelli M L 2009 Optical absorption enhancement in silicon nanowire arrays with a large lattice constant for photovoltaic applications *Opt. Express* **17** 19371
[257] Tsakalakos L *et al* 2007 Strong broadband optical absorption in silicon nanowire films *J. Nanophotonics* **1** 013552
[258] Tian B, Zheng X, Kempa T J, Fang Y, Yu N, Yu G, Huang J and Lieber C M 2007 Coaxial silicon nanowires as solar cells and nanoelectronic power sources *Nature* **449** 885–9
[259] Cao L, White J S, Park J-S, Schuller J A, Clemens B M and Brongersma M L 2009 Engineering light absorption in semiconductor nanowire devices *Nat. Mater.* **8** 643–7
[260] Park J-S *et al* 2017 Enhancement of light absorption in silicon nanowire photovoltaic devices with dielectric and metallic grating structures *Nano Lett.* **17** 7731–6
[261] Hu S, Chi C-Y, Fountaine K T, Yao M, Atwater H A, Dapkus P D, Lewis N S and Zhou C 2013 Optical, electrical, and solar energy-conversion properties of gallium arsenide nanowire-array photoanodes *Energy Environ. Sci.* **6** 1879
[262] LaPierre R R 2011 Numerical model of current–voltage characteristics and efficiency of GaAs nanowire solar cells *J. Appl. Phys.* **109** 034311

[263] Xu Y, Gong T and Munday J N 2015 The generalized Shockley–Queisser limit for nanostructured solar cells *Sci. Rep.* **5** 13536
[264] Wang X, Khan M R, Lundstrom M and Bermel P 2014 Performance-limiting factors for GaAs-based single nanowire photovoltaics *Opt. Express* **22** A344
[265] Tsakalakos L, Balch J, Fronheiser J, Korevaar B A, Sulima O and Rand J 2007 Silicon nanowire solar cells *Appl. Phys. Lett.* **91** 233117
[266] Stelzner T, Pietsch M, Andrä G, Falk F, Ose E and Christiansen S 2008 Silicon nanowire-based solar cells *Nanotechnology* **19** 295203
[267] Kelzenberg M D, Turner-Evans D B, Kayes B M, Filler M A, Putnam M C, Lewis N S and Atwater H A 2008 Photovoltaic measurements in single-nanowire silicon solar cells *Nano Lett.* **8** 710–4
[268] Krogstrup P, Jørgensen H I, Heiss M, Demichel O, Holm J V, Aagesen M, Nygard J and Fontcuberta i Morral A 2013 Single-nanowire solar cells beyond the Shockley–Queisser limit *Nat. Photonics* **7** 306–10
[269] Aberg I *et al* 2016 A GaAs nanowire array solar cell with 15.3% efficiency at 1 Sun *IEEE J. Photovolt.* **6** 185–90
[270] Ghahfarokhi O M, Anttu N, Samuelson L and Aberg I 2016 Performance of GaAs nanowire array solar cells for varying incidence angles *IEEE J. Photovolt.* **6** 1502–8
[271] Trojnar A H, Valdivia C E, LaPierre R R, Hinzer K and Krich J J 2016 Optimizations of GaAs nanowire solar cells *IEEE J. Photovolt.* **6** 1494–501
[272] Im J-H, Luo J, Franckevičius M, Pellet N, Gao P, Moehl T, Zakeeruddin S M, Nazeeruddin M K, Grätzel M and Park N-G 2015 Nanowire perovskite solar cell *Nano Lett.* **15** 2120–6
[273] Anttu N 2015 Shockley–queisser detailed balance efficiency limit for nanowire solar cells *ACS Photonics* **2** 446–53
[274] Anttu N and Xu H Q 2013 Efficient light management in vertical nanowire arrays for photovoltaics *Opt. Express* **21** A558
[275] Li J, Yu H and Li Y 2012 Solar energy harnessing in hexagonally arranged Si nanowire arrays and effects of array symmetry on optical characteristics *Nanotechnology* **23** 194010
[276] Fountaine K T, Whitney W S and Atwater H A 2014 Resonant absorption in semiconductor nanowires and nanowire arrays: Relating leaky waveguide modes to Bloch photonic crystal modes *J. Appl. Phys.* **116** 153106
[277] Dhindsa N, Chia A, Boulanger J, Khodadad I, LaPierre R and Saini S S 2014 Highly ordered vertical GaAs nanowire arrays with dry etching and their optical properties *Nanotechnology* **25** 305303
[278] Walia J, Dhindsa N, Khorasaninejad M and Saini S S 2014 Color generation and refractive index sensing using diffraction from 2D silicon nanowire arrays *Small* **10** 144–51
[279] Khorasaninejad M, Patchett S, Sun J, Mochizuki-Oda N and Saini S S 2013 Diameter dependence of polarization resolved reflectance from vertical silicon nanowire arrays: evidence of tunable absorption *J. Appl. Phys.* **114** 024304
[280] Kupec J, Stoop R L and Witzigmann B 2010 Light absorption and emission in nanowire array solar cells *Opt. Express* **18** 27589
[281] Otnes G and Borgström M T 2017 Towards high efficiency nanowire solar cells *Nano Today* **12** 31–45
[282] Yu P, Wu J, Liu S, Xiong J, Jagadish C and Wang Z M 2016 Design and fabrication of silicon nanowires towards efficient solar cells *Nano Today* **11** 704–37
[283] Joyce H J *et al* 2012 Ultralow surface recombination velocity in InP nanowires probed by terahertz spectroscopy *Nano Lett.* **12** 5325–30
[284] Wallentin J, Ek M, Wallenberg L R, Samuelson L and Borgström M T 2012 Electron trapping in InP nanowire FETs with stacking faults *Nano Lett.* **12** 151–5
[285] Wallentin J and Borgström M T 2011 Doping of semiconductor nanowires *J. Mater. Res.* **26** 2142–56
[286] Nduwimana A and Wang X-Q 2009 Charge carrier separation in modulation doped coaxial semiconductor nanowires *Nano Lett.* **9** 283–6
[287] Murthy D H K *et al* 2011 Efficient photogeneration of charge carriers in silicon nanowires with a radial doping gradient *Nanotechnology* **22** 315710
[288] Parkinson P, Lloyd-Hughes J, Gao Q, Tan H H, Jagadish C, Johnston M B and Herz L M 2007 Transient terahertz conductivity of GaAs nanowires *Nano Lett.* **7** 2162–5
[289] Joyce H J, Docherty C J, Gao Q, Tan H H, Jagadish C, Lloyd-Hughes J, Herz L M and Johnston M B 2013 Electronic properties of GaAs, InAs and InP nanowires studied by terahertz spectroscopy *Nanotechnology* **24** 214006
[290] Mohite A D, Perea D E, Singh S, Dayeh S A, Campbell I H, Picraux S T and Htoon H 2012 Highly efficient charge separation and collection across *in situ* doped axial VLS-grown Si nanowire p–n junctions *Nano Lett.* **12** 1965–71
[291] Saurdi I, Shafura A K, Azhar N E A, Ishak A, Malek M F, Alrokayan A H S, Khan H A, Mamat M H and Rusop M 2016 Effect of Nb-doped TiO_2 on nanocomposited aligned ZnO nanorod/TiO_2:Nb for dye-sensitized solar cells *AIP Conf. Proc.* **1733** 020064
[292] Madel M, Huber F, Mueller R, Amann B, Dickel M, Xie Y and Thonke K 2017 Persistent photoconductivity in ZnO nanowires: influence of oxygen and argon ambient *J. Appl. Phys.* **121** 124301
[293] Mun Wong K, Alay-e-Abbas S M, Fang Y, Shaukat A and Lei Y 2013 Spatial distribution of neutral oxygen vacancies on ZnO nanowire surfaces: an investigation combining confocal microscopy and first principles calculations *J. Appl. Phys.* **114** 034901
[294] Baek M, Kim D and Yong K 2017 Simple but effective way to enhance photoelectrochemical solar-water-splitting performance of ZnO nanorod arrays: charge-trapping $Zn(OH)_2$ annihilation and oxygen vacancy generation by vacuum annealing *ACS Appl. Mater. Interfaces* **9** 2317–25
[295] Czaban J A, Thompson D A and LaPierre R R 2009 GaAs core−shell nanowires for photovoltaic applications *Nano Lett.* **9** 148–54
[296] Christesen J D, Zhang X, Pinion C W, Celano T A, Flynn C J and Cahoon J F 2012 Design principles for photovoltaic devices based on Si nanowires with axial or radial p–n junctions *Nano Lett.* **12** 6024–9
[297] Li J-S, Zhang X, Yan X, Chen X, Li L, Cui J-G, Huang Y-Q and Ren X-M 2014 Fabrication and electrical properties of axial and radial GaAs nanowire pn junction diode arrays *Chin. Phys.* B **23** 128503
[298] Gharghi M, Fathi E, Kante B, Sivoththaman S and Zhang X 2012 Heterojunction silicon microwire solar cells *Nano Lett.* **12** 6278–82
[299] Yoo J, Dayeh S A, Tang W and Picraux S T 2013 Epitaxial growth of radial Si p–i–n junctions for photovoltaic applications *Appl. Phys. Lett.* **102** 093113
[300] Park K-T, Kim H-J, Park M-J, Jeong J-H, Lee J, Choi D-G, Lee J-H and Choi J-H 2015 13.2% efficiency Si nanowire/PEDOT:PSS hybrid solar cell using a transfer-imprinted Au mesh electrode *Sci. Rep.* **5** 12093
[301] Mariani G, Wong P-S, Katzenmeyer A M, Léonard F, Shapiro J and Huffaker D L 2011 Patterned radial GaAs nanopillar solar cells *Nano Lett.* **11** 2490–4
[302] Wallentin J *et al* 2013 InP nanowire array solar cells achieving 13.8% efficiency by exceeding the ray optics limit *Science* **339** 1057–60
[303] Ye Y *et al* 2010 High-performance single CdS nanowire (nanobelt) Schottky junction solar cells with Au/graphene Schottky electrodes *ACS Appl. Mater. Interfaces* **2** 3406–10
[304] Pishekloo S P, Dariani R S and Salehi F 2016 Fabrication of CdS nanowires on TiO_2 nanorods for solar cell application *Mater. Sci. Semicond. Process.* **43** 182–6

[305] Dang H and Singh V P 2015 Nanowire CdS–CdTe solar cells with molybdenum oxide as contact *Sci. Rep.* **5** 14859
[306] Hsueh T-J, Hsu C-L, Chang S-J, Guo P-W, Hsieh J-H and Chen I-C 2007 Cu_2O/n-ZnO nanowire solar cells on ZnO:Ga/glass templates *Scr. Mater.* **57** 53–6
[307] Xu C, Shin P, Cao L and Gao D 2010 Preferential growth of long ZnO nanowire array and its application in dye-sensitized solar cells *J. Phys. Chem.* C **114** 125–9
[308] Jeong S, Garnett E C, Wang S, Yu Z, Fan S, Brongersma M L, McGehee M D and Cui Y 2012 Hybrid silicon nanocone–polymer solar cells *Nano Lett.* **12** 2971–6
[309] Chen Y, Pistol M-E and Anttu N 2016 Design for strong absorption in a nanowire array tandem solar cell *Sci. Rep.* **6** 32349
[310] Royo M, De Luca M, Rurali R and Zardo I 2017 A review on III–V core–multishell nanowires: growth, properties, and applications *J. Phys. D: Appl. Phys.* **50** 143001
[311] Wacaser B A, Dick K A, Johansson J, Borgström M T, Deppert K and Samuelson L 2009 Preferential interface nucleation: an expansion of the VLS growth mechanism for nanowires *Adv. Mater.* **21** 153–65
[312] Dick K A 2008 A review of nanowire growth promoted by alloys and non-alloying elements with emphasis on Au-assisted III–V nanowires *Prog. Cryst. Growth Charact. Mater.* **54** 138–73
[313] Schmidt V, Wittemann J V, Senz S and Gösele U 2009 Silicon nanowires: a review on aspects of their growth and their electrical properties *Adv. Mater.* **21** 2681–702
[314] Wagner R S and Ellis W C 1964 Vapor–liquid–solid mechanism of single crystal growth *Appl. Phys. Lett.* **4** 89–90
[315] Nebol'sin V A, Shchetinin A A, Dolgachev A A and Korneeva V V 2005 Effect of the nature of the metal solvent on the vapor–liquid–solid growth rate of silicon whiskers *Inorg. Mater.* **41** 1256–9
[316] Hochbaum A I, Fan R, He R and Yang P 2005 Controlled growth of si nanowire arrays for device integration *Nano Lett.* **5** 457–60
[317] Schmidt V, Wittemann J V and Gösele U 2010 Growth, thermodynamics, and electrical properties of silicon nanowires *Chem. Rev.* **110** 361–88
[318] Schubert L, Werner P, Zakharov N D, Gerth G, Kolb F M, Long L, Gösele U and Tan T Y 2004 Silicon nanowhiskers grown on ⟨111⟩ Si substrates by molecular-beam epitaxy *Appl. Phys. Lett.* **84** 4968–70
[319] Fuhrmann B, Leipner H S, Höche H-R, Schubert L, Werner P and Gösele U 2005 Ordered arrays of silicon nanowires produced by nanosphere lithography and molecular beam epitaxy *Nano Lett.* **5** 2524–7
[320] Mohan P, Motohisa J and Fukui T 2005 Controlled growth of highly uniform, axial/radial direction-defined, individually addressable InP nanowire arrays *Nanotechnology* **16** 2903–7
[321] Inari M, Takeda J, Motohisa J and Fukui T 2004 Selective area MOVPE growth of InP and InGaAs pillar structures for InP-based two-dimensional photonic crystals *Physica* E **21** 620–4
[322] Zafar F and Iqbal A 2016 Indium phosphide nanowires and their applications in optoelectronic devices *Proc. R. Soc.* A **472** 20150804
[323] Huang Y *et al* 2013 InAs nanowires grown by metal–organic vapor-phase epitaxy (MOVPE) employing PS/PMMA diblock copolymer nanopatterning *Nano Lett.* **13** 5979–84
[324] Goto H, Nosaki K, Tomioka K, Hara S, Hiruma K, Motohisa J and Fukui T 2009 Growth of core–shell InP nanowires for photovoltaic application by selective-area metal organic vapor phase epitaxy *Appl. Phys. Express* **2** 035004
[325] Mariani G, Scofield A C, Hung C-H and Huffaker D L 2013 GaAs nanopillar-array solar cells employing *in situ* surface passivation *Nat. Commun.* **4** 1497
[326] Peng K, Xu Y, Wu Y, Yan Y, Lee S-T and Zhu J 2005 Aligned single-crystalline Si nanowire arrays for photovoltaic applications *Small* **1** 1062–7
[327] Huang Z, Fang H and Zhu J 2007 Fabrication of silicon nanowire arrays with controlled diameter, length, and density *Adv. Mater.* **19** 744–8
[328] Garnett E C and Yang P 2008 Silicon nanowire radial p−n junction solar cells *J. Am. Chem. Soc.* **130** 9224–5
[329] Choi W K, Liew T H, Dawood M K, Smith H I, Thompson C V and Hong M H 2008 Synthesis of silicon nanowires and nanofin arrays using interference lithography and catalytic etching *Nano Lett.* **8** 3799–802
[330] Vinzons L U, Shu L, Yip S, Wong C-Y, Chan L L H and Ho J C 2017 Unraveling the morphological evolution and etching kinetics of porous silicon nanowires during metal-assisted chemical etching *Nanoscale Res. Lett.* **12** 385
[331] Chen Y, Zhang C, Li L, Tuan C-C, Wu F, Chen X, Gao J, Ding Y and Wong C-P 2017 Fabricating and controlling silicon zigzag nanowires by diffusion-controlled metal-assisted chemical etching method *Nano Lett.* **17** 4304–10
[332] Peng K, Zhang M, Lu A, Wong N-B, Zhang R and Lee S-T 2007 Ordered silicon nanowire arrays via nanosphere lithography and metal-induced etching *Appl. Phys. Lett.* **90** 163123
[333] Yu X, Shen X, Mu X, Zhang J, Sun B, Zeng L, Yang L, Wu Y, He H and Yang D 2015 High efficiency organic/silicon-nanowire hybrid solar cells: significance of strong inversion layer *Sci. Rep.* **5** 17371
[334] He J, Gao P, Liao M, Yang X, Ying Z, Zhou S, Ye J and Cui Y 2015 Realization of 13.6% efficiency on 20 μm thick Si/organic hybrid heterojunction solar cells *via* advanced nanotexturing and surface recombination suppression *ACS Nano* **9** 6522–31
[335] Morales A M and Lieber C M 1998 A laser ablation method for the synthesis of crystalline semiconductor nanowires *Science* **279** 208–11
[336] Hsu C-M, Connor S T, Tang M X and Cui Y 2008 Wafer-scale silicon nanopillars and nanocones by Langmuir–Blodgett assembly and etching *Appl. Phys. Lett.* **93** 133109
[337] Li Z, Wang J, Singh N and Lee S 2011 Optical and electrical study of core-shell silicon nanowires for solar applications *Opt. Express* **19** A1057
[338] Arafa M, Youtsey C, Grundbacher R, Adesida I and Klem J 1994 Fabrication of nanostructures in AlGaSb/InAs using electron-beam lithography and chemically assisted ion-beam etching *J. Vac. Sci. Technol.* B **12** 3623
[339] Luo Y, Yan X, Zhang J, Li B, Wu Y, Lu Q, Jin C, Zhang X and Ren X 2018 A graphene/single GaAs nanowire Schottky junction photovoltaic device *Nanoscale* **10** 9212–7
[340] Metaferia W *et al* 2016 GaAsP nanowires grown by aerotaxy *Nano Lett.* **16** 5701–7
[341] Atwater H A and Polman A 2010 Plasmonics for improved photovoltaic devices *Nat. Mater.* **9** 205–13
[342] Erwin W R, Zarick H F, Talbert E M and Bardhan R 2016 Light trapping in mesoporous solar cells with plasmonic nanostructures *Energy Environ. Sci.* **9** 1577–601
[343] Clavero C 2014 Plasmon-induced hot-electron generation at nanoparticle/metal-oxide interfaces for photovoltaic and photocatalytic devices *Nat. Photon.* **8** 95–103
[344] Ritchie R H 1957 Plasma losses by fast electrons in thin films *Phys. Rev.* **106** 874–81
[345] Maier S A, Brongersma M L, Kik P G, Meltzer S, Requicha A A G and Atwater H A 2001 Plasmonics-A route to nanoscale optical devices *Adv. Mater.* **13** 1501–5

[346] Tian Y and Tatsuma T 2005 Mechanisms and applications of plasmon-induced charge separation at TiO_2 films loaded with gold nanoparticles *J. Am. Chem. Soc.* **127** 7632–7
[347] Tian Y and Tatsuma T 2004 Plasmon-induced photoelectrochemistry at metal nanoparticles supported on nanoporous TiO_2 *Chem. Commun.* **16** 1810
[348] Lana-Villarreal T and Gómez R 2005 Tuning the photoelectrochemistry of nanoporous anatase electrodes by modification with gold nanoparticles: development of cathodic photocurrents *Chem. Phys. Lett.* **414** 489–94
[349] Zhang X, Chen Y L, Liu R-S and Tsai D P 2013 Plasmonic photocatalysis *Reports Prog. Phys.* **76** 046401
[350] Linic S, Christopher P and Ingram D B 2011 Plasmonic-metal nanostructures for efficient conversion of solar to chemical energy *Nat. Mater.* **10** 911–21
[351] Cushing S K, Li J, Meng F, Senty T R, Suri S, Zhi M, Li M, Bristow A D and Wu N 2012 Photocatalytic activity enhanced by plasmonic resonant energy transfer from metal to semiconductor *J. Am. Chem. Soc.* **134** 15033–41
[352] Quint M T, Sarang S, Quint D A, Keshavarz A, Stokes B J, Subramaniam A B, Huang K C, Gopinathan A, Hirst L S and Ghosh S 2017 Plasmon-actuated nano-assembled microshells *Sci. Rep.* **7** 17788
[353] Song J, Zhou J and Duan H 2012 Self-assembled plasmonic vesicles of SERS-encoded amphiphilic gold nanoparticles for cancer cell targeting and traceable intracellular drug delivery *J. Am. Chem. Soc.* **134** 13458–69
[354] Maier S A and Atwater H A 2005 Plasmonics: localization and guiding of electromagnetic energy in metal/dielectric structures *J. Appl. Phys.* **98** 011101
[355] Zia R, Selker M D, Catrysse P B and Brongersma M L 2004 Geometries and materials for subwavelength surface plasmon modes *J. Opt. Soc. Am.* A **21** 2442
[356] Fang N, Lee H, Sun C and Zhang X 2005 Sub-diffraction-limited optical imaging with a silver superlens *Science* **308** 534–7
[357] Bai P, Son Chu H, Gu M, Kurniawan O and Li E 2010 Integration of plasmonics into nanoelectronic circuits *Physica* B **405** 2978–81
[358] Muhlschlegel P, Eisler H-J, Martin O J F, Hecht B and Pohl D W 2005 Resonant optical antennas *Science* **308** 1607–9
[359] Cubukcu E, Kort E A, Crozier K B and Capasso F 2006 Plasmonic laser antenna *Appl. Phys. Lett.* **89** 093120
[360] Muskens O L, Giannini V, Sánchez-Gil J A and Rivas J G 2007 Strong enhancement of the radiative decay rate of emitters by single plasmonic nanoantennas *Nano Lett.* **7** 2871–5
[361] Akimov Y A and Koh W S 2010 Resonant and nonresonant plasmonic nanoparticle enhancement for thin-film silicon solar cells *Nanotechnology* **21** 235201
[362] Tan H, Santbergen R, Smets A H M and Zeman M 2012 Plasmonic light trapping in thin-film silicon solar cells with improved self-assembled silver nanoparticles *Nano Lett.* **12** 4070–6
[363] Wang Y, Sun T, Paudel T, Zhang Y, Ren Z and Kempa K 2012 Metamaterial-plasmonic absorber structure for high efficiency amorphous silicon solar cells *Nano Lett.* **12** 440–5
[364] Luoshan M, Bai L, Bu C, Liu X, Zhu Y, Guo K, Jiang R, Li M and Zhao X 2016 Surface plasmon resonance enhanced multi-shell-modified upconversion $NaYF_4$:Yb^{3+}, Er^{3+}@SiO_2@Au@TiO_2 crystallites for dye-sensitized solar cells *J. Power Sources* **307** 468–73
[365] Ding B, Lee B J, Yang M, Jung H S and Lee J-K 2011 Surface-plasmon assisted energy conversion in dye-sensitized solar cells *Adv. Energy Mater.* **1** 415–21
[366] Zarick H F, Hurd O, Webb J A, Hungerford C, Erwin W R and Bardhan R 2014 Enhanced efficiency in dye-sensitized solar cells with shape-controlled plasmonic nanostructures *ACS Photonics* **1** 806–11
[367] Ding I-K *et al* 2011 Plasmonic dye-sensitized solar cells *Adv. Energy Mater.* **1** 52–7
[368] Sheehan S W, Noh H, Brudvig G W, Cao H and Schmuttenmaer C A 2013 Plasmonic enhancement of dye-sensitized solar cells using core–shell–shell nanostructures *J. Phys. Chem.* C **117** 927–34
[369] Nakayama K, Tanabe K and Atwater H A 2008 Plasmonic nanoparticle enhanced light absorption in GaAs solar cells *Appl. Phys. Lett.* **93** 121904
[370] Ferry V E, Sweatlock L A, Pacifici D and Atwater H A 2008 Plasmonic nanostructure design for efficient light coupling into solar cells *Nano Lett.* **8** 4391–7
[371] Saliba M, Zhang W, Burlakov V M, Stranks S D, Sun Y, Ball J M, Johnston M B, Goriely A, Wiesner U and Snaith H J 2015 Plasmonic-induced photon recycling in metal halide perovskite solar cells *Adv. Funct. Mater.* **25** 5038–46
[372] Lu Z *et al* 2015 Plasmonic-enhanced perovskite solar cells using alloy popcorn nanoparticles *RSC Adv.* **5** 11175–9
[373] Willets K A and Van Duyne R P 2007 Localized surface plasmon resonance spectroscopy and sensing *Annu. Rev. Phys. Chem.* **58** 267–97
[374] Chen Y and Ming H 2012 Review of surface plasmon resonance and localized surface plasmon resonance sensor *Photonic Sens.* **2** 37–49
[375] Jain P K, Huang X, El-Sayed I H and El-Sayed M A 2007 Review of some interesting surface plasmon resonance-enhanced properties of noble metal nanoparticles and their applications to biosystems *Plasmonics* **2** 107–18
[376] Mayer K M and Hafner J H 2011 Localized surface plasmon resonance sensors *Chem. Rev.* **111** 3828–57
[377] Hou W and Cronin S B 2013 A review of surface plasmon resonance-enhanced photocatalysis *Adv. Funct. Mater.* **23** 1612–9
[378] Enrichi F, Quandt A and Righini G C 2018 Plasmonic enhanced solar cells: summary of possible strategies and recent results *Renew. Sustain. Energy Rev.* **82** 2433–9
[379] Chang Y C, Chou F Y, Yeh P H, Chen H W, Chang S-H, Lan Y C, Guo T F, Tsai T C and Lee C T 2007 Effects of surface plasmon resonant scattering on the power conversion efficiency of organic thin-film solar cells *J. Vac. Sci. Technol.* B **25** 1899
[380] Chen X, Jia B, Zhang Y and Gu M 2013 Exceeding the limit of plasmonic light trapping in textured screen-printed solar cells using Al nanoparticles and wrinkle-like graphene sheets *Light Sci. Appl.* **2** e92–92
[381] Singh G, Sekhon J S and Verma S S 2016 Cu nanoparticle plasmons to enhance GaAs solar cell efficiency *13th Int. Conf. on Fiber Optics and Photonics* (Washington, DC: OSA) p W3A.14
[382] Dhonde M, Sahu K, Murty V V S, Nemala S S and Bhargava P 2017 Surface plasmon resonance effect of Cu nanoparticles in a dye sensitized solar cell *Electrochim. Acta* **249** 89–95
[383] Mertz J 2000 Radiative absorption, fluorescence, and scattering of a classical dipole near a lossless interface: a unified description *J. Opt. Soc. Am.* B **17** 1906
[384] Ringe E, McMahon J M, Sohn K, Cobley C, Xia Y, Huang J, Schatz G C, Marks L D and Van Duyne R P 2010 Unraveling the effects of size, composition, and substrate on the localized surface plasmon resonance frequencies of gold and silver nanocubes: a systematic single-particle approach *J. Phys. Chem.* C **114** 12511–6
[385] Ringe E *et al* 2009 Effect of size, shape, composition, and support film on localized surface plasmon resonance frequency: a single particle approach applied to silver bipyramids and gold and silver nanocubes *MRS Proc.* **1208** 52–7

[386] Malinsky M D, Kelly K L, Schatz G C and Duyne R P V 2001 Nanosphere lithography: effect of substrate on the localized surface plasmon resonance spectrum of silver nanoparticles *J. Phys. Chem.* A **105** 2343–50
[387] Derkacs D, Lim S H, Matheu P, Mar W and Yu E T 2006 Improved performance of amorphous silicon solar cells via scattering from surface plasmon polaritons in nearby metallic nanoparticles *Appl. Phys. Lett.* **89** 93103–5
[388] Catchpole K R and Polman A 2008 Design principles for particle plasmon enhanced solar cells *Appl. Phys. Lett.* **93** 191113
[389] Pala R A, White J, Barnard E, Liu J and Brongersma M L 2009 Design of plasmonic thin-film solar cells with broadband absorption enhancements *Adv. Mater.* **21** 3504–9
[390] Novotny L and van Hulst N 2011 Antennas for light *Nat. Photon.* **5** 83–90
[391] Green M A and Pillai S 2012 Harnessing plasmonics for solar cells *Nat. Photon.* **6** 130–2
[392] Beck F J, Polman A and Catchpole K R 2009 Tunable light trapping for solar cells using localized surface plasmons *J. Appl. Phys.* **105** 114310
[393] Liu Y, Cheng R, Liao L, Zhou H, Bai J, Liu G, Liu L, Huang Y and Duan X 2011 Plasmon resonance enhanced multicolour photodetection by graphene *Nat. Commun.* **2** 579
[394] Sherry L J, Chang S-H, Schatz G C, Van D R P, Wiley B J and Xia Y 2005 Localized surface plasmon resonance spectroscopy of single silver nanocubes *Nano Lett.* **5** 2034–8
[395] Krug J T, Sánchez E J and Xie X S 2002 Design of near-field optical probes with optimal field enhancement by finite difference time domain electromagnetic simulation *J. Chem. Phys.* **116** 10895–901
[396] Perney N M B, Baumberg J J, Zoorob M E, Charlton M D B, Mahnkopf S and Netti C M 2006 Tuning localized plasmons in nanostructured substrates for surface-enhanced Raman scattering *Opt. Express* **14** 847
[397] Chang S, Li Q, Xiao X, Wong K Y and Chen T 2012 Enhancement of low energy sunlight harvesting in dye-sensitized solar cells using plasmonic gold nanorods *Energy Environ. Sci.* **5** 9444
[398] Wang K X, Yu Z, Liu V, Cui Y and Fan S 2012 Absorption enhancement in ultrathin crystalline silicon solar cells with antireflection and light-trapping nanocone gratings *Nano Lett.* **12** 1616–9
[399] Kim S-S, Na S-I, Jo J, Kim D-Y and Nah Y-C 2008 Plasmon enhanced performance of organic solar cells using electrodeposited Ag nanoparticles *Appl. Phys. Lett.* **93** 073307
[400] Wu J-L, Chen F-C, Hsiao Y-S, Chien F-C, Chen P, Kuo C-H, Huang M H and Hsu C-S 2011 Surface plasmonic effects of metallic nanoparticles on the performance of polymer bulk heterojunction solar cells *ACS Nano* **5** 959–67
[401] Sebo B, Huang N, Liu Y, Tai Q, Liang L, Hu H, Xu S and Zhao X-Z 2013 Dye-sensitized solar cells enhanced by optical absorption, mediated by TiO_2 nanofibers and plasmonics Ag nanoparticles *Electrochim. Acta* **112** 458–64
[402] Muduli S, Game O, Dhas V, Vijayamohanan K, Bogle K A, Valanoor N and Ogale S B 2012 TiO_2–Au plasmonic nanocomposite for enhanced dye-sensitized solar cell (DSSC) performance *Sol. Energy* **86** 1428–34
[403] Ng S-P, Lu X, Ding N, Wu C-M L and Lee C-S 2014 Plasmonic enhanced dye-sensitized solar cells with self-assembly gold-TiO_2@core–shell nanoislands *Sol. Energy* **99** 115–25
[404] Chen H-W, Hong C-Y, Kung C-W, Mou C-Y, Wu K C-W and Ho K-C 2015 A gold surface plasmon enhanced mesoporous titanium dioxide photoelectrode for the plastic-based flexible dye-sensitized solar cells *J. Power Sources* **288** 221–8
[405] Dong H, Wu Z, Lu F, Gao Y, El-Shafei A, Jiao B, Ning S and Hou X 2014 Optics-electrics highways: plasmonic silver nanowires@TiO_2 core–shell nanocomposites for enhanced dye-sensitized solar cells performance *Nano Energy* **10** 181–91
[406] Chander N, Khan A F, Thouti E, Sardana S K, Chandrasekhar P S, Dutta V and Komarala V K 2014 Size and concentration effects of gold nanoparticles on optical and electrical properties of plasmonic dye sensitized solar cells *Sol. Energy* **109** 11–23
[407] Zhang W, Saliba M, Stranks S D, Sun Y, Shi X, Wiesner U and Snaith H J 2013 Enhancement of perovskite-based solar cells employing core–shell metal nanoparticles *Nano Lett.* **13** 4505–10
[408] Lenzmann F, Krueger J, Burnside S, Brooks K, Grätzel M, Gal D, Rühle S and Cahen D 2001 Surface photovoltage spectroscopy of dye-sensitized solar cells with TiO_2, Nb_2O_5, and $SrTiO_3$ nanocrystalline photoanodes: indication for electron injection from higher excited dye states *J. Phys. Chem.* B **105** 6347–52
[409] Würfel P 1997 Solar energy conversion with hot electrons from impact ionisation *Sol. Energy Mater. Sol. Cells* **46** 43–52
[410] Li J, Cushing S K, Meng F, Senty T R, Bristow A D and Wu N 2015 Plasmon-induced resonance energy transfer for solar energy conversion *Nat. Photon.* **9** 601–7
[411] White T P and Catchpole K R 2012 Plasmon-enhanced internal photoemission for photovoltaics: theoretical efficiency limits *Appl. Phys. Lett.* **101** 073905
[412] Yu K, Tian Y and Tatsuma T 2006 Size effects of gold nanaoparticles on plasmon-induced photocurrents of gold–TiO_2 nanocomposites *Phys. Chem. Chem. Phys.* **8** 5417–20
[413] Toyoda T, Tsugawa S and Shen Q 2009 Photoacoustic spectra of Au quantum dots adsorbed on nanostructured TiO_2 electrodes together with the photoelectrochemical current characteristics *J. Appl. Phys.* **105** 034314
[414] Ide Y, Matsuoka M and Ogawa M 2010 Efficient visible-light-induced photocatalytic activity on gold-nanoparticle-supported layered titanate *J. Am. Chem. Soc.* **132** 16762–4
[415] Gomes Silva C, Juárez R, Marino T, Molinari R and García H 2011 Influence of excitation wavelength (UV or visible light) on the photocatalytic activity of titania containing gold nanoparticles for the generation of hydrogen or oxygen from water *J. Am. Chem. Soc.* **133** 595–602
[416] Yuan Z *et al* 2015 Hot-electron injection in a sandwiched TiO_x -Au-TiO_x structure for high-performance planar perovskite solar cells *Adv. Energy Mater.* **5** 1500038
[417] Liu D, Yang D, Gao Y, Ma J, Long R, Wang C and Xiong Y 2016 Flexible near-infrared photovoltaic devices based on plasmonic hot-electron injection into silicon nanowire arrays *Angew. Chem., Int. Ed.* **55** 4577–81
[418] Barad H-N, Ginsburg A, Cohen H, Rietwyk K J, Keller D A, Tirosh S, Bouhadana Y, Anderson A Y and Zaban A 2016 Hot electron-based solid state TiO_2|Ag solar cells *Adv. Mater. Interfaces* **3** 1500789
[419] Ginsburg A, Priel M, Barad H N, Keller D A, Borvick E, Rietwyk K, Kama A, Meir S, Anderson A Y and Zaban A 2018 Solid state ITO|Au-NPs|TiO_2 plasmonic based solar cells *Sol. Energy Mater. Sol. Cells* **179** 254–9
[420] Zhang Y, Yam C and Schatz G C 2016 Fundamental limitations to plasmonic hot-carrier solar cells *J. Phys. Chem. Lett.* **7** 1852–8
[421] Anderson A, Deryckx K S, Xu X G, Steinmeyer G and Raschke M B 2010 Few-femtosecond plasmon dephasing of a single metallic nanostructure from optical response function reconstruction by interferometric frequency resolved optical gating *Nano Lett.* **10** 2519–24
[422] Jing C, Shi L, Liu X and Long Y-T 2014 A single gold nanorod as a plasmon resonance energy transfer based nanosensor for high-sensitivity Cu(ii) detection *Analyst* **139** 6435–9
[423] Ma X-C, Dai Y, Yu L and Huang B-B 2016 Energy transfer in plasmonic photocatalytic composites *Light Sci. Appl.* **5** e16017–16017

[424] Cushing S K, Li J, Bright J, Yost B T, Zheng P, Bristow A D and Wu N 2015 Controlling plasmon-induced resonance energy transfer and hot electron injection processes in metal@TiO_2 core–shell nanoparticles *J. Phys. Chem.* C **119** 16239–44

[425] Wu D, Wang F, Wang H, Cao K, Gao Z, Xu F and Jiang K 2016 Plasmon resonance energy transfer and hot electron injection induced high photocurrent density in liquid junction Ag@Ag_2S sensitized solar cells *Dalton Trans.* **45** 16275–82

[426] Conibeer G 2007 Third-generation photovoltaics *Mater. Today* **10** 42–50

[427] Richards B S, Ivaturi A, MacDougall S K W and Marques-Hueso J 2012 Up- and down-conversion materials for photovoltaic devices *Photonics for Solar Energy Systems IV* (*SPIE Proc.* vol 8438) ed R Wehrspohn and A Gombert p 843802

[428] Verma D, Saetre T O and Midtgard O-M 2012 Review on up/down conversion materials for solar cell application *2012 38th IEEE Photovoltaic Specialists Conf.* (Piscataway, NJ: IEEE) pp 002608–13

[429] Cheng Y Y *et al* 2012 Improving the light-harvesting of amorphous silicon solar cells with photochemical upconversion *Energy Environ. Sci.* **5** 6953

[430] de Wild J, Meijerink A, Rath J K, van Sark W G J H M and Schropp R E I 2010 Towards upconversion for amorphous silicon solar cells *Sol. Energy Mater. Sol. Cells* **94** 1919–22

[431] Rajeswari R, Susmitha K, Jayasankar C K, Raghavender M and Giribabu L 2017 Enhanced light harvesting with novel photon upconverted $Y_2CaZnO_5:Er^{3+}/Yb^3$ nanophosphors for dye sensitized solar cells *Sol. Energy* **157** 956–65

[432] Han G, Wang M, Li D, Bai J and Diao G 2017 Novel upconversion Er, Yb–CeO_2 hollow spheres as scattering layer materials for efficient dye-sensitized solar cells *Sol. Energy Mater. Sol. Cells* **160** 54–9

[433] Wu J, Song Y, Han B, Wei J, Wei Z and Yang Y 2015 Synthesis and characterization of UV upconversion material $Y_2 SiO_5:Pr^{3+}$, Li^+/TiO_2 with enhanced the photocatalytic properties under a xenon lamp *RSC Adv.* **5** 49356–62

[434] Huang X 2017 Broadband dye-sensitized upconversion: a promising new platform for future solar upconverter design *J. Alloys Compd.* **690** 356–9

[435] Wen X, Yu P, Toh Y-R, Ma X and Tang J 2014 On the upconversion fluorescence in carbon nanodots and graphene quantum dots *Chem. Commun.* **50** 4703–6

[436] Zhou J, Liu Q, Feng W, Sun Y and Li F 2015 Upconversion luminescent materials: advances and applications *Chem. Rev.* **115** 395–465

[437] Gnach A and Bednarkiewicz A 2012 Lanthanide-doped up-converting nanoparticles: merits and challenges *Nano Today* **7** 532–63

[438] Liao J, Yang Z, Lai S, Shao B, Li J, Qiu J, Song Z and Yang Y 2014 Upconversion emission enhancement of $NaYF_4$:Yb,Er nanoparticles by coupling silver nanoparticle plasmons and photonic crystal effects *J. Phys. Chem.* C **118** 17992–9

[439] Singh-Rachford T N and Castellano F N 2010 Photon upconversion based on sensitized triplet–triplet annihilation *Coord. Chem. Rev.* **254** 2560–73

[440] Auzel F 2004 Upconversion and anti-stokes processes with f and d ions in solids *Chem. Rev.* **104** 139–74

[441] Auzel F E 1973 Materials and devices using double-pumped-phosphors with energy transfer *Proc. IEEE* **61** 758–86

[442] Weingarten D H, LaCount M D, van de Lagemaat J, Rumbles G, Lusk M T and Shaheen S E 2017 Experimental demonstration of photon upconversion via cooperative energy pooling *Nat. Commun.* **8** 14808

[443] Dong H, Sun L-D and Yan C-H 2015 Energy transfer in lanthanide upconversion studies for extended optical applications *Chem. Soc. Rev.* **44** 1608–34

[444] Favilla E, Cittadino G, Veronesi S, Tonelli M, Fischer S, Goldschmidt J C, Cassanho A and Jenssen H P 2016 Comparative analysis of upconversion efficiencies in fluoride materials for photovoltaic application *Sol. Energy Mater. Sol. Cells* **157** 415–21

[445] Ding M, Yin S, Chen D, Zhong J, Ni Y, Lu C, Xu Z and Ji Z 2015 Hexagonal $NaYF_4:Yb^{3+}/Er^{3+}$ nano/micro-structures: controlled hydrothermal synthesis and morphology-dependent upconversion luminescence *Appl. Surf. Sci.* **333** 23–33

[446] Yang D, Kang X, Ma P, Dai Y, Hou Z, Cheng Z, Li C and Lin J 2013 Hollow structured upconversion luminescent $NaYF_4:Yb^{3+}$, Er^{3+} nanospheres for cell imaging and targeted anti-cancer drug delivery *Biomaterials* **34** 1601–12

[447] Cresswell P J, Robbins D J and Thomson A J 1978 Rhenium(IV) as a sensitizer for two-step blue up-converters *J. Lumin.* **17** 311–24

[448] Pires A M, Serra O A and Davolos M R 2005 Morphological and luminescent studies on nanosized Er, Yb–Yttrium oxide up-converter prepared from different precursors *J. Lumin.* **113** 174–82

[449] Kijima T, Isayama T, Sekita M, Uota M and Sakai G 2009 Emission properties of Tb^{3+} in $Y_2O_2SO_4$ derived from their precursory dodecylsulfate-templated concentric- and straight-layered nanostructures *J. Alloys Compd.* **485** 730–3

[450] Tymiński A and Grzyb T 2017 Are rare earth phosphates suitable as hosts for upconversion luminescence? Studies on nanocrystalline $REPO_4$ (RE = Y, La, Gd, Lu) doped with Yb^{3+} and Eu^{3+}, Tb^{3+}, Ho^{3+}, Er^{3+} or Tm^{3+} ions *J. Lumin.* **181** 411–20

[451] Boyer J-C, Manseau M-P, Murray J I and van Veggel F C J M 2010 Surface modification of upconverting $NaYF_4$ nanoparticles with PEG−phosphate ligands for NIR (800 nm) biolabeling within the biological window *Langmuir* **26** 1157–64

[452] Wang F, Yang B, Chen X, Ma W and Xu B 2016 Color-tunable and upconversion luminescence of Gd_2O_2S:Er,Tb phosphor *Mater. Chem. Phys.* **169** 113–9

[453] Wang N, Liu Z, Tong H, Zhang X and Bai Z 2017 Preparation of $Gd_2O_2S:Yb^{3+}$, Er^{3+}, Tm^{3+} sub-micro phosphors by sulfurization of the oxides derived from sol-gel method and the upconversion luminescence properties *Mater. Res. Express* **4** 076205

[454] Martín-Rodríguez R, Fischer S, Ivaturi A, Froehlich B, Krämer K W, Goldschmidt J C, Richards B S and Meijerink A 2013 Highly efficient IR to NIR upconversion in Gd_2O_2S: Er^{3+} for photovoltaic applications *Chem. Mater.* **25** 1912–21

[455] Boccolini A, Favilla E, Tonelli M, Richards B S and Thomson R R 2015 Highly efficient upconversion in Er^{3+} doped BaY_2F_8 single crystals: dependence of quantum yield on excitation wavelength and thickness *Opt. Express* **23** A903

[456] Boccolini A, Faoro R, Favilla E, Veronesi S and Tonelli M 2013 BaY_2F_8 doped with Er^{3+}: an upconverter material for photovoltaic application *J. Appl. Phys.* **114** 064904

[457] Huang F, Liu X, Hu L and Chen D 2015 Spectroscopic properties and energy transfer parameters of Er^{3+}-doped fluorozirconate and oxyfluoroaluminate glasses *Sci. Rep.* **4** 5053

[458] Ivanova S and Pellé F 2009 Strong 153 μm to NIR–VIS–UV upconversion in Er-doped fluoride glass for high-efficiency solar cells *J. Opt. Soc. Am.* B **26** 1930

[459] Shalav A, Richards B S, Trupke T, Krämer K W and Güdel H U 2005 Application of $NaYF_4:Er^{3+}$ up-converting phosphors for enhanced near-infrared silicon solar cell response *Appl. Phys. Lett.* **86** 013505

[460] Kuisheng Y, Yan L, Chaoyi Y, Liping L, Chanhua Y and Xiyan Z 2006 Upconversion luminescence properties of Ho^{3+}, Tm^{3+}, Yb^{3+} Co-doped nanocrystal $NaYF_4$ synthesized by hydrothermal method *J. Rare Earths* **24** 757–60

[461] Chen D, Liu L, Huang P, Ding M, Zhong J and Ji Z 2015 Nd^{3+}-sensitized Ho^{3+} single-band red upconversion luminescence in core–shell nanoarchitecture *J. Phys. Chem. Lett.* **6** 2833–40

[462] Gibart P, Auzel F, Guillaume J-C and Zahraman K 1996 Below band-gap IR response of substrate-free GaAs solar cells using two-photon up-conversion *Jpn. J. Appl. Phys.* **35** 4401–2

[463] Trupke T, Green M A and Würfel P 2002 Improving solar cell efficiencies by up-conversion of sub-band-gap light *J. Appl. Phys.* **92** 4117–22

[464] Liang X F, Huang X Y and Zhang Q Y 2009 $Gd_2(MoO_{4)3}$:Er^{3+} nanophosphors for an enhancement of silicon solar-cell near-infrared response *J. Fluoresc.* **19** 285–9

[465] Shan G-B and Demopoulos G P 2010 Near-infrared sunlight harvesting in dye-sensitized solar cells via the insertion of an upconverter-TiO_2 nanocomposite layer *Adv. Mater.* **22** 4373–7

[466] Wang H-Q, Batentschuk M, Osvet A, Pinna L and Brabec C J 2011 Rare-earth ion doped up-conversion materials for photovoltaic applications *Adv. Mater.* **23** 2675–80

[467] Fischer S, Goldschmidt J C, Löper P, Bauer G H, Brüggemann R, Krämer K, Biner D, Hermle M and Glunz S W 2010 Enhancement of silicon solar cell efficiency by upconversion: optical and electrical characterization *J. Appl. Phys.* **108** 044912

[468] Luitel H N, Mizuno S and Takeda Y 2017 $CaTiO_3$:Er^{3+}, Ni^{2+} broadband-sensitive upconverter: an effective way to harvest unused NIR solar irradiation for crystalline silicon solar cells *Phys. Status Solidi* **214** 1600899

[469] He M, Pang X, Liu X, Jiang B, He Y, Snaith H and Lin Z 2016 Monodisperse dual-functional upconversion nanoparticles enabled near-infrared organolead halide perovskite solar cells

[470] MacDougall S K W, Ivaturi A, Marques-Hueso J, Krämer K W and Richards B S 2014 Broadband photoluminescent quantum yield optimisation of Er^{3+}-doped β-$NaYF_4$ for upconversion in silicon solar cells *Sol. Energy Mater. Sol. Cells* **128** 18–26

[471] Fischer S, Favilla E, Tonelli M and Goldschmidt J C 2015 Record efficient upconverter solar cell devices with optimized bifacial silicon solar cells and monocrystalline BaY_2F_8:30% Er^{3+} upconverter *Sol. Energy Mater. Sol. Cells* **136** 127–34

[472] Ding Y, Qiao H, Yang T, Yin N, Li P, Zhao Y and Zhang X 2017 Upconversion luminescence co-enhanced by Li^+ ions doping and localized surface plasmon resonance for perovskite solar cells *Opt. Mater.* **73** 617–22

[473] Zhang Z, Qin J, Shi W, Liu Y, Zhang Y, Liu Y, Gao H and Mao Y 2018 Enhanced power conversion efficiency of perovskite solar cells with an up-conversion material of Er^{3+}-Yb^{3+}-Li^+ tri-doped TiO_2 *Nanoscale Res. Lett.* **13** 147

[474] Zou W, Visser C, Maduro J A, Pshenichnikov M S and Hummelen J C 2012 Broadband dye-sensitized upconversion of near-infrared light *Nat. Photonics* **6** 560–4

[475] Trupke T, Green M A and Würfel P 2002 Improving solar cell efficiencies by down-conversion of high-energy photons *J. Appl. Phys.* **92** 1668–74

[476] de la Mora M B, Amelines-Sarria O, Monroy B M, Hernández-Pérez C D and Lugo J E 2017 Materials for downconversion in solar cells: perspectives and challenges *Sol. Energy Mater. Sol. Cells* **165** 59–71

[477] Lakshminarayana G, Yang H, Ye S, Liu Y and Qiu J 2008 Cooperative downconversion luminescence in Pr^{3+}/Yb^{3+}:SiO_2–Al_2O_3–BaF_2–GdF_3 glasses *J. Mater. Res.* **23** 3090–5

[478] Vergeer P, Vlugt T J H, Kox M H F, den Hertog M I, van der Eerden J P J M and Meijerink A 2005 Quantum cutting by cooperative energy transfer in $Yb_xY_{1-x}PO_4$:Tb^{3+} *Phys. Rev.* B **71** 014119

[479] Chen D, Wang Y, Yu Y, Huang P and Weng F 2008 Quantum cutting downconversion by cooperative energy transfer from Ce^{3+} to Yb^{3+} in borate glasses *J. Appl. Phys.* **104** 116105

[480] Chen D, Yu Y, Wang Y, Huang P and Weng F 2009 Cooperative energy transfer up-conversion and quantum cutting down-conversion in Yb^{3+}:TbF_3 nanocrystals embedded glass ceramics *J. Phys. Chem.* C **113** 6406–10

[481] Feng W, Liu J and Yu X 2014 Efficiency enhancement of mono-Si solar cell with CdO nanotip antireflection and down-conversion layer *RSC Adv.* **4** 51683–7

[482] Elleuch R, Salhi R, Deschanvres J-L and Maalej R 2015 Antireflective downconversion ZnO:Er^{3+}, Yb^{3+} thin film for Si solar cell applications *J. Appl. Phys.* **117** 055301

[483] hang Q Y, Yang G F and Jiang Z H 2007 Cooperative downconversion in $GdAl_3(BO_3)_4$:RE^{3+},Yb^{3+} (RE = Pr, Tb, and Tm) *Appl. Phys. Lett.* **91** 051903

[484] Meijer J-M, Aarts L, van der Ende B M, Vlugt T J H and Meijerink A 2010 Downconversion for solar cells in YF_3: Nd^{3+}, Yb^{3+} *Phys. Rev.* B **81** 035107

[485] Yu D-C, Martín-Rodríguez R, Zhang Q-Y, Meijerink A and Rabouw F T 2015 Multi-photon quantum cutting in Gd_2O_2S:Tm^{3+} to enhance the photo-response of solar cells *Light Sci. Appl.* **4** e344

[486] Yasaka P and Kaewkhao J 2015 Luminescence from lanthanides-doped glasses and applications: a review *2015 4th Int. Conf. on Instrumentation, Communications, Information Technology, and Biomedical Engineering (ICICI-BME)* (Piscataway, NJ: IEEE) pp 4–15

[487] Wu D M, García-Etxarri A, Salleo A and Dionne J A 2014 Plasmon-enhanced upconversion *J. Phys. Chem. Lett.* **5** 4020–31

[488] Park K, Jung K, Kwon S J, Jang H S, Byun D, Han I K and Ko H 2016 Plasmonic nanowire-enhanced upconversion luminescence for anticounterfeit devices *Adv. Funct. Mater.* **26** 7836–46

[489] Martin G 2003 *Third Generation Photovoltaics* vol 12 (Berlin: Springer)

[490] Debije M G and Verbunt P P C 2012 Thirty years of luminescent solar concentrator research: solar energy for the built environment *Adv. Energy Mater.* **2** 12–35

[491] Meinardi F, Bruni F and Brovelli S 2017 Luminescent solar concentrators for building-integrated photovoltaics *Nat. Rev. Mater.* **2** 1–9

[492] Weber W H and Lambe J 1976 Luminescent greenhouse collector for solar radiation *Appl. Opt.* **15** 2299

[493] Batchelder J S, Zewai A H and Cole T 1979 Luminescent solar concentrators: I. Theory of operation and techniques for performance evaluation *Appl. Opt.* **18** 3090

[494] Goetzberger A and Greube W 1977 Solar energy conversion with fluorescent collectors *Appl. Phys.* **14** 123–39

[495] Swartz B A, Cole T and Zewail A H 1977 Photon trapping and energy transfer in multiple-dye plastic matrices: an efficient solar-energy concentrator *Opt. Lett.* **1** 73

[496] Drake J M, Lesiecki M L, Sansregret J and Thomas W R L 1982 Organic dyes in PMMA in a planar luminescent solar collector: a performance evaluation *Appl. Opt.* **21** 2945

[497] El-Shahawy M A and Mansour A F 1996 Optical properties of some luminescent solar concentrators *J. Mater. Sci., Mater. Electron.* **7** 171–4

[498] Baumberg I, Berezin O, Drabkin A, Gorelik B, Kogan L, Voskobojnik M and Zaidman M 2001 Effect of polymer matrix on photo-stability of photo-luminescent dyes in multi-layer polymeric structures *Polym. Degrad. Stab.* **73** 403–10

[499] Batchelder J S, Zewail A H and Cole T 1981 Luminescent solar concentrators: II. Experimental and theoretical analysis of their possible efficiencies *Appl. Opt.* **20** 3733

[500] Sark W G J H M *et al* 2008 Luminescent solar concentrators—a review of recent results *Opt. Express* **16** 21773

[501] Seybold G and Wagenblast G 1989 New perylene and violanthrone dyestuffs for fluorescent collectors *Dyes Pigment.* **11** 303–17

[502] Al-Kaysi R O, Sang Ahn T, Müller A M and Bardeen C J 2006 The photophysical properties of chromophores at high (100 mM and above) concentrations in polymers and as neat solids *Phys. Chem. Chem. Phys.* **8** 3453–9

[503] Sanguineti A, Sassi M, Turrisi R, Ruffo R, Vaccaro G, Meinardi F and Beverina L 2013 High Stokes shift perylene dyes for luminescent solar concentrators *Chem. Commun.* **49** 1618–20
[504] Wilson L R and Richards B S 2009 Measurement method for photoluminescent quantum yields of fluorescent organic dyes in polymethyl methacrylate for luminescent solar concentrators *Appl. Opt.* **48** 212
[505] Currie M J, Mapel J K, Heidel T D, Goffri S and Baldo M A 2008 High-efficiency organic solar concentrators for photovoltaics *Science* **321** 226–8
[506] van Sark W G J H M 2013 Luminescent solar concentrators—a low cost photovoltaics alternative *Renew. Energy* **49** 207–10
[507] Desmet L, Ras A J M, de Boer D K G and Debije M G 2012 Monocrystalline silicon photovoltaic luminescent solar concentratorent solar concentrator with 42% power conversion efficiency *Opt. Lett.* **37** 3087
[508] Slooff L H, Bende E E, Burgers A R, Budel T, Pravettoni M, Kenny R P, Dunlop E D and Büchtemann A 2008 A Luminescent Solar Concentrator with 7.1% power conversion efficiency *Phys. Status Solidi* **2** 257–9
[509] Mansour A 2004 Photostability and optical parameters of copolymer styrene/MMA as a matrix for the dyes used in fluorescent solar collectors *Polym. Test.* **23** 247–52
[510] Mićić O I, Cheong H M, Fu H, Zunger A, Sprague J R, Mascarenhas A and Nozik A J 1997 Size-dependent spectroscopy of InP quantum dots *J. Phys. Chem.* B **101** 4904–12
[511] Chatten A J, Barnham K W J, Buxton B F, Ekins-Daukes N J and Malik M A 2003 A new approach to modelling quantum dot concentrators *Sol. Energy Mater. Sol. Cells* **75** 363–71
[512] Norris D J and Bawendi M G 1996 Measurement and assignment of the size-dependent optical spectrum in CdSe quantum dots *Phys. Rev.* B **53** 16338–46
[513] Micic O I, Curtis C J, Jones K M, Sprague J R and Nozik A J 1994 Synthesis and characterization of InP quantum dots *J. Phys. Chem.* **98** 4966–9
[514] Shcherbatyuk G V, Inman R H, Wang C, Winston R and Ghosh S 2010 Viability of using near infrared PbS quantum dots as active materials in luminescent solar concentrators *Appl. Phys. Lett.* **96** 191901
[515] Kennedy M, McCormack S J, Doran J and Norton B 2009 Improving the optical efficiency and concentration of a single-plate quantum dot solar concentrator using near infra-red emitting quantum dots *Sol. Energy* **83** 978–81
[516] Gallagher S J, Norton B and Eames P C 2007 Quantum dot solar concentrators: electrical conversion efficiencies and comparative concentrating factors of fabricated devices *Sol. Energy* **81** 813–21
[517] Sholin V, Olson J D and Carter S A 2007 Semiconducting polymers and quantum dots in luminescent solar concentrators for solar energy harvesting *J. Appl. Phys.* **101** 123114
[518] Erickson C S, Bradshaw L R, McDowall S, Gilbertson J D, Gamelin D R and Patrick D L 2014 Zero-reabsorption doped-nanocrystal luminescent solar concentrators *ACS Nano* **8** 3461–7
[519] Meinardi F, Akkerman Q A, Bruni F, Park S, Mauri M, Dang Z, Manna L and Brovelli S 2017 Doped halide perovskite nanocrystals for reabsorption-free luminescent solar concentrators *ACS Energy Lett.* **2** 2368–77
[520] Bradshaw L R, Knowles K E, McDowall S and Gamelin D R 2015 Nanocrystals for luminescent solar concentrators *Nano Lett.* **15** 1315–23
[521] Knowles K E, Kilburn T B, Alzate D G, McDowall S and Gamelin D R 2015 Bright $CuInS_2$/CdS nanocrystal phosphors for high-gain full-spectrum luminescent solar concentrators *Chem. Commun.* **51** 9129–32
[522] Chen W *et al* 2017 Heavy metal free nanocrystals with near infrared emission applying in luminescent solar concentrator *Sol. RRL* **1** 1700041
[523] Hu X, Kang R, Zhang Y, Deng L, Zhong H, Zou B and Shi L-J 2015 Ray-trace simulation of $CuInS(Se)_2$ quantum dot based luminescent solar concentrators *Opt. Express* **23** A858
[524] Meinardi F, McDaniel H, Carulli F, Colombo A, Velizhanin K A, Makarov N S, Simonutti R, Klimov V I and Brovelli S 2015 Highly efficient large-area colourless luminescent solar concentrators using heavy-metal-free colloidal quantum dots *Nat. Nanotechnol.* **10** 878–85
[525] Meinardi F, Ehrenberg S, Dhamo L, Carulli F, Mauri M, Bruni F, Simonutti R, Kortshagen U and Brovelli S 2017 Highly efficient luminescent solar concentrators based on earth-Abundant indirect-bandgap silicon quantum dots *Nat. Photon.* **11** 177–85
[526] Nie W *et al* 2015 Solar cells. High-efficiency solution-processed perovskite solar cells with millimeter-scale grains *Science* **347** 522–5
[527] Leijtens T, Eperon G E, Noel N K, Habisreutinger S N, Petrozza A and Snaith H J 2015 Stability of metal halide perovskite solar cells *Adv. Energy Mater.* **5** 1500963
[528] Saba M *et al* 2014 Correlated electron–hole plasma in organometal perovskites *Nat. Commun.* **5** 5049
[529] Löper P, Stuckelberger M, Niesen B, Werner J, Filipič M, Moon S-J, Yum J-H, Topič M, De Wolf S and Ballif C 2015 Complex refractive index spectra of $CH_3NH_3PbI_3$ perovskite thin films determined by spectroscopic ellipsometry and spectrophotometry *J. Phys. Chem. Lett.* **6** 66–71
[530] Chen C-W, Hsiao S-Y, Chen C-Y, Kang H-W, Huang Z-Y and Lin H-W 2015 Optical properties of organometal halide perovskite thin films and general device structure design rules for perovskite single and tandem solar cells *J. Mater. Chem.* A **3** 9152–9
[531] Nikolaidou K, Sarang S, Hoffman C, Mendewala B, Ishihara H, Lu J Q, Ilan B, Tung V and Ghosh S 2016 Hybrid perovskite thin films as highly efficient luminescent solar concentrators *Adv. Opt. Mater.* **4** 2126–32
[532] Li X, Li W, Guo X, Lou J and Tong L 2013 All-fiber hybrid photon-plasmon circuits: integrating nanowire plasmonics with fiber optics *Opt. Express* **21** 15698
[533] Xu D, Li A, Yao L, Lin H, Yang S and Zhang Y 2017 Lanthanide-doped KLu_2F_7 nanoparticles with high upconversion luminescence performance: a comparative study by judd-ofelt analysis and energy transfer mechanistic investigation *Sci. Rep.* **7** 43189
[534] de Wild J, Meijerink A, Rath J K, van Sark W G J H M and Schropp R E I 2011 Upconverter solar cells: materials and applications *Energy Environ. Sci.* **4** 4835
[535] Saxena V N 1983 Phosphors for solar-cells Tb-doped lanthanum fluoride and Tm-doped calcium tungstate *Indian J. Pure Appl. Phys.* **21** 306–7
[536] Liu J, Yao Q and Li Y 2006 Effects of downconversion luminescent film in dye-sensitized solar cells *Appl. Phys. Lett.* **88** 173119
[537] Yao N, Huang J, Fu K, Liu S, Dong E, Wang Y, Xu X, Zhu M and Cao B 2014 Efficiency enhancement in dye-sensitized solar cells with down conversion material ZnO: Eu^{3+}, Dy^{3+} *J. Power Sources* **267** 405–10
[538] Fix T, Nonat A, Imbert D, Di Pietro S, Mazzanti M, Slaoui A and Charbonnière L J 2016 Enhancement of silicon solar cells by downshifting with Eu and Tb coordination complexes *Prog. Photovolt., Res. Appl.* **24** 1251–60
[539] Yu Y, Lan L and Cai H 2018 Integrating down-shifting and down-conversion into metal–organic frameworks to enhance the spectral conversion for solar cells *J. Phys. Chem.* C **122** 96–104

[540] Tsai M-L, Tu W-C, Tang L, Wei T-C, Wei W-R, Lau S P, Chen L-J and He J-H 2016 Efficiency enhancement of silicon heterojunction solar cells via photon management using graphene quantum dot as downconverters *Nano Lett.* **16** 309–13
[541] Zhou D, Liu D, Pan G, Chen X, Li D, Xu W, Bai X and Song H 2017 Cerium and ytterbium codoped halide perovskite quantum dots: a novel and efficient downconverter for improving the performance of silicon solar cells *Adv. Mater.* **29** 1704149
[542] Gardelis S and Nassiopoulou A G 2014 Evidence of significant down-conversion in a Si-based solar cell using $CuInS_2$/ZnS core shell quantum dots *Appl. Phys. Lett.* **104** 183902